# INFORMATION TO USERS

This manuscript has been reproduced from the microfilm master. UMI films the text directly from the original or copy submitted. Thus, some thesis and dissertation copies are in typewriter face, while others may be from any type of computer printer.

**The quality of this reproduction is dependent upon the quality of the copy submitted.** Broken or indistinct print, colored or poor quality illustrations and photographs, print bleedthrough, substandard margins, and improper alignment can adversely affect reproduction.

In the unlikely event that the author did not send UMI a complete manuscript and there are missing pages, these will be noted. Also, if unauthorized copyright material had to be removed, a note will indicate the deletion.

Oversize materials (e.g., maps, drawings, charts) are reproduced by sectioning the original, beginning at the upper left-hand corner and continuing from left to right in equal sections with small overlaps.

Photographs included in the original manuscript have been reproduced xerographically in this copy. Higher quality 6" x 9" black and white photographic prints are available for any photographs or illustrations appearing in this copy for an additional charge. Contact UMI directly to order.

Bell & Howell Information and Learning
300 North Zeeb Road, Ann Arbor, MI 48106-1346 USA
800-521-0600

# ACTIVE-PASSIVE CORROSION OF Fe-Cr-Ni ALLOYS IN HOT CONCENTRATED SULPHURIC ACID SOLUTIONS

By

JOSEPH R. KISH, B. Eng.

A Thesis

Submitted to the School of Graduate Studies

in Partial Fulfilment of the Requirements

for the Degree

Doctor of Philosophy

McMaster University

# ACTIVE-PASSIVE CORROSION OF Fe-Cr-Ni ALLOYS IN HOT CONCENTRATED SULPHURIC ACID SOLUTIONS

DOCTOR OF PHILOSOPHY
(Materials Science and Engineering)

McMASTER UNIVERSITY
Hamilton, Ontario

| | |
|---|---|
| TITLE: | Active-Passive Corrosion of Fe-Cr-Ni Alloys in Hot Concentrated Sulphuric Acid Solutions |
| AUTHOR: | Joesph R. Kish, B. Eng. (McMaster University) |
| SUPERVISOR: | Professor M.B. Ives |
| NUMBER OF PAGES: | xvi, 237 |

IN LOVING MEMORY OF
JOSEPH J. KISH (S.N. 7729938) AND
HILDA ROMANO

# ABSTRACT

In the manufacture of sulphuric acid more stringent environmental standards and operation economics have forced the industry to improve product utilization, energy efficiency and reliability. A key to improving both the thermal efficiency and reliability is the use and/or development of more corrosion resistance materials including stainless steels, especially in the parts of the plant that handle the condensed acid. Application of more corrosion resistant material requires a better understanding of the corrosion mechanism involved in concentrated $H_2SO_4$-$H_2O$ (>90 wt.%) solutions. While corrosion kinetics of carbon steel, the traditional material of construction, are relatively well understood, this is much less true in the case of the cyclic active-passive corrosion of stainless steels. Models proposed to explain the cyclic active-passive corrosion involve a periodic formation of either a protective metal sulphate film or an insoluble sulphur layer.

To better understand the reactivity and/or passivity of stainless steel in concentrated $H_2SO_4$-$H_2O$ solutions a study employing immersion and electrochemical techniques, including rotating electrodes, was conducted in order to clarify the following:

1. The state of stainless steel passivity.
2. The conditions in which passivity is stable.
3. The role played by the major alloying elements in establishing and maintaining the passive state.

The study involved evaluating the corrosion behaviour of stainless steels S30403 and S43000 along with iron, chromium and nickel in 93.5 wt.% $H_2SO_4$ at temperatures between 25-80°C.

Major discoveries of the study include:

1. A content of 17-18 wt.% chromium is sufficient to anodically passivate S43000 as the potential is made more noble. Passivity is not stable and requires anodic polarization.
2. Alloyed nickel plays an active role in improving the corrosion resistance of stainless steel. A content of 8 wt.% nickel is sufficient promote a periodic passivation of the base Fe-(17-18)wt.% Cr stainless steel under open-circuit conditions which reduces the corrosion rate by at least an order of magnitude.
3. The electrolysis of concentrated $H_2SO_4$-$H_2O$ solutions involves a potential-dependent reduction of $H_2SO_4$ molecules to sulphur-containing species with an oxidation state lower than six (6). The various reduction products have a significant effect on the stainless steel corrosion resistance.
4. Successful modelling of the corrosion of nickel has been accomplished by using a galvanic interaction between a noncontinuous nickel sulphide (NiS) deposit, formed *in situ*, and the uncovered nickel metal.
5. Successful modelling of the active-passive corrosion of S30403 has been accomplished using a galvanic interaction between NiS(Ni) and S43000.

# ACKNOWLEDGEMENTS

I wish to express my deepest gratitude to my academic mentor, Professor M. Brian Ives, for his guidance, wisdom and encouragement throughout the challenge of conducting this research. My committee members, Professor A. Petric and Professor O.E. Hileman Jr., also deserve my appreciation for providing timely suggestions, advice and support.

My co-workers in the Walter W. Smeltzer Corrosion Laboratory have provided me with a truly enjoyable environment in which to spend those may hours required in the lab to "push the envelope" of corrosion science. The following deserve appreciation: John Rodda, Yucheng Lu, Jingli Luo, Sanna Virtanen, Fred Hua and Sladjana Zdero. Of the group, John Rodda deserves special gratitude for sharing with me his enthusiasm for, and his expertise in, conducting corrosion research in concentrated sulphuric acid.

My professional mentors, Gordon Cameron at Cecebe Technologies Inc. and Dave Hodgson at D.&M. Hodgson and Associates Inc., deserve appreciation for never letting me lose sight of the technical importance of this research. My employer, NORAM Engineering & Constructors Ltd. also deserves my appreciation for providing the encouragement, time and financial resources required to finish writing the manuscript.

The following individuals at the National Research Council of Canada (NRC) are acknowledged for conducting the surface microanalysis: M.J. Graham, P. Schmuki and I. Sproule. J. McAndrew at McMaster is acknowledged for conducting the XRF analysis. C. Butcher and M. Van Oosten are acknowledged for providing various technical support throughout the research.

My fellow MSE "MisFits" have provided the necessary balance for a successful and memorable graduate research experience. The following deserve appreciation for being the wall: Craig Zaluski, Brian Reeves, Ed Becze, Dave Novog, Mike Flynn, Kelly Conlon, Dwayne Wasylyshyn, Andrew Holm and Colin Scott.

Finally, I cannot adequately express gratitude to my family whose encouragement and support played the greatest role in sustaining me through my career as a student.

# TABLE OF CONTENTS

# LIST OF FIGURES

# LIST OF TABLES

# CHAPTER 1

## 1. INTRODUCTION

In recent years, the chemical process industry has been forced to improve product utilization, energy efficiency and reliability in response to more stringent environmental standards and operation economics. The manufacture of sulphuric acid ($H_2SO_4$) is no exception. While the sulphuric acid contact process has a production efficiency of 98-99%, the same cannot be said of the thermal efficiency. The contact process involves several exothermic reactions: the catalytic conversion of sulphur dioxide ($SO_2$) to sulphur trioxide ($SO_3$), the absorption of $SO_3$ in 98 wt.% $H_2SO_4$ and the dilution with water ($H_2O$) to maintain 98 wt.% or to produce 93 wt.% acid. Removal of this reaction heat is a process requirement. Useful recovery of this reaction heat, however, is a process challenge. A key to improving both the thermal efficiency and reliability of the process is more corrosion resistant materials,

especially in the parts of the plant that handle the condensed acid[1,2].

Normal conditions encountered during manufacturing include 98-99 wt.% $H_2SO_4$ up to 120°C and 93 wt.% $H_2SO_4$ up to 70°C. The performance limit of the construction materials dictate the process temperature. Generally, stainless steel S31603 is specified for pump tanks, piping, heat exchangers and for internal components in drying and absorption towers. The limited resistance of S31603 to temperatures above ambient requires the application of anodic protection for acceptable performance. The principle of anodic protection is the formation and/or stabilization of protective surface films on film-forming metals and alloys by an externally impressed anodic current. In this case, anodic protection stabilizes a protective surface film on S31603 which would otherwise undergo a periodic breakdown resulting in increased corrosion[3,4,5].

A major materials related development in sulphuric acid production is the recent introduction of S30601, a silicon-stainless steel, to contain the hot condensed $H_2SO_4$ acid[6]. Corrosion data shows silicon-stainless steel has a marked improvement in the unprotected corrosion resistance over S31603 to typical process environments[7,8]. The economic attraction is the ability to use non-anodically protected stainless steel at elevated temperatures. A less reliable performance in acids weaker than 93 wt.%, however, limits successful retrofitting of anodically protected S31603 components[7].

Further improvements in corrosion resistance of the construction materials are required to meet the environmental and economic demands. To permit such improvement,

a better understanding of the nature of passivity that allows stainless steel to resist corrosion in concentrated $H_2SO_4$-$H_2O$ solutions is necessary. The material developments to date have been made without a fundamental understanding of the corrosion processes involved[4,5,8].

## 1.1 Research Objective

The objective of this study is to develop a better understanding of the reactivity and/or passivity of stainless steel in concentrated $H_2SO_4$-$H_2O$ solutions by establishing the anodic and cathodic reactions involved. In particular, to characterize the following:

1. The state of stainless steel passivity in concentrated $H_2SO_4$-$H_2O$ solutions.
2. The conditions under which stainless steel passivity is stable in concentrated $H_2SO_4$-$H_2O$.
3. The role played by the major alloying elements in establishing and maintaining stainless steel passivity in concentrated $H_2SO_4$-$H_2O$.

## 1.2 Research Scope

The investigation began with a critical review of the relevant literature pertaining to the corrosion of stainless steel in concentrated $H_2SO_4$-$H_2O$ solutions. The review provided a better idea of what to expect while investigating the reactivity and/or passivity of stainless steel and identified inconsistencies and shortcomings that require clarification through

further research.

The adopted experimental approach involved establishing, developing and testing a model that best explains the corrosion of stainless steels S43000 and S30403 in 93.5 wt.% $H_2SO_4$-$H_2O$ solutions. Techniques employed in this study include weight loss, electrochemical DC polarization and X-ray spectroscopy (XPS and XFR).

The experimental portion of the study began by comparing and contrasting the corrosion behaviour of S43000 and S30403 and their major alloying elements in 93.5 wt.% $H_2SO_4$ at 60°C. The purpose of such experiments is to test preconceived ideas regarding the state of passivity, the conditions in which it is stable and the role of the major alloying elements in determining that state. The attempt to establish a model describing the active-passive corrosion of S30403 identify two areas that required clarification through further research. Experiments subsequently conducted on the corrosion of nickel in 93.5 wt.% $H_2SO_4$ characterized its reactivity and elucidated its role in the active-passive corrosion of S30403. Exploring the anodic behaviour of stainless steel S43000 and its galvanic interaction with more noble materials in 93.5 wt.% $H_2SO_4$ defined the conditions necessary for galvanic passivation. Applying the galvanic-induced passivation model of the active-passive corrosion state to predict the corrosion dependence on $H_2SO_4$ concentration tested its validity.

### 1.3 Major Findings

Stainless steel S43000 and S30403 possess the ability to passivate at anodic potentials in 90-96.4 wt.% $H_2SO_4$ at all temperatures and electrode rotation rates studied between 25-80°C and 0-2000 rpm respectively. Passivity likely involves the formation of a chromium- enriched oxide film via a solid-state mechanism and not a sulphate film via a dissolution-precipitation mechanism or an insoluble sulphur layer. A content of about 17 wt.% is sufficient in conveying chromium's passive properties to an iron-based alloy. Without anodic polarization, the passive state essentially has no stability and a rapid passive to active transition ensues upon release of potential control.

Stainless steel S43000 corrodes in an active state under open-circuit conditions without showing any tendency to spontaneously passivate. The dominant cathodic process is the evolution of hydrogen gas. Anodic passivation is attained by applying a sufficient anodic current or by galvanically coupling with a more noble material with a sufficient cathode/anode surface area ratio. Anodic passivation of S43000 reduces the corrosion rate by at least a factor of 10, independent of the method employed.

The addition of nickel significantly improves the corrosion resistance. The corrosion rate of stainless steel S30403, assumed to be essentially S43000 alloyed with 8 wt.% nickel, is an order of magnitude lower than S43000. The improved resistance results from periodic passivation. A regular oscillatory potential consisting of a series of potential spikes characterizes the active-passive corrosion of nickel-stainless steel. Active state corrosion

occurs during the spikes, whereas passive state corrosion occurs during the period between the spikes.

The mechanism through which nickel-stainless steel spontaneously passivates is believed to be due in part to the unique reactivity of nickel in concentrated $H_2SO_4$-$H_2O$ solutions. The corrosion of nickel involves the formation and subsequent dissolution of a solid nickel sulphide (NiS) corrosion product. The electroactive nature of NiS is believed to establish a galvanic couple with the nickel metal which significantly polarizes the anodic reaction. No reduction in the anodic kinetics occurs as nickel does not passivate at the more positive potentials attained during the galvanic interaction.

The situation is quite different for stainless steel S43000. The electroactive nature of NiS, formed *in situ* on a nickel electrode, anodically passivates S43000 during galvanic coupling with a sufficient anode/cathode area ratio. The active-passive corrosion of nickel-stainless steel is believed to occur through a similar mechanism, a periodic formation of a galvanic couple between the stainless steel alloy and a solid NiS deposit.

From a technical point of view the results of the study better clarify the factors that influence the corrosion resistance of stainless steel to concentrated $H_2SO_4$-$H_2O$ solutions. A significantly improved resistance occurs in conditions where a passive state is stable. The factors that affect the stability of passivity include the alloyed nickel content, temperature, sample rotation velocity and acid concentration. Furthermore, the results provide insight into possible ways to improve the corrosion resistance such as altering the chemical composition

or making a galvanic couple with a more noble material.

From a scientific point of view the findings provide a better understanding of stainless steel passivity in strongly acidic, concentrated $H_2SO_4$-$H_2O$ solutions. The results suggest that passivity of stainless steel occurs with the formation of an oxide-type film in which chromium plays a major role. Spontaneous passivity of nickel-stainless steel involves a synergistic interaction between chromium and nickel. Inherent to the results of the study is a better understanding of the electrochemical properties of concentrated $H_2SO_4$-$H_2O$ solutions. Cathodic processes include a potential-dependent reduction of $H_2SO_4$ molecules to sulphur- containing species with a valence lower than six along with the hydrogen evolution reaction. The main reduction products change from sulphur dioxide ($SO_2$) to elemental sulphur (S) to hydrogen sulphide ($H_2S$) and hydrogen gas ($H_2$) as the overpotential of the cathodic reaction increases.

This dissertation contains seven chapters. Chapter 2 discusses the review of the relevant literature regarding the reactivity and/or passivity of stainless steel and its major alloying elements in concentrated $H_2SO_4$-$H_2O$ solutions and presents the associated set of inconsistencies and shortcomings. Chapter 3 describes the various techniques and procedures employed to meet the objective stated in Section 1.2. Chapters 4 through 6 present and discuss the experimental results in the following order: Chapter 4 contains the results of experiments conducted to compare and contrast the corrosion behaviour of S43000 and S30403 and their major alloying elements in 93.5 wt.% $H_2SO_4$ at 60°C, Chapter 5

contains the results of experiments conducted to characterize the corrosion of nickel in 93.5 wt.% $H_2SO_4$ as a function of temperature and stirring and Chapter 6 contains the results of experiments conducted to explore the galvanic passivation of S43000 by NiS in 93.5 wt.% $H_2SO_4$ as a means to model the active-passive corrosion of S30403. Chapter 7 summarizes the major contributions to knowledge generated by the study and identifies areas requiring further research.

# CHAPTER 2

## 2. LITERATURE REVIEW

The research programme adopted to meet the objectives defined in Section 1.1 began with a critical review of the literature. The system under investigation in this study is stainless steel S43000 and S30403 in 93.5 wt.% $H_2SO_4$. A review of the relevant literature provided a better idea of what to expect prior to and, thus, monitor during subsequent experiments and to identify those areas requiring further research. The review began by determining the current state of knowledge regarding the phenomenon of metallic passivity and of the relevant properties, with respect to corrosion, of $H_2SO_4$-$H_2O$ mixtures. This insight proved essential to understand the literature regarding the corrosion and electrochemical behaviour of stainless steel and its major alloying elements in this medium.

This chapter contains five major sections. The first two sections discuss the essential features of metallic passivity and the properties of concentrated $H_2SO_4$-$H_2O$ solutions respectively. The next two sections discuss the corrosion and electrochemical behaviour of stainless steel and its major alloying elements in concentrated $H_2SO_4$-$H_2O$ solutions respectively. The fifth section summarizes the insight gained, the shortcomings in the literature and those areas requiring further research to meet the objectives defined in Section 1.1.

## 2.1 Essential Features of Metallic Passivity

One of the more important and interesting methods for improving the corrosion resistance of metals and alloys involves the phenomenon of passivity. From a technical point of view, an understanding of the mechanism of passivity is essential because its breakdown or loss of stability is the principal reason for corrosion failures.

The rate of any thermodynamically probable electrochemical corrosion process depends on the degree of thermodynamic instability, the principal resistive factors being the anodic and cathodic polarization. When an electrochemical reaction is forced away from equilibrium by the passing of a current, the electrode potential changes. According to the generally accepted "mixed potential" theory[9,10], polarization of both the anodic and cathodic half cell reactions occurs during the corrosion of metals and alloys. Each must polarize to a common intermediate potential $E_{corr}$, the corrosion potential and a common current, $i_{corr}$ to

maintain charge conservation.

Several control conditions may be identified during corrosion[11] . Anodic control exists when the polarization occurs mostly for the anodic reaction and the corrosion current (rate) is sensitive to small changes in cathodic polarization. Cathodic control exists when the polarization occurs mostly for the cathodic reaction and the corrosion current is sensitive to small changes in the anodic polarization. Mixed control occurs when both the anodic and cathodic reactions are polarized to some degree.

For a corrosion process, the anodic reaction is a metal dissolution reaction, which proceeds according to the general form,

$$M = M^{n+} + ne^- \qquad [2.1]$$

where M is the metal atom of a metal or alloy, $M^{n+}$ is the cation with n valence , which is also the is the number of electrons produced. The cathodic reaction, which is required to consume electrons, depends partly on the environment and partly on the metal itself. The cathodic processes most commonly encountered may be summarized as follows:

1. Evolution of hydrogen gas ($H_2$) from acid [2.2], or alkaline solutions, [2.3],

$$2H^+ + 2e^- = H_2 \qquad [2.2]$$

$$2H_2O + 2e^- = H_2 + 2OH^- \qquad [2.3]$$

2. Reduction of dissolved oxygen in acid, [2.4], or alkaline solutions, [2.5],

$$O_2 + 4H^+ + 4e^- = 2H_2O \qquad [2.4]$$

$$O_2 + 2H_2O + 4e^- = 4OH^- \qquad [2.5]$$

3. Reduction of a dissolved oxidizer in a redox reaction,

$$Ox + \upsilon e^- = Rd^{\upsilon-} \qquad [2.6]$$

where Ox is the oxidized from and Rd is the reduced form.

In all cases of metallic passivity, a sharp increase in the inhibition of the anodic process, [2.1], is observed. Therefore, passivity may be defined as a state of improved corrosion resistance resulting from the inhibition of the anodic process of metal dissolution despite a marked thermodynamic tendency to react[12,13]. Metallic materials that fulfill this definition display a distinctive behaviour during anodic polarization, Figure 2.1[14,15], which is characteristic to a specific environment.

In the active state, polarizing the metal or alloy from its equilibrium potential enhances the dissolution reaction, [2.1], as the current increases sharply with potential. At a certain potential $E_p$, the passivation potential, the current decreases rapidly to much lower values. The sharp inhibition of the anodic process is the onset of passivity. A state of passivity forms and is maintained at potentials above $E_p$. The current $i_p$, the passive current, remains relatively independent of potential. At higher potentials, the current may start to increase sharply due either to the breakdown of passivity or to the onset of an additional

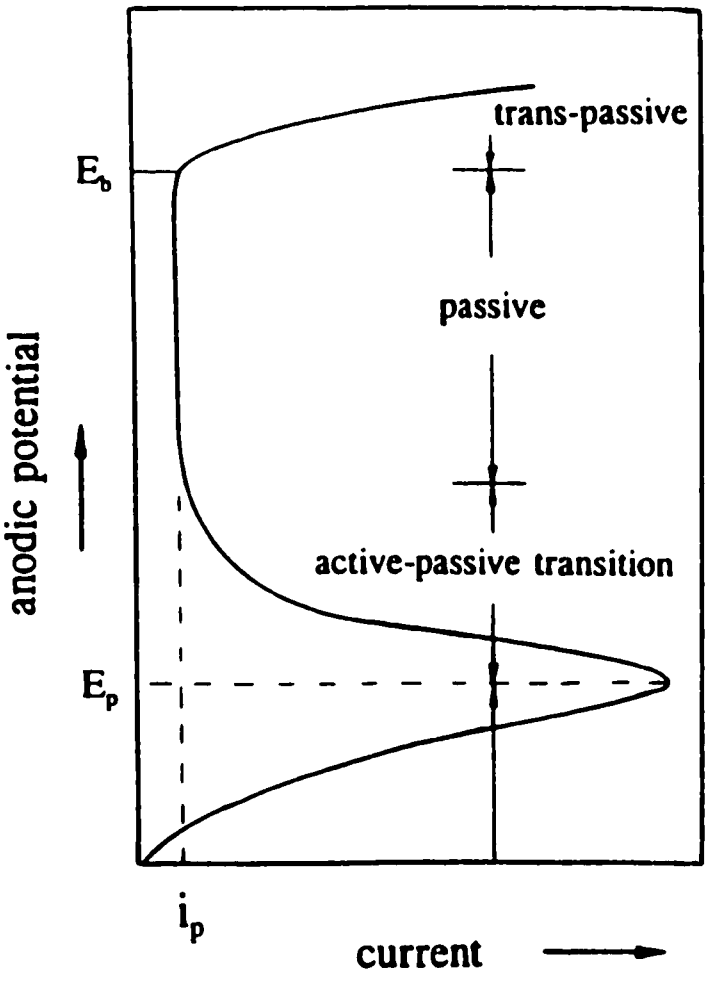


Figure 2.1. Schematic of active-passive polarization behaviour[14,15].

anodic process.

Many passivity theories have been presented in the literature, all of which fall into either the adsorption theory or the three-dimensional oxide theory. In the adsorption theory[16,17,18,19,20], the essential cause of passivity is the formation of a monolayer of adsorbed oxygen. The inhibition of the anodic process is achieved through the formation of chemical bonds which satisfy the surface affinities of the metal without metal atoms leaving their lattice site. In the three-dimensional oxide theory[21,22,23,24,25], the dissolution of the metal produces a situation in which the solubility of a salt or hydroxide is exceeded and a film (10-100 Å in thickness) forms. The inhibition of the anodic process is achieved through a change in film property such as conductivity. Sato[26] presented a generalized theory in which the passivity of transition metals is attributed to a thin oxide film which may involve the adsorption of oxygen or hydroxyl ($OH^-$) ions in the initial stages. The passivity of metals is generally accepted to proceed in aqueous systems with the participation of $H_2O$ molecules as sources of oxygen for oxide formation[26]. A decrease in the $H_2O$ activity has been found to hinder the passivation process[27,28,29].

Whether or not spontaneous passivation occurs during corrosion depends on the oxidizing power of the environment and the extent of polarization of both the anodic and cathodic partial processes. The polarization behaviour for possible corrosion conditions is schematically illustrated in Figure 2.2[66]. The most desirable condition from a technical point is when $E_{corr}$ is established in the region of passivity as the dissolution rate (current) is

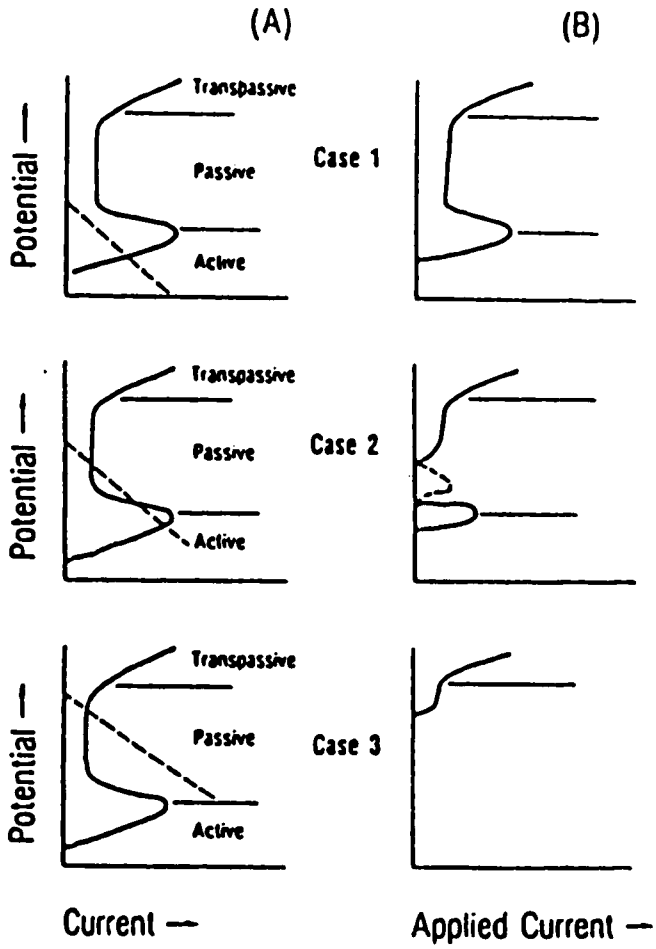


Figure 2.2. Schematic polarization behaviour for possible corrosion conditions. (A) theoretical, (B) experimentally measured[66].

minimized, Case 3. In this case, the equilibrium potential of the cathodic half cell reaction is more noble than the passivation potential of the anodic half cell reaction and the cathodic current is greater than the critical passivating anodic current. An unique situation arises when the cathodic half cell reaction intersects the anodic half cell reaction in three different places, Case 2. Here, the cathodic current is less than the critical anodic current required for passivity. Consequently, the system may exist in the either the active or passive state. The middle intersection point is not a stable potential state and is never observed when passivity is established by the dissolved oxidizer.

## 2.2 Properties of $H_2SO_4$-$H_2O$ Mixtures

Corrosion of metallic materials is sensitive to the properties of the medium. The properties of $H_2SO_4$ as a solvent system have been extensively studied and discussed in several reviews[30,31,32]. The following discussion provides a general introduction to those physical, chemical and electrochemical properties which affect corrosion.

### 2.2.1 Physical Properties

Pure liquid $H_2SO_4$ is readily obtained. The liquid has a layer-type structure in which each $H_2SO_4$ is hydrogen bonded to four others[33]. Table 2.1 compares several physical constants of liquid $H_2SO_4$ with those of liquid $H_2O$. The high viscosity, boiling point and density of $H_2SO_4$ indicate its highly associated nature. The relatively high dielectric

constants of both liquids reflect their ability to act as solvent systems.

Table 2.1. Selected Physical Constants of Sulphuric Acid[31] and Water[34]

| Property | $H_2SO_4$ | | $H_2O$ | |
|---|---|---|---|---|
| freezing point | 10.4°C | | 0°C | |
| boiling point | 290-317°C | | 100°C | |
| viscosity | 24.54 cP | 25°C | 1.0 cP | 25°C |
| specific gravity | 1.8292 | 25°C | 1.0 | 25°C |
| dielectric constant | 100 | 25°C | 82 | 25°C |
| specific conductivity | $1.044\times10^{-2}\ \Omega^{-1}cm^{-1}$ | 25°C | $5.5\times10^{-8}\ \Omega^{-1}cm^{-1}$ | 25°C |

In metallic corroding systems the conductivity of the electrolyte plays an important role since current flows in the electrolyte adjacent to the metal surface and electrons flow through the metal to complete the circuit. The conductivity of pure $H_2SO_4$ is five orders of magnitude higher than pure $H_2O$, a striking result considering both are molecular liquids. The conductivity of $H_2SO_4$-$H_2O$ mixtures depends on the concentration of $H_2SO_4$[35]. In the range from 82 to 95 wt.% $H_2SO_4$, the conductivity is relatively constant (1.25 $ohm^{-1}cm^{-1}$ at 18°C) and decreases with higher $H_2SO_4$ concentration. The conductivity increases with temperature for all concentrations from 0 to 100 wt.% $H_2SO_4$[36]. Therefore, metallic corrosion would not appear to be limited by electrolyte conductivity in concentrated $H_2SO_4$-$H_2O$ solutions.

A second physical property of the medium that affects corrosion is viscosity. Corrosion invariably involves the transport of ions and molecules to and from the metal-solution interface. Transport processes such as diffusion and convection rely on the mobility of ions and molecules in the solution. The lower the viscosity of the solution, the higher the mobility. The viscosity of pure liquid $H_2SO_4$ is significantly higher than that for pure liquid $H_2O$ (Table 2.1). In $H_2SO_4$-$H_2O$ mixtures, the viscosity decreases with a decrease in the concentration of $H_2SO_4$ and temperature[37]. For example, the viscosity decreases from 25.4 to ~18 cP as the $H_2SO_4$ concentration decreases from 100 to 90 wt.% at 25°C. An increase in temperature from 25 to 75°C decreases the viscosity of 90 wt.% $H_2SO_4$ from ~18 to ~5 cP. The relatively high viscosity and its sensitivity to concentration and temperature indicate it may play a role in the corrosion of metallic materials to concentrated $H_2SO_4$-$H_2O$ solutions.

### 2.2.2 Chemical Structure

Gillespie and Robinsen[32] summarized the extensive self-dissociation processes that occur in pure $H_2SO_4$. The pure liquid is amphoteric which is shown by the appreciable autoprotolysis,

$$2H_2SO_4 = H_3SO_4^+ + HSO_4^- \qquad [2.7]$$

In addition to the autoprotolysis, $H_2SO_4$ is self-dissociated in other ways which are a consequence of the primary dissociation into $H_2O$ and $SO_3$ according to,

$$H_2SO_4 = H_2O + SO_3 \quad [2.8]$$

The water produced from this dissociation is ionized according to,

$$H_2O + H_2SO_4 = H_3O^+ + HSO_4^- \quad [2.9]$$

whereas the $SO_3$ forms disulphuric acid,

$$SO_3 + H_2SO_4 = H_2S_2O_7 \quad [2.10]$$

which is partially ionized according to,

$$H_2S_2O_7 + H_2SO_4 = H_3SO_4^+ + HS_2O_7^- \quad [2.11]$$

Thus, since the $H_3SO_4^+$ and $HSO_4^-$ ions are in equilibrium as a result of [2.7] it follows that the $H_3O^+$ and $HS_2O_7^-$ ions must also be in equilibrium, [2.12].

$$2H_2SO_4 = H_3O^+ + HS_2O_7^- \quad [2.12]$$

The complete self-dissociation of $H_2SO_4$ may be described by equations [2.7], [2.9], [2.11] and [2.12]. Values of the corresponding dissociation constant for these reactions at 25°C are given in Table 2.2. The total molar concentration of ionic species is 0.0424 M at 25°C which is in striking contrast with the value of $2\times10^{-7}$ M for pure liquid $H_2O$.

Table 2.2. Equilibrium Constants for the Self-Dissociation of $H_2SO_4$ at 25°C[32]

| Equation | K |
|---|---|
| [2.2] $K = [H_3SO_4^+][HSO_4^-]$ | $2.7\times10^{-4}$ |
| [2.7] $K = [H_3O^+][HS_2O_7^-]$ | $5.1\times10^{-5}$ |
| [2.6] $K = [H_3SO_4^+][HS_2O_7^-]/[H_2S_2O_7]$ | $1.4\times10^{-2}$ |
| [2.4] $K = [H_3O^+][HSO_4^-]$ | 1 |

Gable *et al.*[38] found $H_2SO_4$ to be completely miscible with $H_2O$ in all proportions. Young *et al.*[39] and Zarakhani and Vinnik[40] characterized the chemical composition of $H_2SO_4$-$H_2O$ mixtures using Raman spectroscopy, the results of which Liler[41] summarized as shown in Figure 2.3. In dilute solutions, the medium consists of both $HSO_4^-$ and $SO_4^{2-}$ ions, which is consistent with the well known dissociation of $H_2SO_4$ in $H_2O$,

$$H_2SO_4 + H_2O = HSO_4^- + H_3O^+ \qquad [2.13]$$

$$HSO_4^- + H_2O = SO_4^{2-} + H_3O^+ \qquad [2.14]$$

The dissociation constant at 25°C is >>1 for [2.13] and $1.2\times10^{-3}$ for [2.14][42]. In more concentrated solutions, the medium consists of $H_2SO_4$ molecules with $H_3O^+$ and $HSO_4^-$ ions. According to Högfeldt[43], the proton ($H^+$) forms the various hydrated complexes shown in Figure 2.4.

The chemical composition may be divided into three structural ranges:

1. 0-8 M $H_2SO_4$ - In this range $H_2O$ molecules dominate the medium.

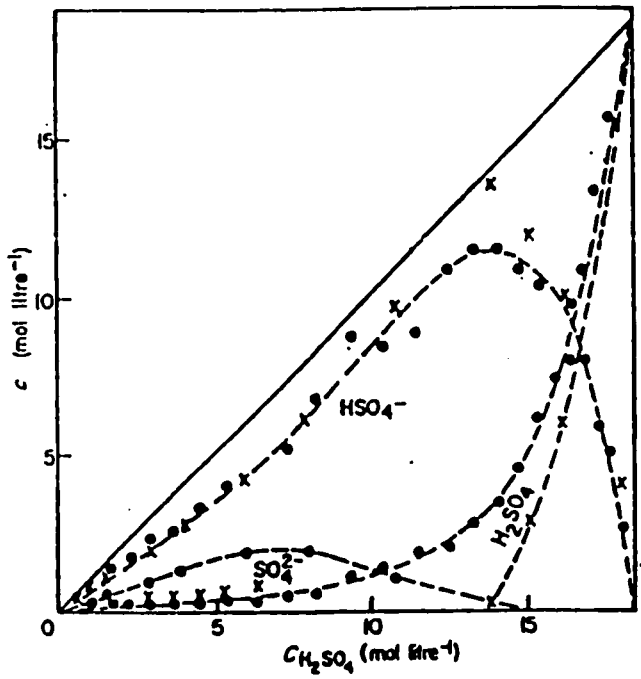


Figure 2.3. Concentrations of species in $H_2SO_4$-$H_2O$ solutions from Raman spectra[41], (x) Young *et al.*[39]; (•) Zarakhani and Vinnik[40].

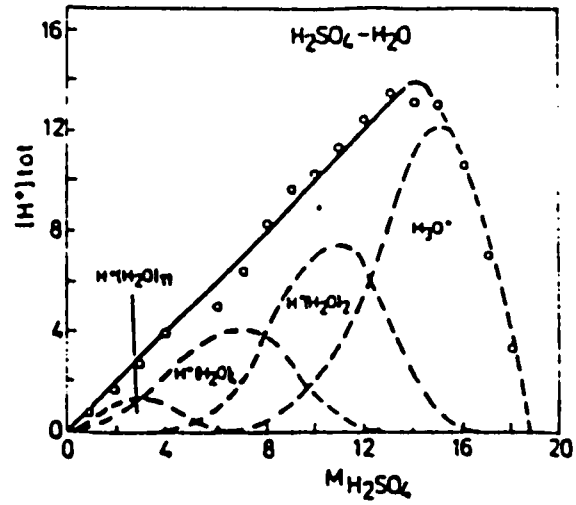


Figure 2.4. Concentration and structure of hydrated protons in $H_2SO_4$-$H_2O$ solutions[43].

2. 8-14 M $H_2SO_4$ - In this range $HSO_4^-$ ions dominate the medium and the $H_2O$ molecules are bound in the proton complex $H^+(H_2O)_n$ where $1<n<4$.
3. 14-18 M $H_2SO_4$ - In this range $H_2SO_4$ molecules appear and the $H_2O$ molecules are bound in the proton complex $H_3O^+$.

The $H_2SO_4$-$H_2O$ medium of interest to this study (14-18 M) is essentially a solution consisting of molecular $H_2SO_4$ with $H_3O^+$ and $HSO_4^-$ ions.

### 2.2.3 Solution Acidity

An important chemical property affecting the corrosion of metals is the solution acidity, that is, the proton activity. The proton activity affects the thermodynamic stability of the metal and its corrosion products along with the corrosion rate. The monograph by Pourbaix[44] summarizes the influence of the proton activity on the thermodynamic stability of metals in $H_2O$ in the form of potential-pH (Pourbaix) diagrams. The influence of the proton activity on the corrosion rate is linked with the fact that hydrogen evolution is one of the more common reduction reactions in corrosion.

The acidity of a mixture can be describe by an acidity function, which is based on the quantitative response of some probe molecule to the proton-donating ability of the acidic medium. Although pH is an acidity function, it is of limited applicability concentrated $H_2SO_4$-$H_2O$ solutions, being a measure of the ability of dissolved $H_2SO_4$ to transfer a proton

to bulk water. The Hammet acidity function is a widely used and familiar measure of acidity. The function is defined as,

$$pK_{BH^+} - \log_{10}\frac{[B]}{[BH^+]} = -\log_{10} a_{H^+} - \log_{10}\frac{\gamma_B}{\gamma_{BH^+}} \equiv H_o \qquad [2.15]$$

where [B] is the concentration of the weak base nitroaniline indicator B, [$BH^+$] is the concentration of the protonated weak base nitroaniline indicator $HB^+$, $pK_{BH^+}$ the negative logarithm of the weak base dissociation constant $K_{BH^+}$, $a_{H^+}$ is the activity of the proton and $\gamma_B$ and $\gamma_{BH^+}$ are the activity coefficients of B and $HB^+$ respectively. The measured Hammet acidity function of $H_2SO_4$-$H_2O$ solutions shows the acidity has a monotonic increase as the concentration of $H_2SO_4$ increases up to 100 wt.%[45,46].

### 2.2.4 Electrochemical Properties

Evans and Hart[47] studied the corrosion behaviour of a nickel-silicon alloy in boiling 10-96 wt.% $H_2SO_4$-$H_2O$ solutions and found the cathodic process depended on the $H_2SO_4$ concentration. The dominant cathodic process in dilute solutions (10-53 wt.%) involved the formation of hydrogen ($H_2$), whereas in intermediate solutions (55-75 wt.%) it involved the formation of elemental sulphur (S) and hydrogen sulphide ($H_2S$). In concentrated solutions (75-96 wt.%), the dominant cathodic process was postulated to involve the formation of sulphur dioxide ($SO_2$).

Sridhar[48] and Banas and Stypula[97] measured the redox potential of $H_2SO_4$-$H_2O$ solutions on a platinized platinum inert electrode. Both found a significant change in the linear dependence of the redox potential on acidity ($H_2SO_4$ concentration), Figure 2.5. In both studies, the measured redox potential dependence on acidity (pH, $H_0$) in solutions less than about 8 M $H_2SO_4$ coincided with the theoretical acidity dependence of the hydrogen evolution reaction. The more sensitive acidity dependence in solutions greater than 8 M $H_2SO_4$ was attributed to the reduction of $H_2SO_4$ molecules and/or $HSO_4^-$ ions to sulphur-containing compounds with a valence lower than six[97]. The measured value of the slope ($\partial E/\partial H_0$) correlated best with the reduction of $HSO_4^-$ ions to $SO_2$ according to the following:[97]

$$HSO_4^- + 3H^+ + 2e^- = SO_2 + 2H_2O \qquad [2.16]$$

The electrolysis of concentrated $H_2SO_4$-$H_2O$ solutions has been studied in some detail. Hoffmann[49] studied the electrolysis of 98.5 wt.% $H_2SO_4$ using platinum electrodes at temperatures between 50-280°C. Various products such as $H_2S$, sulphur and $SO_2$ were found to form at the cathode. At high temperatures (>200°C) $SO_2$ was practically the only substance formed during cathodic electrolysis. Beck[50] studied the cathodic electrolysis of 85-100 wt.% $H_2SO_4$-$H_2O$ solutions as a function of electrode material, temperature and $H_2O$ concentration. The marked increase in current, signifying a cathodic reaction, occurred at more positive potentials in solutions greater than 90 wt.% $H_2SO_4$, Figure 2.6. It was concluded that $H_3O^+$ ions were reduced to $H_2$ in 85-90 wt.% $H_2SO_4$-$H_2O$ solutions, whereas

(A)

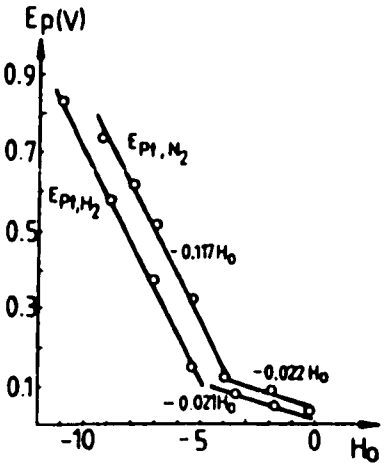


(B)

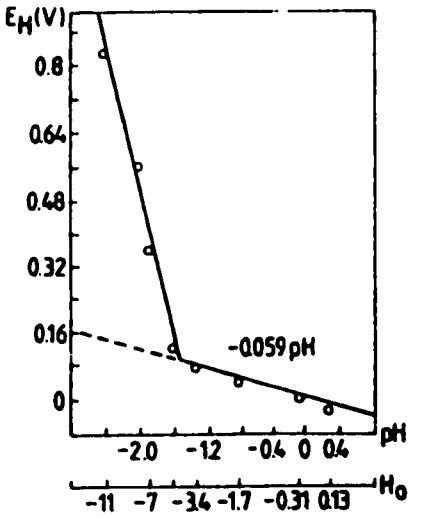


Figure 2.5. Redox potential of $H_2SO_4$-$H_2O$ solutions at 25°C. (A) Banas and Stypula[97], (B) Sridhar[48].

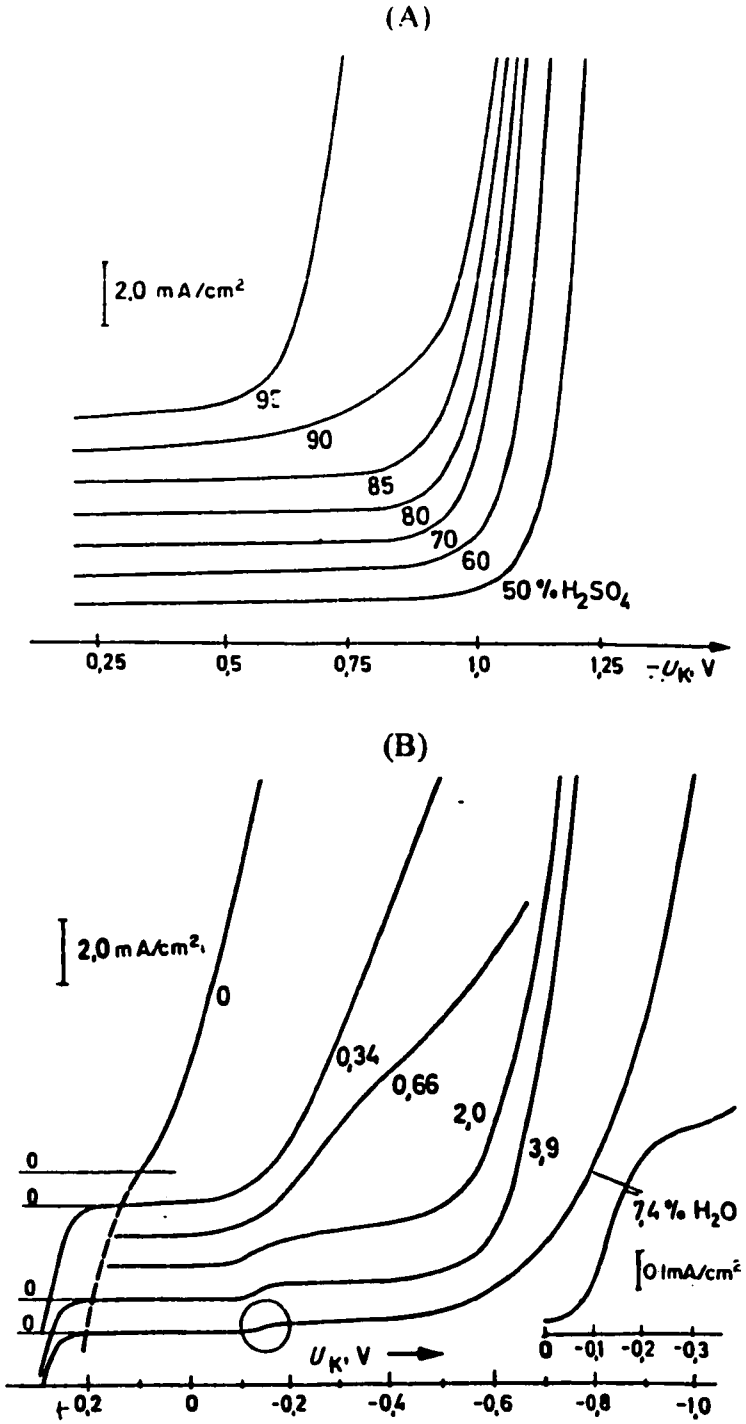


Figure 2.6. Cathodic polarization of $H_2SO_4$-$H_2O$ solutions on a mercury electrode[50]. (A) 50-96 wt.% $H_2SO_4$, (B) 92.6-100 wt.% $H_2SO_4$.

$H_2SO_4$ molecules were reduced to $H_2S$, sulphur and $SO_2$ in 90-100 wt.% solutions.

Arvía *et al.*[51,52,53,54] studied the electrolysis of fuming $H_2SO_4$ (100 wt.% $H_2SO_4$ with dissolved $SO_3$) with 5-28 wt.% $SO_3$ on a platinum electrode. Various cathodic reaction products were observed as the overpotential was increased. At low overpotentials (0-0.5 V), $SO_2$ was the main reduction product, whereas at higher overpotentials (>0.5 V) the reduction reaction involved the formation of $H_2$, $S_2O_3$ and sulphur. The formation of the reduced sulphur-containing species was attributed to the reduction of solvated $SO_3$ ($H_2S_2O_7$), whereas, $H_2$ formation was attributed to the reduction of solvated $H^+$ ($H_3SO_4^+$).

## 2.3 Corrosion of Stainless Steel in Concentrated $H_2SO_4$-$H_2O$ Solutions

Kiefer and Renshaw[55] and Phelps and Vreeland[56] studied the corrosion of various grades of austenitic stainless steel in 0-96 wt.% $H_2SO_4$-$H_2O$ solutions at 25-50°C. For a given temperature, the corrosion rate initially increased as the $H_2SO_4$ concentration increased before reaching a maximum in the 40-60 wt.% range; thereafter it decreased as the concentration approached 100 wt.%. Despite the decreased corrosion rate in more concentrated solutions, a high level of corrosion resistance (<5 mpy) occurred only at ambient temperatures. Spontaneous passivation during corrosion was concluded to occur in all $H_2SO_4$-$H_2O$ concentrations at ambient temperatures. Electrochemical measurements were not performed in either study to verify this conclusion.

The ability of stainless steel to anodically passivate in concentrated and dilute $H_2SO_4$-$H_2O$ solutions is well known. Edeleanu[57], while gathering support for anodic protection, found the anodic polarization of stainless steel consisted of an active to passive transition at practically all concentrations at temperatures up to the boiling point. It was through such studies on anodic protection that the complex corrosion behaviour of stainless steel in concentrated $H_2SO_4$-$H_2O$ solutions became known.

Kain and Morris[3] noted that difficulties could arise when determining the optimum potential region for anodic protection of S31603 in 93-98 wt.% $H_2SO_4$-$H_2O$ solutions because of the instability of the corrosion potential. For example, the corrosion potential in 93.5 wt.% $H_2SO_4$ oscillated in time, consisting of a series of spikes with an amplitude of ~0.6 V and a frequency that increased with an increase in temperature. By comparing the potential extremities with the corresponding anodic polarization curve, Kain and Morris concluded that S31603 dissolved in an *active-passive* state in 93-98 wt.% $H_2SO_4$. It is emphasised here that spontaneous oscillatory behaviour involving an electrochemical system is unusual[58,59,60,61]. Most electrochemical oscillatory phenomena arise during applied anodic or cathodic polarization[62,63,64].

In a more detailed study, Chang[4] provided evidence supporting an active-passive corrosion state. Weight loss measurements of a S31603 electrode in 98 wt.% $H_2SO_4$ suggest that the majority of weight loss occurs during the potential spikes where the alloy dissolves in an active state. The weight loss per cycle was found to be sensitive to stirring and the acid

concentration, but not temperature. Potential oscillations, characteristic to the active-passive corrosion state, occurred in all concentrations studied between 80-100 wt.% $H_2SO_4$.

Matsuhashi *et al.*[65] provided evidence that alloyed nickel has a strong influence on the active-passive corrosion of stainless steel in concentrated $H_2SO_4$-$H_2O$ solutions. Weight loss measurements show that alloyed nickel (4-40 wt.%) significantly lowers the corrosion rate of a Fe-18Cr-2.5Mo base stainless steel in 97 wt.% $H_2SO_4$ regardless of temperature between 40-80°C. The lower corrosion rate is attributed to the state in which corrosion occurs. The nickel-containing alloys corroded in an cyclic active-passive state, whereas the base alloy corroded in a stable active state. In the cyclic active-passive corrosion state, increasing the nickel content of the alloys beyond 8 wt.% increased the corrosion rate. Corrosion potential measurements suggest this increase in corrosion rate results from the increase in the cycle frequency. They propose that the ability of nickel-stainless steel to spontaneously passivate is related to a reduced overpotential for the reduction of $H_2SO_4$ molecules on the nickel-containing surfaces. Here, the reduction of $H_2SO_4$ molecules provides the necessary driving force and current required to anodically passivate the alloy.

Several mechanistic models have been proposed to explain the cyclic active-passive corrosion of stainless steel in concentrated $H_2SO_4$-$H_2O$ solutions. The proposed models involve a mild oxidizing cathodic reaction, the periodic formation and dissolution of a protective sulphate film and the periodic formation and dissolution of a protective sulphur barrier layer.

Tong[66] and Renner[67] believe that mechanism through which active-passive corrosion occurs involves a mild oxidizing cathodic reaction that intersects the anodic polarization curve in the active-passive transition region (Figure 2.2, Case 2). According to Tong[66], the cathodic reaction is under concentration polarization and is the unspecified reduction of $SO_4^{2-}$ ions. According to Renner[67], the cathodic reaction is the reduction of $H_2SO_4$ molecules to $SO_2$, which proceeds as,

$$H_2SO_4 + 2e^- = SO_4^- + SO_2 + 2H_2O \qquad [2.17]$$

Although the oscillatory potential behaviour is attributed to the multiple intersecting polarization curves, no evidence of a cathodic loop that supports this conclusion was found during anodic polarization measurements in either study.

Chang[4] and Matsuhashi *et al.*[5] believe that the mechanism involves a periodic formation and dissolution of a protective sulphate film. Figure 2.7 illustrates the Matsuhashi *et al.* model. According to this model, metal dissolution occurring in the active state leads to the formation of a supersaturated solution adjacent to the surface, which then causes the precipitation of a metal sulphate film. Once the film forms, a significant anodic polarization occurs due to the inhibiting nature of the film which then shift the potential to a more electropositive value. The shift in the potential then favours the cathodic reduction of $H_2SO_4$ to sulphur according to,

$$5H_2SO_4 + 2H^+ + 6e^- = 4HSO_4^- + S + 4H_2O \qquad [2.18]$$

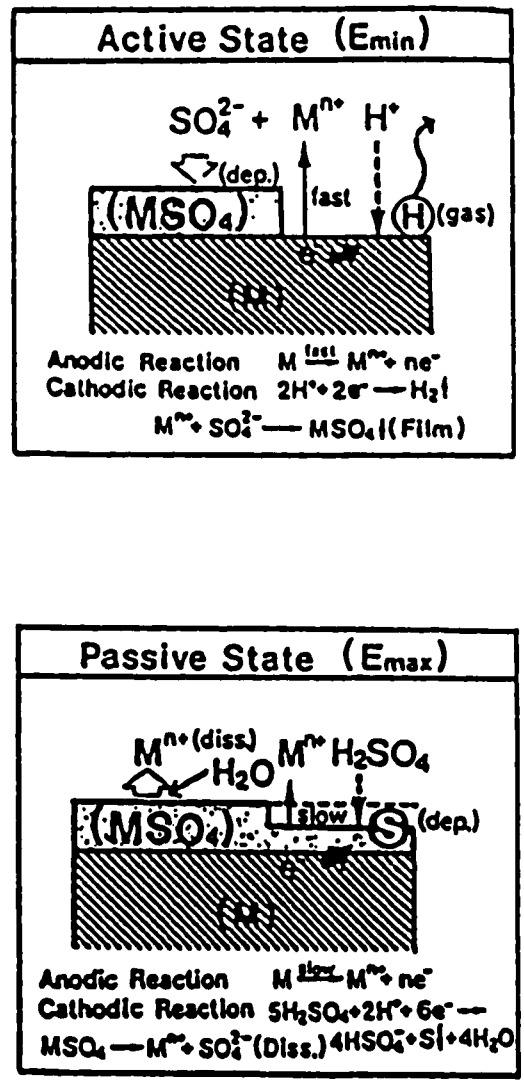


Figure 2.7. Matsuhashi *et al.*[5] model illustrating a stainless steel corrosion mechanism in concentrated $H_2SO_4$-$H_2O$ solutions.

over the hydrogen evolution reaction. The water produced as reaction product then dissolves the sulphate film, ultimately returning the alloy to its active state. The process is believed to occur repeatedly as a result of the nature of the cyclic reactions.

The idea that stainless steel passivity in concentrated $H_2SO_4$-$H_2O$ solutions involves the formation of a protective sulphate film is consistent with an earlier study performed by Kuron *et al.*[68]. Auger electron spectroscopy (AES) found enrichment of sulphur and oxygen at the surface region of UNS S31600 anodically polarized at +1.35 $V_{SHE}$ in 98 wt.% $H_2SO_4$ at 140°C. X-ray diffraction (XRD) showed the anodic passive layer consisted of $(Fe,Cr,Ni)[HSO_4]_2.4H_2O$. Renner and Maughan[69] studied the anodic polarization of N08028 through to +1.65 $V_{SHE}$ in 92.5 wt.% $H_2SO_4$ at 100°C and found both a crystalline and globular surface deposit. Energy dispersive X-ray (EDX) analysis found the crystalline deposit consisted primarily of iron and sulphur with traces of nickel and chromium. The globular deposit consisted only of sulphur. They concluded that anodic passivity of involves the formation of a $Fe(HSO_4)_2$ surface film.

Kuzub *et al.*[70] believe that the mechanism involves the periodic formation and dissolution of a protective sulphur barrier layer. According to this model, corrosion in the active state leads to the formation of a protective barrier sulphur layer. Here, sulphur forms as a product of the cathodic reaction involving the reduction of $H_2SO_4$ molecules. Once formed, the sulphur barrier layer then dissolves slowly according to the following reaction with $H_2SO_4$ molecules:

$$S + 2H_2SO_4 = 3SO_2 + 2H_2O \quad [2.19]$$

The composition of the anodic passive layer formed on stainless steel alloys in concentrated $H_2SO_4$-$H_2O$ solutions has been found to be quite different from that formed in dilute solutions. The chemical composition of the passive layer formed on stainless steel under various passivation conditions in dilute $H_2SO_4$-$H_2O$ solutions has been studied extensively by surface analytical techniques such as XPS and AES[71,72,73,74,75,76,77,78]. The majority of investigations utilized the solute action of $H_2SO_4$ in $H_2O$ to study the effect of aqueous acidity (pH) on passivity. The passive layer has been found to be significantly enriched in chromium, most likely in a hydrated oxy-hydroxide form, and depleted in nickel.

## 2.4 Behaviour of Major Alloying Elements

According to the literature, the presence of about 17 wt.% chromium, as found in S30400 and S31600, may be incapable of promoting the formation of a protective oxy-hydroxide passive film in 80-100 wt.% $H_2SO_4$. Banas *et al.*[79,80,81] found that the passivity of transition metals, including chromium, occurs in anhydrous $H_2SO_4$-$CH_3OH$ solutions and involves the formation of an oxide-type film. The undissociated $H_2SO_4$ molecules are believed to be the source of oxygen for oxide formation in such solutions. An anodic inhibition mechanism involving the formation of a protective sulphate is plausible, however, since a similar mechanism occurs for iron in concentrated $H_2SO_4$-$H_2O$ solutions; iron being the major component in stainless steel. Since stainless steel is composed of iron, chromium

and nickel, the corrosion and anodic polarization behaviour of these metals in concentrated $H_2SO_4$-$H_2O$ solutions are of particular interest to this study.

### 2.4.1 Behaviour of Iron

Hines and Williamson[82,83] and Gilli and Zucchi[84] studied the anodic polarization behaviour of iron in 5-18 M $H_2SO_4$ and found that a sulphation stage, involving the formation of a sulphate layer, always preceded a passivation stage. In the sulphation stage (low overpotentials), the formation of a hydrated ferrous sulphate corrosion product film governs the anodic dissolution[84]. In the passivation stage (high overpotentials), a passivation phenomenon occurs that is believed to involve the formation of an oxide-type film with the oxidation of ferrous sulphate to ferric sulphate playing an initiating role. X-ray diffraction (XRD) measurements showed that the composition of the iron sulphate films formed at various potentials depends on the $H_2SO_4$ concentration[84]. The adherent $FeSO_4 \cdot 7H_2O$ film formed in 14-18 M $H_2SO_4$ was more effective in resisting anodic dissolution than the $FeSO_4 \cdot H_2O$ film formed in 7.5-14 M $H_2SO_4$.

Mazurkiewicz[85] explored the surface composition of iron in the passivation stage in stagnant 1-18.8 M $H_2SO_4$-$H_2O$ solutions in an attempt to better understand the effect of electrolyte structure on passivity. X-ray photoelectron spectroscopy (XPS) analysis showed that in the passivation stage the metal was covered with a hydrated oxy-hydroxide film. The thickness and the degree of hydration of the film varied with the $H_2SO_4$ concentration.

Sulphur-containing compounds found in the layers formed in 10-18.8 M are believed to be sulphate ($SO_4^{2-}$) and its corresponding reduction products. It was concluded that the passivity of iron involves the formation of an oxide-type film via a solid state reaction with $H_2O$ molecules in dilute solutions (<10 M) and with $H_2SO_4$ molecules and/or $HSO_4^-$ ions in concentrated solutions (>10 M).

The corrosion of iron in 70-100 wt.% $H_2SO_4$-$H_2O$ solutions has been studied extensively[86,87,88,89,90] since iron has been widely used as a construction material in systems handling the acid. Consequently, the corrosion mechanism is well understood. Ellison and Schmeal[87] found the rate controlling process in the steady state corrosion of iron in 60-96 wt.% $H_2SO_4$ was the dissolution and diffusion of ferrous sulphate into the bulk solution from the saturated solution at the film/acid interface,

$$Fe + H^+ + HSO_4^- + 7H_2O = FeSO_4 \cdot 7H_2O + 2H_2 \qquad [2.20]$$

$$FeSO_4 \cdot 7H_2O + H^+ = Fe^{2+} + HSO_4^- + 7H_2O \qquad [2.21]$$

A steady state film thickness is maintained when the rate of metal oxidation and ion diffusion through the film balances the rate of ion diffusion into the bulk solution. A diffusion layer model was successfully applied by Pohlman and Andersen[90] to predict and explain the corrosion rate as a function of temperature, $H_2SO_4$ concentration, acid flow rate and selected impurities.

### 2.4.2 Behaviour of Nickel

Epelboin and Keddam[91] studied the anodic polarization of nickel in $H_2SO_4$-$H_2O$ solutions up to 12 M $H_2SO_4$ in an attempt to determine the nature of the products that reduced the limiting anodic current density during the active to passive transition. In concentrations exceeding 4M, a crystalline product appeared near the active peak and disappeared in the region of passivity. Observations made with an optical microscope suggested the film was $\beta$-$NiSO_4 \cdot 6H_2O$.

Ebersbach *et al.*[92] studied the anodic polarization of nickel in 15 M $H_2SO_4$-$H_2O$ and found that a formation of a salt layer impeded the anodic current to a considerable extent. The passivation current decreased with increasing temperature, contrary to what happened in dilute acid. A different passivation mechanism was believed to occur in 15 M $H_2SO_4$. Due to the small $H_2O$ content and the possibility of $SO_4^{2-}$ replacing $H_2O$ at the metal surface, the protective layer was believed to consist of anhydrous $NiSO_4$. Gilli *et al.*[93]. provided further evidence that a different passivation mechanism existed for nickel in concentrated $H_2SO_4$-$H_2O$ solutions. Passivity disappeared as the $H_2SO_4$ concentration increased from 1 to 10 M and then was restored with a further increase to 18 M. The passive current density reached a maximum at 10 M (30 $mA/cm^2$) and then decreased as the $H_2SO_4$ concentration was increased to 18 M (~ 0.1 $mA/cm^2$). XRD analysis of the crystalline phase formed during polarization in 10-18 M $H_2SO_4$ showed the film most likely was $\beta$-$NiSO_4 \cdot 6H_2O$, the formation of which was due to the decreased nickel sulphate solubility in the more

concentrated solutions. The improved inhibition of the salt film in the more concentrated solutions was believed to be due to the film becoming more compact and less conductive. Turner *et al.*[94] reported a similar anodic polarization of nickel in 1-18.8 M $H_2SO_4$ while attempting to elucidate some of the problems associated the anodic dissolution of nickel and its passivation.

Mazurkiewicz[95] found that an anodic passive oxide film formed on anodically polarized amorphous $Ni_{83}B_{17}$ binary alloy in concentrated $H_2SO_4$-$H_2O$ solutions. XPS analysis revealed the anodic film formed in 13.5 M $H_2SO_4$ at +1.00 $V_{SCE}$ consisted of nickel ($Ni^{2+}$) oxy-hydroxide and sulphate. The presence of sulphate was attributed to its low solubility in $H_2SO_4$ at concentrations exceeding 10 M. The anodic film formed in 18 M $H_2SO_4$ at +1.00 $V_{SCE}$ consisted of a thinner nickel ($Ni^{2+}$) oxy-hydroxide film which contained a smaller sulphate component. The formation of an oxide-type film on anodically polarized $Ni_{83}B_{17}$ was believed to involve the reduction of $H_2SO_4$ molecules to $SO_2$.

### 2.4.3 Behaviour of Chromium

Stypula *et al.*[96,97,98,99] studied the anodic polarization of chromium in 1-18 M $H_2SO_4$ in an attempt to better understand the effect of electrolyte structure on the passivation process. An active to passive transition occurred in all $H_2SO_4$-$H_2O$ solutions studied. A marked decrease in the steady state passive current occurred as the $H_2SO_4$ concentration increased despite the decrease in water activity. The passivation potential was found to have

a linear dependence on the $H_2SO_4$ concentration and acidity in 14-18 M solutions. Furthermore, a significant quantity of dissolved $SO_2$ was measured in solutions greater than 8 M $H_2SO_4$. It was concluded that in 14-18 M solutions, the passivation process involved the reduction of undissociated $H_2SO_4$.

XPS analysis of the anodic layer formed in 1, 8 and 18 M $H_2SO_4$ at +0.8 $V_{SCE}$ showed the presence of a chromium-rich oxide-type film which is independent of acid concentration[96,97,98]. The major difference between the layers formed in dilute and concentrated acids was the sulphur content and the extent of hydration. In 14-18 M, the passive film essentially consisted of chromium ($Cr^{3+}$) oxy-hydroxide with no $H_2O$ but with sulphur species in the $S^0$ and $S^{2-}$ valence state. The presence of sulphur compounds of lower valence states in the film was believed to be due to the reduction of the $H_2SO_4$ molecules required in the passivation process. The anodic passivation of chromium in 14-18 M $H_2SO_4$ was proposed to occur by the following solid state reaction mechanism[97,98].

$$Cr + H_2SO_4 = Cr(HSO_4)_{ad} + H^+ + e^- \qquad [2.22]$$

$$Cr(HSO_4)_{ad} = CrOOH + SO_2 \qquad [2.23]$$

## 2.5 Summary

The corrosion behaviour of stainless steel in concentrated $H_2SO_4$-$H_2O$ solutions has been discussed within the context of passivity. The contributions of the previously reported

work revealed several important differences concerning corrosion and passivity in dilute and concentrated acid solutions:

1. In dilute solutions (1-14 M $H_2SO_4$), stainless steel dissolves in an active state due to the non-oxidizing hydrogen evolution cathodic process. Passivity is attained with sufficient anodic polarization and involves the formation an oxy-hydroxide film, which is significantly enriched with chromium.
2. In concentrated solutions (14-18.8 M $H_2SO_4$), stainless steel can dissolve in a cyclic active-passive state that is characterized by regular potential oscillations. The behaviour is due in part to a more oxidizing cathodic process, which most likely involves the reduction of $H_2SO_4$ molecules. Passivity is attained with sufficient anodic polarization and involves the formation of a protective sulphate film without any significant enrichment of iron, chromium or nickel.

Although models have been proposed to explain the complex corrosion behaviour exhibited in concentrated solutions, there are certain weaknesses.

### 2.5.1 Shortcomings in the Literature

It is rather odd that the passivity of about 17 wt.% chromium-stainless steel in concentrated $H_2SO_4$-$H_2O$ mixtures is derived from the formation of a protective sulphate film

and not an oxide film considering chromium's ability to anodically passivate in identical solutions with the formation of an oxide film. It may be that the alloyed chromium level is too low to significantly improve the passivity of iron in these environments. In dilute $H_2SO_4$-$H_2O$ solutions, however, the addition of 18 wt.% chromium is more than sufficient to significantly improve the passivity of iron[100]. There is no adequate explanation as to why this is not the case in concentrated solutions.

Assuming that the passivity of 17 wt.% chromium-stainless steel involves the formation of a protective sulphate film through a dissolution-precipitation mechanism, it is rather odd that the non-nickel stainless steels do not passivate under open-circuit conditions. There is no suitable explanation as to why the active corrosion of non-nickel stainless steel does not supersaturate the alloy-solution interface as does nickel-stainless steel. Furthermore, there is no explanation as to why the metals iron and nickel do not show potential oscillations during corrosion as both are known to form protective sulphate films.

The complex, active-passive corrosion behaviour of stainless steel is due in part to a more oxidizing cathodic process which most likely involves the reduction of $H_2SO_4$ molecules either to sulphur and $H_2O$[5,68] or to $SO_2$ and $H_2O$[67]. The measured redox potential in concentrated solutions suggests that the reduction of $H_2SO_4$ to sulphur is unlikely as its redox potential is too low. Although the reduction of $H_2SO_4$ to $SO_2$ is more consistent with the measured redox potential, it does not account for the sulphur which is found to form during corrosion[4,5]. Thus, the cathodic reduction mechanism responsible for the active-

passive corrosion behaviour remains to be resolved.

# CHAPTER 3

## 3. EXPERIMENTAL APPROACH

A review of the relevant literature regarding the corrosion behaviour of stainless steel and its major alloying elements in concentrated $H_2SO_4$-$H_2O$ solutions identified the areas requiring clarification. The review also provided necessary insight into the applicability of possible experimental techniques to study the reactivity and/or passivity of stainless steels and their major alloying elements in concentrated $H_2SO_4$-$H_2O$ solutions. The purpose of this chapter is to introduce and describe the various procedures and techniques employed in this study. The following sections introduce and discuss the materials employed (Section 3.1), the solution conditions studied (Section 3.2) and the techniques employed (Section 3.3).

### 3.1 Materials

Stainless steel samples employed in this study were prepared from ~1 cm thick annealed plates of alloys S43000 and S30403. The composition in wt.% of each alloy, as determined by spectrographic analysis, is shown in Table 3.1. Rectangular electrodes ~2 cm by ~1.5 cm were cut from the plates and were subsequently drilled and tapped to facilitate mounting. Cylindrical electrodes of ~1.2 cm outer diameter and ~0.7 cm inner diameter were machined from S43000 and S30403 plates by the McMaster University Engineering Machine Shop.

**Table 3.1.** Stainless Steel Alloy Composition (wt.%)

| Alloy | Fe | Cr | Ni | C | Co, Cu, Mn, Mo, P, S, Si |
|---|---|---|---|---|---|
| UNS S43000 | 82.3 | 16.7 | < .01 | < .01 | < 1 |
| UNS S30403 | 71.6 | 18.1 | 7.9 | < .01 | < 1 |

This study employed stainless steel S30403 instead of S31603 because it contains no alloyed molybdenum. Selecting an stainless steel without alloyed molybdenum reduced the number of major alloying elements from four to three. Selecting stainless steel S43000 provided a non-nickel grade with a chromium content most similar to that in S30403. This particular selection of stainless steels provided two grades that vary essentially in only the nickel content.

Polycrystalline (>99.9 wt.%) Armco iron and electrolytic grade chromium electrodes employed in this study were previously prepared by the W.W. Smeltzer Corrosion Laboratory at McMaster University. Polycrystalline nickel electrodes employed in this study were prepared from an ~2.54 cm diameter annealed nickel 270 rod. Rectangular (~2 cm by ~1.5 cm) and cylindrical (~1.2 cm outer diameter and ~0.7 inner diameter) electrodes were machined from the rod by the McMaster University Engineering Machine Shop. Table 3.2 shows the nominal compositions of the three metals studied.

**Table 3.2.** Nominal Composition of Metals Studied (wt.%)

| | Iron | Chromium | Nickel |
|---|---|---|---|
| Fe | 99.9 | 0.35 | 0.05 |
| Cr | >0.001 | 99.4 | >0.001 |
| Ni | >0.001 | >0.001 | 99.9 |
| C | 0.012 | 0.05 | 0.02 |
| Mn | 0.017 | 0.01 | >0.005 |
| S | 0.025 | 0.01 | >0.001 |
| Si | >0.001 | 0.10 | >0.005 |

### 3.2 Acid Solutions

The majority of the dissolution experiments were performed in 93.5 wt.% $H_2SO_4$ solutions that were prepared from BDH reagent grade sulphuric acid and distilled water. Table 3.3 displays the composition of the BDH reagent grade sulphuric acid. A Nusonic Model 6080 Concentration Analyzer, which measures the velocity at which ultrasonic pulses travel through the acid, verified the strength of the prepared solutions. The instrument was previously calibrated against different acid strengths at different temperatures[101]. Acid solutions other than 93.5 wt.% examined were prepared in a similar manner. No attempt was made to aerate or deaerate the acid solutions. A Cole-Palmer Model 2186-20 Digi-Sense[a] Platinum RTD Temperature Controller maintained solutions temperatures to within ±0.5°C in all experiments. A virgin acid solution was used for each test.

**Table 3.3.** Composition of BDH Reagent Grade Sulphuric Acid

| Assay 95.0 - 98.0 wt.% | | | |
|---|---|---|---|
| $Cl^-$ | 0.2 ppm | Pb | 1 ppm |
| $NO_3^-$ | 0.5 ppm | Fe | 0.2 ppm |
| $NH_4^+$ | 2 ppm | As | 0.01 ppm |
| $SO_2$ | 2 ppm | Hg | 5 ppb |

a Digi-Sense is a trademark of the Cole-Parmer Instrument Co.

### 3.3 Immersion Measurements

All electrodes were wet-ground with emery paper up to 400 grit, cleaned in soap solution, rinsed with methanol, dried with absorbent paper and then weighed immediately prior to immersion. Upon removal all electrodes were rinsed with distilled water, cleaned in soap solution, rinsed with methanol, dried with absorbent paper and then weighed. A Mettler Type H15 Analytical Balance weighed the electrodes to ± 0.0001 g prior to and after immersion. Rectangular electrodes were mounted according to the ASTM G-5 specification[102]. Electrical contact with chromium was achieved by joining the electrode, via a silver solder, with a stainless steel contact rod. Cylindrical electrodes were mounted using the Pine Instrument Company Style QC Cylindrical Electrode Assembly. Figure 3.1 shows a schematic diagram of the two sample mounts.

### 3.4 Electrochemical Measurements

Electrochemical direct current (DC) polarization was the main experimental technique employed in this study. The technique measures the potential-current-time relationships by using a direct current source to control the potential. The main instrument is a dual potentiostat/galvanostat electronic device, which comprises a potentiostat and galvanostat circuit. The majority of electrochemical measurements in this study utilized the potentiostat circuit. The monograph by von Fraunhofer and Banks[103] provides an excellent description and detailed electronics of the modern potentiostat.

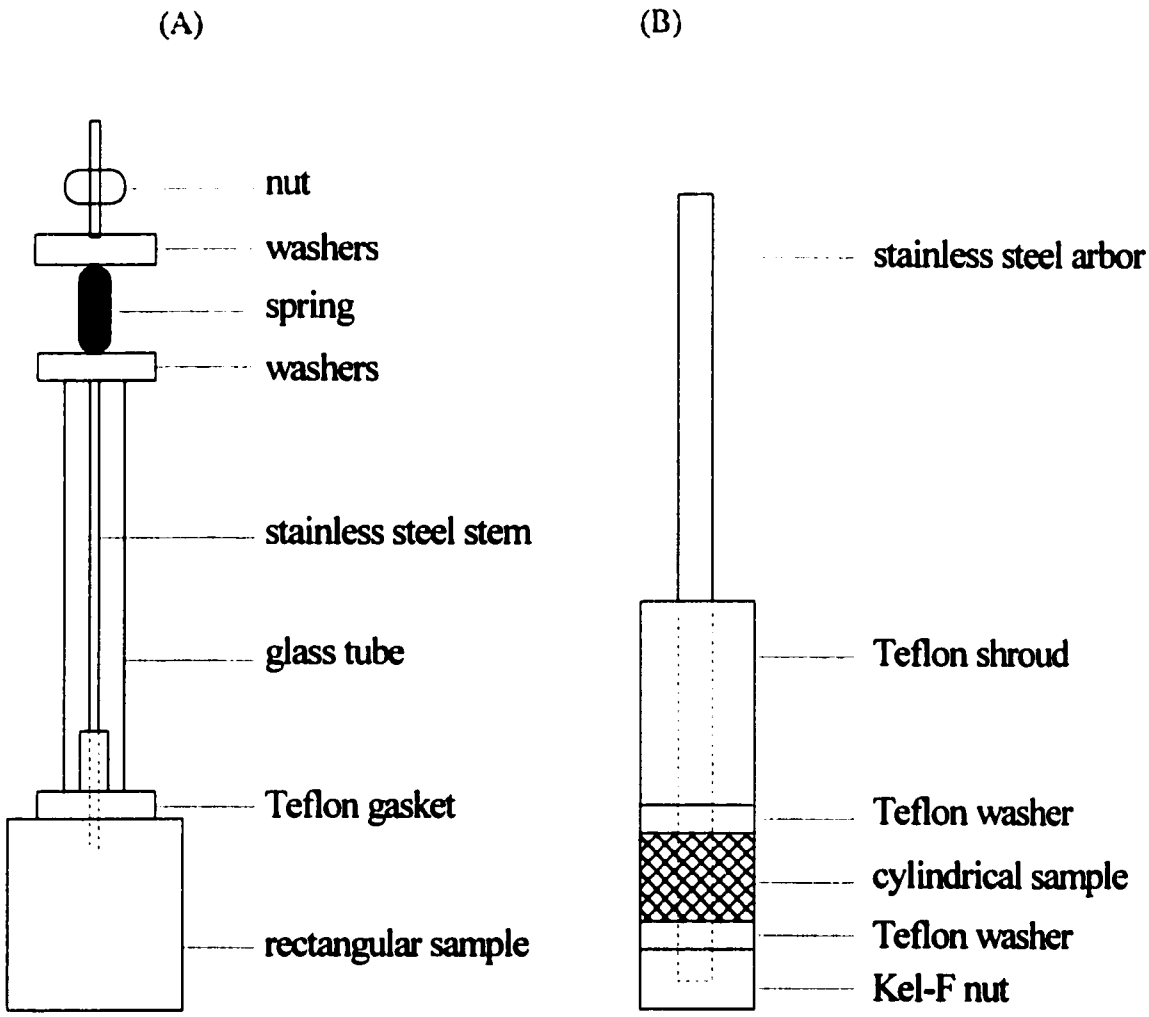


Figure 3.1. Schematic diagram of sample mounts. (A) ASTM G-5 rectangular sample mount, (B) Pine Instrument Company rotating cylinder mount.

Electrochemical measurements were performed in a conventional Pyrex glass electrochemical cell (250 ml) with a EG&G Princeton Applied Research Model 273 Potentiostat/Galvanostat controlled by Model 352 SOFTCORR[b] Corrosion Software run on a Packard Bell Force 545 Computer. All potentials were measured against a platinum wire electrode. Rotating cylinder electrode (RCE) measurements were conducted using a Pine Instrument Company Model AFMSRX Rotator and MSRX Speed Control Unit. Figure 3.2 shows a schematic diagram of the apparatus and electrical circuitry.

A platinum reference electrode was chosen because it has been successfully employed in commercial anodic protection systems for handling concentrated $H_2SO_4$-$H_2O$ solutions[104] and in the oleum and concentrated $H_2SO_4$-$H_2O$ solution research of Arvia *et al.*[49,50,51,52]. Measuring the platinum reference potential against a standard calomel electrode (SCE) in stagnant 93.5 wt.% as a function of time, Figure 3.3, verified its stability. For the measurement, the standard calomel electrode was placed in a separate, air-cooled compartment that contained an equivalent $H_2SO_4$ acid solution at 25°C. The compartment was connected to the rest of the cell by means of a Luggin-Haber capillary tip. The redox potential rapidly stabilized within the first few minutes and remained constant at +0.601 $V_{SCE}$ for the duration of the test.

During the course of this study the potential of the platinum reference electrode was checked numerous times against a SCE. The platinum reference potential of +0.601 $V_{SCE}$

---

b SOFTCORR is a trademark of EG&G Princeton Applied Research Corporation

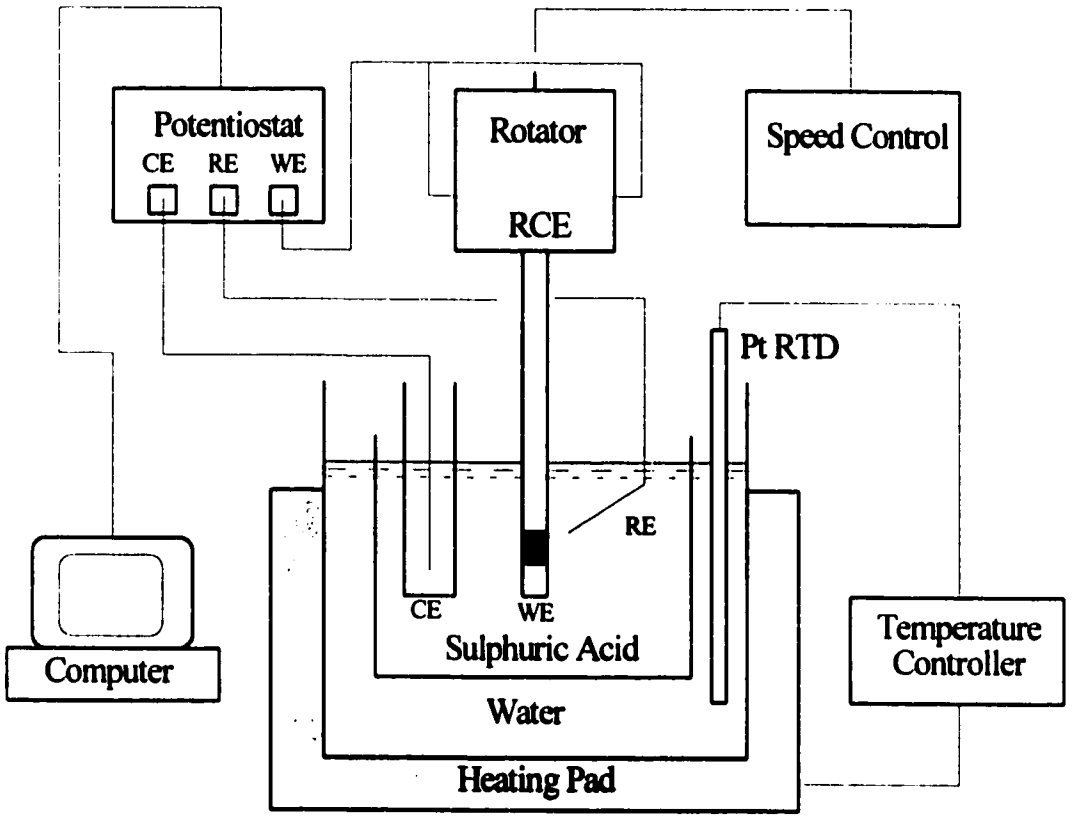


Figure. 3.2. Schematic diagram of experimental set-up. WE = working electrode, CE = counter electrode and RE = reference electrode.

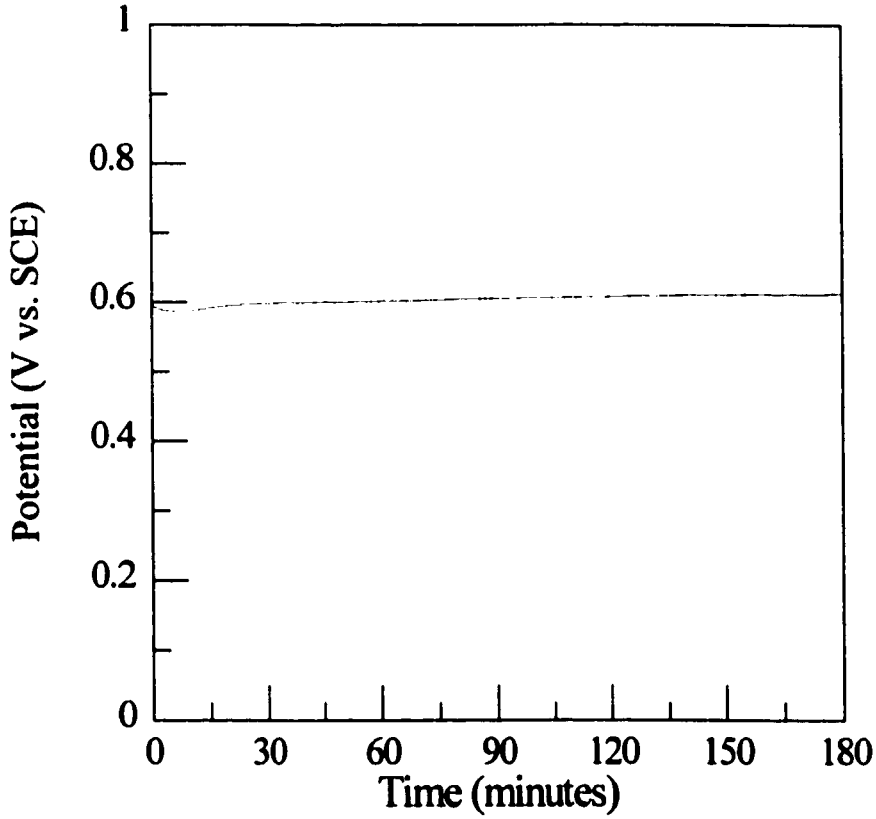


Figure 3.3. Redox potential of quiet 93.5 wt.% $H_2SO_4$ at 60°C measured on a platinum electrode.

was stable and reproducible in 93.5 wt.% $H_2SO_4$ at 60°C. According to Banas and Stypula[97], the reaction responsible for the measured redox potential of 14-18 M $H_2SO_4$-$H_2O$ is likely the reduction of $HSO_4^-$ ions to $SO_2$:

$$HSO_4^- + 3H^+ + 2e^- = SO_2 + 2H_2O \qquad [3.1]$$

The corrosion potential of the various samples under investigation verse the platinum reference electrode was recorded at a frequency of 0.5 Hz. The measurement frequency was increased to 10 Hz when monitoring the potential transient behaviour during a potential spike.

Current-potential curves were obtained by potentiodynamic polarization with an arrangement employing an isolated counter electrode compartment that was connected to the working and reference electrode cell with a porous glass frit. A platinum wire was used as a counter electrode in all polarization measurements. The scan rate was 0.33 mV/s. A platinum (99.99 wt.%) disk working electrode was employed to measure the current-potential characteristics of the concentrated sulphuric acid.

Potentiostatic polarization experiments were conducted using the same two compartment cell as described for the potentiodynamic experiments. In these experiments the potential difference between the sample and the reference electrode was kept constant and the applied current transient was recorded at a frequency of 0.5 Hz.

### 3.5 X-ray Spectroscopic Techniques

This study employed X-ray spectroscopic techniques to characterize the solid deposits that formed during the corrosion of stainless steel S30403 and S43000 along with the corrosion of nickel in 93.5 wt.% $H_2SO_4$. The techniques include X-ray fluorescence spectroscopy (XRF) and X-ray photoelectron spectroscopy (XPS).

The XRF measurements were carried out on a Philips PW 1480 XRF Spectrometer by Mr. J. Andrews of the Department of Chemistry at McMaster University. This technique was employed to characterize the elemental composition of insoluble non-adherent corrosion products. The procedure to collect the insoluble non-adherent products involved removing the deposit from the surface of the electrode by rinsing the covered electrode with distilled $H_2O$ and subsequent filtering. All deposits collected in this manner were dried in air for a period of at least 24 hours prior to analysis. The monographs by Bertin[105,106] provide an excellent discussion of the theory and the practice of XRF.

The XPS measurements were carried out on a Perkin Elmer PHI 5500 system with a monochromated Al $K_\alpha$ source by P. Schmuki, M.J. Graham and I. Sproule of the National Research Council of Canada. This technique was employed to characterize the composition of insoluble adherent corrosion products, including passive films. The system collected the data using a pass energy of 29.4 eV with a take off angle of 75°. Sample preparation prior to analysis involved rinsing the electrodes with methanol, cleaning in a ultrasonic methanol bath and drying using high purity nitrogen gas. The monograph by Roy and Carette[107]

provides an excellent discussion on the theory and practice of XPS.

# CHAPTER 4

## 4. CORROSION OF STAINLESS STEEL IN 93.5 WT.% $H_2SO_4$

The investigation began by conducting a series of corrosion tests designed to test preconceived ideas regarding the state of stainless steel passivity, the conditions in which it is stable, the role played by the major alloying elements in determining that state and to identify specific areas that require further research. The experimental approach used to meet these objectives involved making weight loss and electrochemical measurements on electrodes constructed of S43000, S43000, iron, chromium and nickel respectively in stirred 93.5 wt.% $H_2SO_4$ at 60°C. Testing preconceived ideas regarding the state of passivity involved comparing the corrosion and electrochemical behaviour of a S43000 to that of a S30403 electrode. Testing preconceived ideas regarding the conditions in which the passive state is stable involved exploring the influence of temperature, stirring (RCE rotation rate)

and the concentration of dissolved oxygen on the corrosion behaviour of a S30403 RCE. Testing preconceived ideas regarding the role of the alloying elements in determining passivity involved comparing and contrasting the corrosion and electrochemical behaviour of iron, chromium and nickel electrodes. Identifying areas for further investigation involved establishing a tentative theory that provides a reasonable interpretation of all the observations.

This chapter is organized into six major sections. The first section presents the results of the tests conducted using a S43000 and a S30403 electrode in stirred 93.5 wt.% $H_2SO_4$ at 60°C. The second section presents the results of the tests conducted on a S30403 RCE in 93.5 wt.% $H_2SO_4$ as a function of temperature, stirring (RCE rotation rate) and the concentration of dissolved oxygen. The third section presents the results of the tests conducted on iron, chromium and nickel electrodes in stirred 93.5 wt.% $H_2SO_4$ at 60°C. The fourth section proposes the theory that provides a reasonable explanation of the corrosion mechanism of S43000 and S30403 in stirred 93.5 wt.% $H_2SO_4$ and identifies the areas requiring further research to meet the overall objectives of the study. The fifth section summarizes the major conclusions drawn from the research conducted.

## 4.1 Passivity of 17 wt.% Chromium-Stainless Steels in 93.5 wt.% $H_2SO_4$ at 60°C

The first step taken to meet the objective defined above involved exploring the state of stainless steel passivity in 93.5 wt.% $H_2SO_4$. The relevant literature discussed in Section

2.3 provided an idea of what to expect. For convenience, the current state of knowledge regarding the passive state in stainless steel is reviewed below.

Alloyed nickel promotes a periodic spontaneous passivation of stainless steel alloys in concentrated $H_2SO_4$-$H_2O$ solutions[65]. This unique *active-passive* corrosion state is characterized by a corrosion potential that oscillates in time between two distinct potential extremities[3,4,5]. The oscillatory potential consists of a series of spikes separated by an extended period where the potential is significantly more positive. Active state corrosion occurs during the spikes with the formation of hydrogen, whereas passive state corrosion occurs during the period between the spikes with the formation of sulphur[4,5]. Passivation mechanisms proposed include the periodic formation and dissolution of a metal sulphate film[4,5] and the periodic formation and dissolution of a sulphur barrier layer[68]. Regardless of the barrier layer, the proposed cathodic reaction that provides the necessary driving force and current to anodically passivate the stainless steel involves the reduction of $H_2SO_4$ molecules to sulphur; the overpotential of which being significantly reduced on nickel sites[4,5,65,68].

Taking the literature review into account, experiments conducted to explore the state of passivity involved studying the corrosion of stainless steels S43000 and S30403 in stirred 93.5 wt.% $H_2SO_4$ at 60°C. Comparing and contrasting the potential and anodic polarization behaviour confirmed the beneficial influence of alloyed nickel on the corrosion resistance of 17 wt.% chromium-stainless steels. The same anodic polarization measurements coupled with a surface analysis provided more information regarding their state of passivity. The

following subsections present and discuss the results of the various measurements made.

### 4.1.1 Influence of Alloyed Nickel on Corrosion Behaviour

The first test compared and contrasted the short term (4 hours) corrosion behaviour of S43000 and S30403 in 93.5 wt.% $H_2SO_4$ at 60°C. Figure 4.1 shows the corrosion potential of a S43000 RCE and a S30403 RCE, both at 1000 rpm, in 93.5 wt.% $H_2SO_4$ at 60°C as a function of time. A marked difference in the time dependence occurred for the two stainless steels. Without any alloyed nickel, the corrosion potential of S43000 quickly established and remained reasonably stable at -0.775 $V_{Pt}$. In contrast, the corrosion potential of the nickel-stainless steel S30403 oscillated in time with a reasonably regular amplitude of ~0.6 $V_{Pt}$ and a period of ~90 minutes. The potential changed rapidly in the range from about -0.4 to -0.8 $V_{Pt}$, whereas it changed significantly more slowly in the range from about -0.2 to -0.4 $V_{Pt}$. If the S30403 samples employed in the study are essentially S43000 samples alloyed with 7.9 wt.% nickel, then the oscillatory potential of S30403 is a direct result of the presence of 7.9 wt.% alloyed nickel.

The oscillatory corrosion potential of S30403 consists of a series of spikes separated by an extended period where the potential is significantly more positive. Figure 4.2 shows the typical potential dependence on time during a spike. Although the plot shows only one spike, the observed behaviour was reproducible in the next four consecutive spike measurements. The plot shows a finite time exists at which the corrosion potential remains

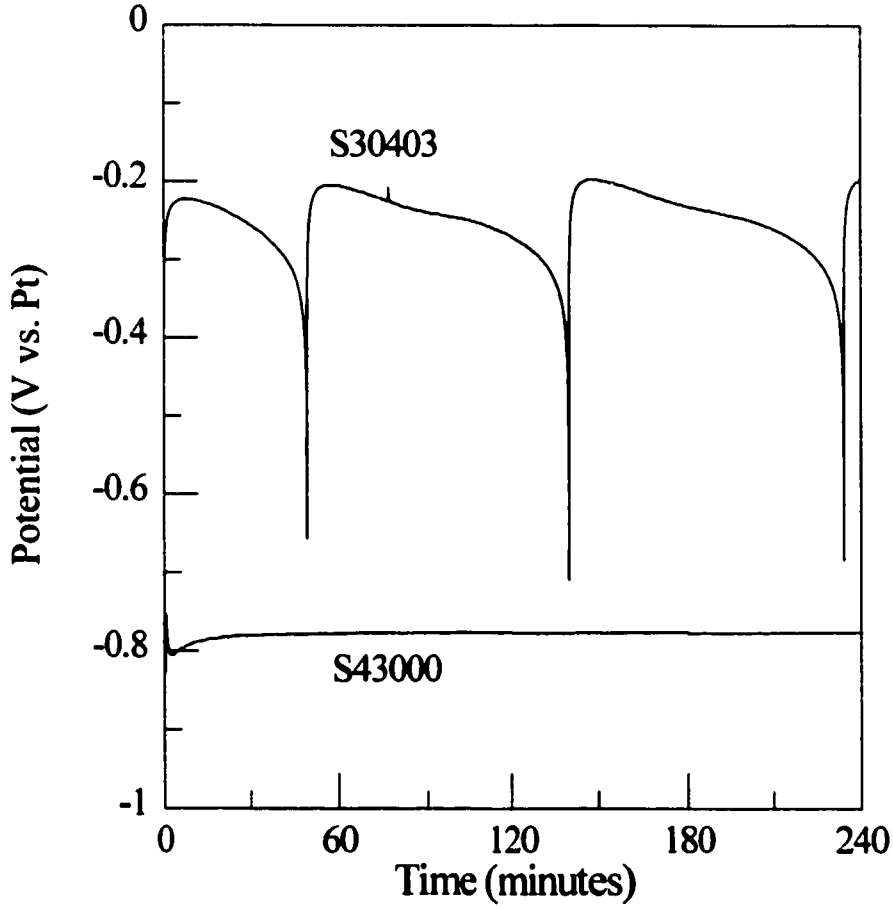


Figure 4.1. Corrosion potential of a S43000 RCE (1000 rpm) and a S30403 RCE (1000 rpm) in 93.5 wt.% $H_2SO_4$ at 60°C as a function of time immediately after immersion.

at the more negative potentials of the cycle before it increases rapidly towards the more positive maximum. Therefore, the corrosion potential of S30403 cycles between two distinct potential extremes. Superimposed in Figure 4.2 is the stable corrosion potential behaviour of the S43000 RCE. Comparing the two curves shows that the finite corrosion potential plateau of the S30403 RCE that occurs during the spike coincides with the stable corrosion potential of the S43000 RCE.

Visible gas evolution occurred on the surface of the S30403 RCE during the short potential plateau (~-0.8 $V_{Pt}$) attained during the spikes. No new gas evolution was visibly evident when the potential reached the more positive plateau (~-0.2 $V_{Pt}$). The observation suggests that different corrosion products form at the different potential plateaus.

According to Chang[4] and Matsuhashi *et al.*[5,65], the insoluble gas formed as a cathodic reaction product during corrosion at the more negative potentials is hydrogen. The cathodic formation of insoluble hydrogen gas is plausible during the spike since the corrosion potential at which the evolution occurs is likely more negative than the equilibrium potential of the hydrogen evolution reaction. According to published data[48,97], the equilibrium potential of the hydrogen evolution reaction in 93.5 wt.% $H_2SO_4$ at 25°C is -0.607 $V_{Pt}$. Furthermore, hydrogen has a limited solubility in concentrated $H_2SO_4$-$H_2O$ solutions. According to Christoff[108], the solubility of $H_2$ in 95.6 wt.% $H_2SO_4$ at 25°C is $4.89\times10^{-4}$ mol/l which is lower than the solubility of $9.27\times10^{-4}$ mol/l in 0 wt.% $H_2SO_4$ (100 wt.% $H_2O$).

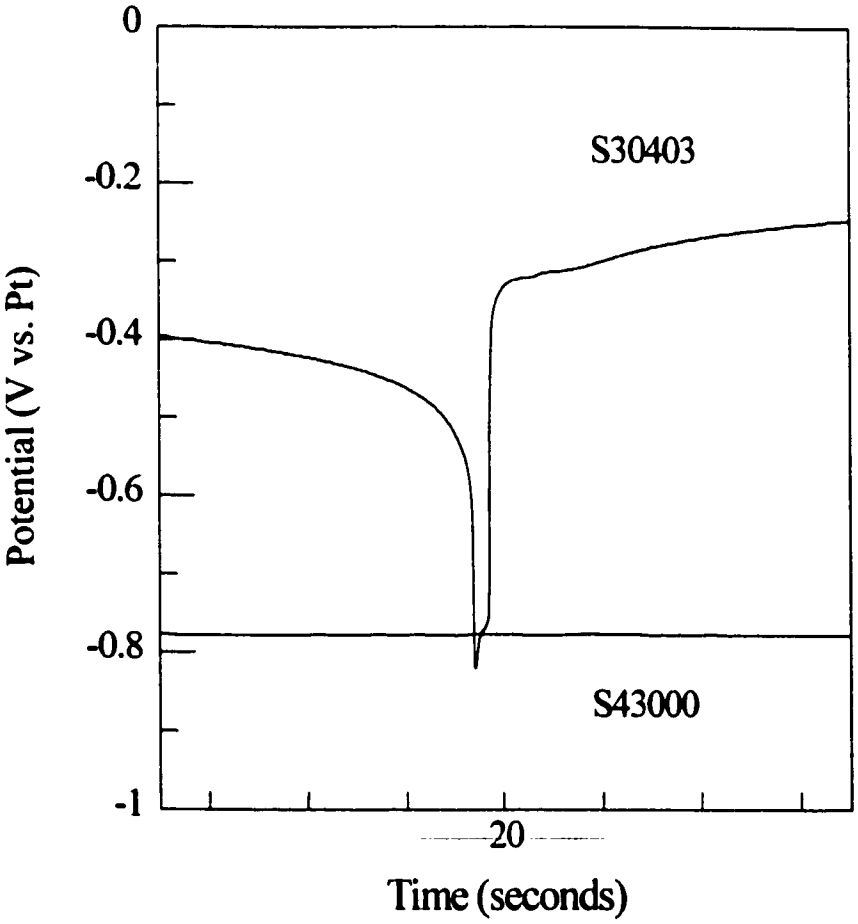


Figure. 4.2. Corrosion potential of a S30403 RCE (1000 rpm) in 93.5 wt.% $H_2SO_4$ at 60°C during a potential spike. Superimposed is the steady state corrosion potential of a S43000 RCE (1000 rpm) shown in Figure 4.1.

Visible gas evolution occurred on the surface of the S43000 RCE during the entire four hour exposure. The rate of evolution decreased with increasing exposure time. For reasons discussed above, the insoluble gas is likely hydrogen formed as a cathodic reaction product during corrosion. Hydrogen formation occurs during the entire four hours since the corrosion potential remains essentially constant during the same time period.

Table 4.1 displays the weight loss measured after the four hour test. Comparing the data shows that the weight loss of the S30403 RCE is 20.5 times lower than that for the S43000 RCE. The difference in weight loss is likely related to the respective corrosion potential behaviour. For the S43000 RCE, a large weight loss occurred while the corrosion potential remained essentially constant at -0.775 $V_{Pt}$. The corrosion potential of the S30403 RCE spent a small fraction of the time at a similar potential. The majority of the time was spent at a significantly higher potential. A lower weight loss rate at the more positive corrosion potentials can account for the lower total lower weight loss measured for the S30403 RCE.

**Table 4.1.** Stainless Steel RCE Weight Loss in 93.5 wt.% $H_2SO_4$ at 60°C (Rotation rate = 1000 rpm; Exposure Time = 4 hours)

| Alloy | Weight Loss ($mg/cm^2$) |
|---|---|
| S43000 | 3.69 |
| S30403 | 0.18 |

A potential dependent weight loss of the S30403 RCE in 93.5 wt.% $H_2SO_4$ is consistent with the belief that nickel-stainless steel can corrode in a active-passive state in concentrated $H_2SO_4$-$H_2O$. The weight loss data confirm that alloyed nickel plays an active role in providing corrosion resistance to stainless steel alloys in concentrated $H_2SO_4$-$H_2O$ solutions despite being present mainly to retain the austenitic phase.

### 4.1.2 Influence of Alloyed Nickel on Anodic Polarization Behaviour

Potentiodynamic anodic polarization measurements provided more information regarding the corrosion behaviour. Figure 4.3 shows the anodic polarization behaviour of the two stainless steel rotating electrodes (1000 rpm) in 93.5 wt.% $H_2SO_4$ at 60°C. Both electrodes show the distinctive anodic polarization behaviour characteristic of a metallic material that undergoes passivity (Figure 2.1). An active-passive transition occurred at ~-0.5 $V_{Pt}$ for both alloys. A region of passivity followed the transition where the anodic current density was two orders of magnitude lower than the critical current density required for passivity. The limiting anodic current that occurred prior to the transition suggests that passivation may involve the formation of a semi-protecting precursor film. Assuming that S30403 is essentially S43000 alloyed with 7.9 wt.% nickel, adding 7.9 wt.% nickel shifted the corrosion potential in the positive direction, decreased the critical current density required for passivity and slightly increased the passive current density of S43000. The comparable passivation potential and passive current density suggests that the two stainless steels

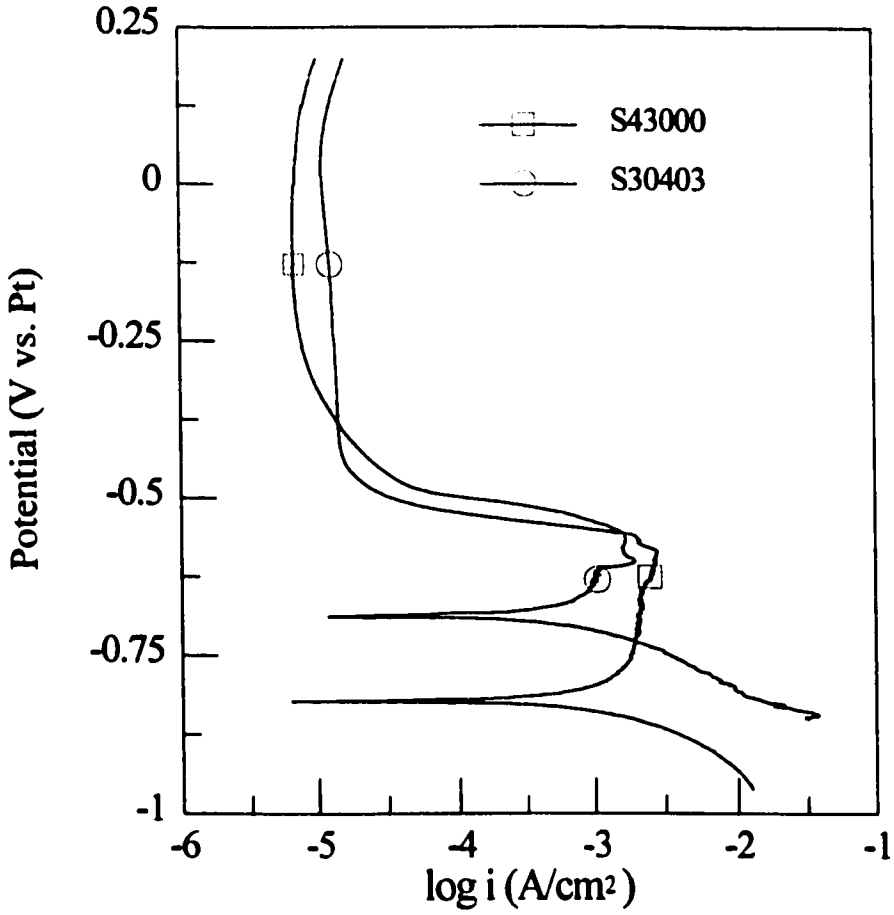


Figure 4.3. Potentiodynamic anodic polarization of a S43000 RCE (1000 rpm) and a S30403 RCE (1000 rpm) in 93.5 wt.% $H_2SO_4$ at 60°C. Scan rate = 20 mV/min.

passivate through a similar mechanism.

Superimposing the anodic polarization behaviour of the S30403 RCE with its corrosion potential spike behaviour, Figure 4.4, supports the idea that the rate of the corrosion process characterized by the oscillatory potential is potential-dependent. The maximum and minimum potentials attained during the cycle reside on either side of the active-passive transition. Therefore, according to Figure 4.4, corrosion proceeds in an active state during the spikes with an appreciable rate and in a passive state during the period between the spikes with a much reduced rate.

### 4.1.3 Potential-Dependent Corrosion Rate of S30403

Comparing the measured weight loss with an expected weight loss calculated using the measured anodic polarization data and Faraday's Law provided additional evidence supporting a potential-dependent corrosion rate. This exercise involved measuring and calculating the weight loss for a 24 hour exposure of a S30403 RCE (1000 rpm) in 93.5 wt.% $H_2SO_4$ at 60°C.

Faraday's Law is expressed mathematically as,

$$m = \frac{Qw_e}{F} \qquad [4.1]$$

where m is the weight loss (g), Q is the charge passed during dissolution (C), $W_e$ is the

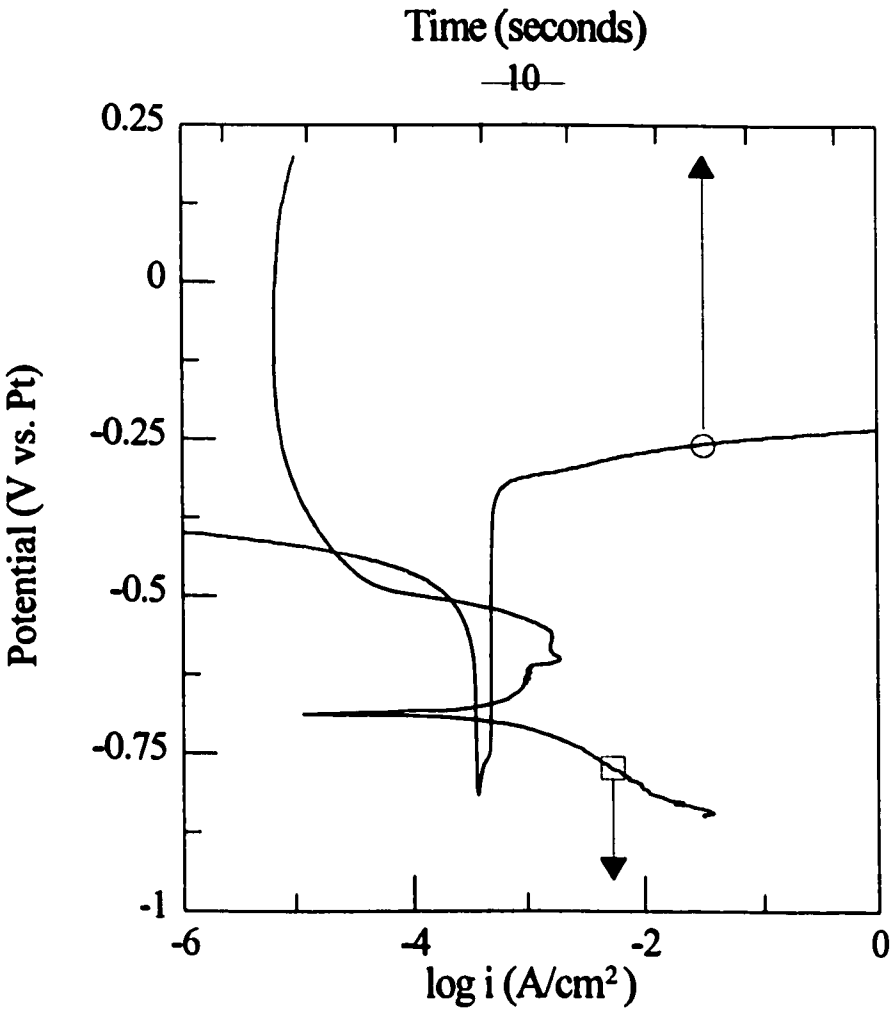


Figure 4.4. Superimposed corrosion potential (during a potential spike) of the S30403 RCE (1000 rpm) and anodic polarization of the S30403 RCE (1000 rpm) in 93.5 wt.% $H_2SO_4$ at 60°C. Scan rate = 20 mV/min.

equivalent weight (25.12 g/equivalent for S30403) and F is Faraday's constant (96 486 C/equivalent). Therefore, the weight loss can be calculated using [4.1] providing the total charge consumed during corrosion is known. For the corrosion situation under consideration, the total charge Q is the sum of the charge $Q_a$ consumed during active state dissolution and charge $Q_p$ consumed during passive state dissolution. The charge $Q_a$ and $Q_p$ are given by the following,

$$Q_a = i_a A t_a \qquad [4.2]$$

$$Q_p = i_p A t_p \qquad [4.3]$$

where $i_a$ is the active state current density ($A/cm^2$), $i_p$ is the passive state current density ($A/cm^2$), A is the area ($cm^2$), $t_a$ is the total time spent in the active state (s) and $t_p$ is the total time spent in the passive state (s).

The weight loss of the S30403 RCE (1000 rpm) measured after 24 hours exposure in 93.5 wt.% $H_2SO_4$ at 60°C is 6.0 mg. A total of 24 spikes occurred during course of the exposure. The calculation of the expected weight loss using [4.1]-[4.3] involved the following five assumptions:

1. The active-passive transition occurred at -0.45 $V_{Pt}$ (the midpoint potential of the measured transition).
2. Corrosion in the active state occurred at potentials more negative than -0.45 $V_{Pt}$ with a current density of 1.66 $mA/cm^2$ (the limiting anodic

current density measured in the active state).

3. Corrosion in the passive state occurred at all potentials more positive than -0.45 $V_{Pt}$ with a current density of 7.11 $x10^{-3}$ $mA/cm^2$ (the current density measured at the maximum potential -0.2 $V_{Pt}$ attained during the cycle).

4. Corrosion in the active state occurred during the spikes with a period of 1.5 s/spike (measured from the potential spike-time plot in Figure 4.2). A total of 24 spikes occurred during the 24 hour exposure. Thus, for the 24 hour exposure, the total active state time was 36 s.

5. Corrosion in the passive state occurred during the period between the spikes. For the 24 hour exposure, the total passive state time was 86 364 s.

Substitution of the respective quantities into [4.1]-[4.3] leads to a calculated expected weight loss of 0.41 mg for the 24 hour exposure. The expected weight loss is significantly lower than the measured weight loss.

The rate of corrosion on a freshly depassivated surface provides a plausible explanation of the weight loss discrepancy since the rate is likely much larger than that recorded on an anodic polarization curve. The corrosion potential of the S30403 RCE attained during in situ depassivation is more negative than the corrosion potential (zero current potential) determined from the anodic polarization measurement. Consequently, the

rate of corrosion is likely higher. The rate of the cathodic reaction ($H_2$ evolution) is likely rate-limiting, but is faster on a freshly depassivated surface because of an increased exchange current density ($i_o$).

### 4.1.4 Influence of Solid Products on Stainless Steel Corrosion

The anodic polarization behaviour in Figure 4.3 show that both the S43000 RCE and the S30403 RCE possess the ability to passivate in 93.5 wt.% $H_2SO_4$ at 60°C. The similar passivation potential and critical current required for passivity suggest passivation occurs by a similar mechanism; one which is independent of the alloyed nickel content. The measurements, however, provide little information regarding nature of the passive film. A 96 hour corrosion test provided a better understanding of the influence of insoluble corrosion products on the resulting corrosion rate in 93.5 wt.% $H_2SO_4$ at 60°C. For this test, a rectangular electrode of each alloy was immersed in its own cell containing 1000 ml of the acid solution. A glass impeller driven by an overhead motor mechanically agitated each test solution.

Potential measurements conducted during the exposure showed no significant change in the corrosion potential behaviour with the extended exposure time. The corrosion potential of the S30403 electrode oscillated during the entire exposure without a significant change in the amplitude or period. The corrosion potential of the S43000 electrode remained stable but had a slow positive drift with increased exposure time.

A distinct, visible surface deposit covered each stainless steel electrode prior to the end of the 96 hours exposure. A dark grey deposit covered the S43000 electrode, whereas a brownish yellow deposit covered the S30403 electrode. Attempting to collect the dark grey deposit from the surface of the S43000 electrode showed the deposit was non-adherent and soluble in water. Attempting to collect the brownish yellow deposit from the S30403 electrode showed the deposit was non-adherent and insoluble in $H_2O$. The insolubility in $H_2O$ allowed collection of a sufficient quantity for subsequent chemical analysis. An XRF analysis conducted on the brownish-yellow deposit showed that the deposit is very rich in sulphur (>99 wt.%) and very lean in metallic elements (<1 wt.%). Appendix A.1 contains the results of the analysis. The analysis is consistent with the formation of insoluble elemental sulphur.

Table 4.2 displays the weight loss measured and the weight loss calculated from the dissolved iron concentration measured analytically after the 96 hour test. The dissolved iron ($Fe^{2+}$) concentration in the acid solution was analyzed spectrophotometrically, using 1,10 phenanthroline as the complexing agent, according to the procedure of Harvey *et al.*[109]. Converting the dissolved iron concentration to a weight loss involved assuming that the stainless steel electrode dissolved in proportion to its respective stoichiometry. The excellent agreement shows that both stainless steel electrodes dissolved according to their respective stoichiometries. The significance is that no preferential leaching occurred. Comparing the data shows that the weight loss of the S30403 electrode is 6.3 times lower

than that for the S43000 electrode. The 96 hour weight loss ratio of 6.3 is lower than the 4 hour ratio of 20.5. The different ratios suggest that the corrosion products do inhibit the corrosion rate to some extent. Regardless of the ratio, the nickel-containing S30403 electrode has a lower corrosion rate. The improved resistance of the S30403 electrode results from periodic passivation.

**Table 4.2.** Stainless Steel Weight Loss in Agitated 93.5 wt.% $H_2SO_4$ at 60°C (After 96 hours)

| Alloy | Weight Loss ($mg/cm^2$) | Iron Analysis ($mg/cm^2$) |
|---|---|---|
| S43000 | 45.80 | 44.54 |
| S30403 | 7.27 | 7.33 |

As reported above, the S43000 electrode had a water-soluble grey deposit form during the course of the test. The observations are consistent with, at least in part, anhydrous $FeSO_4$. The solubility of $FeSO_4$ in 93.5 wt.% $H_2SO_4$ at 60°C is 0.265 wt.%[110]. A weight loss of 45.80 $mg/cm^2$ after 96 hours exposure corresponds to a calculated $FeSO_4$ concentration of 0.098 wt.% which is lower than the equilibrium solubility. It is reasonable to postulate that the build up of corrosion products at the metal-solution interface, due to the high solution viscosity, leads to the precipitation of a film made of, at least in part, $FeSO_4$ from a super-saturated solution at a time much sooner than required to saturate the bulk solution.

An optical microscopic examination after exposure provided information regarding the mode of attack. Under a magnification of 400x, the surface of both stainless steels revealed uniform attack occurred; the attack being more severe for S43000. There was no evidence of intergranular attack. Corrosion occurred without any clearly defined anodic or cathodic surfaces.

According to the weight loss data in Table 4.2, the sulphur deposit formed on the S30403 electrode appears to be the more protective layer. This observation is consistent with the conclusion that stainless steel passivity in concentrated $H_2SO_4$-$H_2O$ solutions proposed by Kuzob *et al.*[68]. If both the S43000 and S30403 electrodes anodically passivated through a similar mechanism, then sulphur should be detected on the surface of an anodically passivated S43000 electrode along with a passivated S30403 electrode. An XPS and AES analysis of the passivated surfaces shows this is not the case. Anodic passivity of stainless steels S43000 and S30403 likely involves the formation of an oxide film.

### 4.1.5 Surface Analysis of Passivated Stainless Steel

Figure 4.5(a) shows the XPS sulphur 2p spectrum measured on the surface of a S30403 electrode after 90 minutes exposure in stirred 93.5 wt.% $H_2SO_4$ at 60°C. The sulphur region exhibits a strong peak at 163.99 eV and a shoulder at 163.30 eV. The reported binding energies were adjusted using the carbon peak as the reference. The adjusted binding energies of the peak and its shoulder are consistent with the literature values reported for elemental

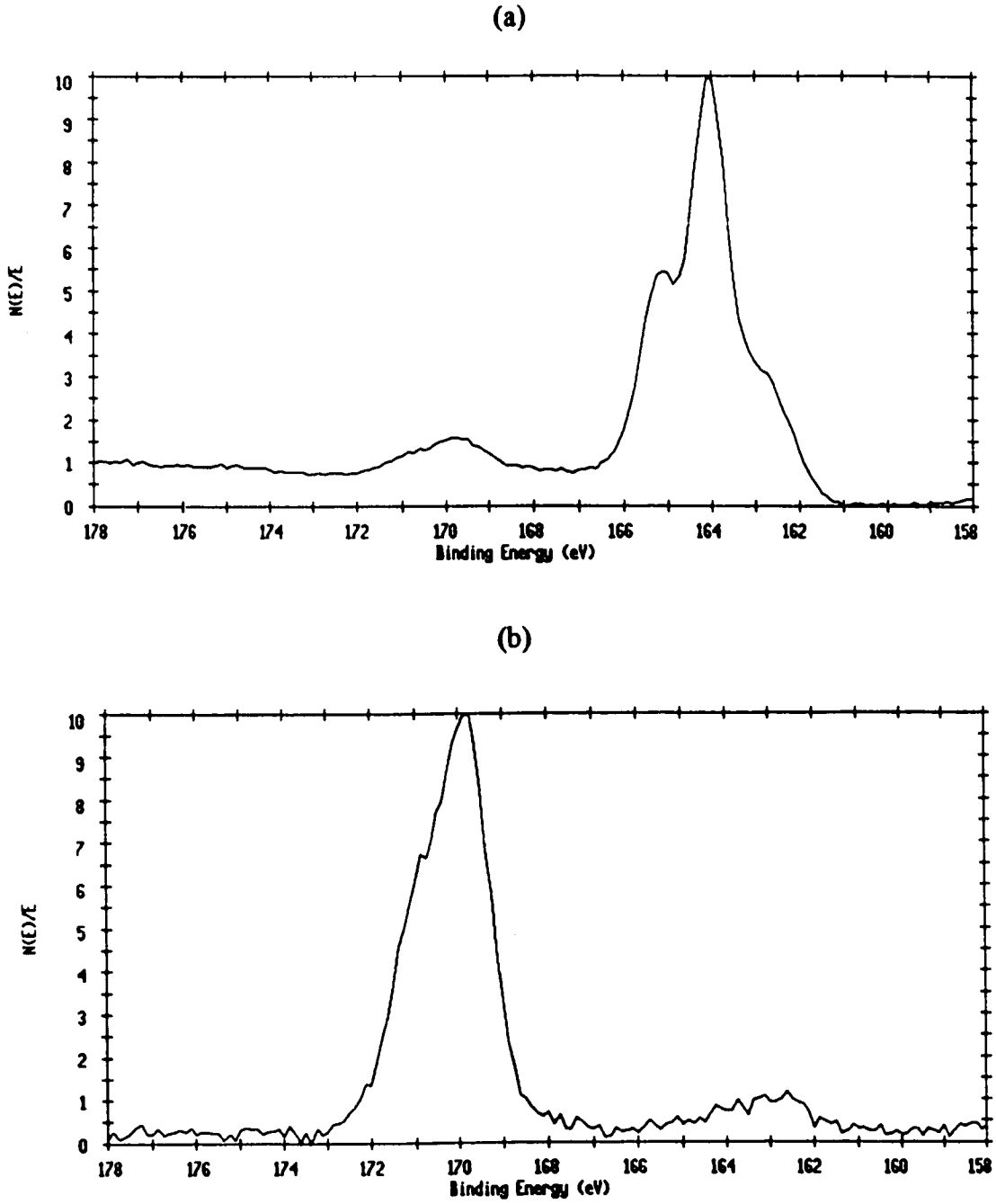


Figure 4.5. XPS sulphur 2p spectra: (a) obtained from the surface of a S30403 electrode after 90 minutes exposure in 93.5 wt.% $H_2SO_4$ at 60°C and (b) obtained from the surface of a S43000 electrode after 60 minutes of potentiostatic polarization at -0.2 $V_{Pt}$ in 93.5 wt.% $H_2SO_4$ at 60°C.

sulphur[111]. Therefore, the XPS results confirm the interpretation of the XRF results discussed above. Although the XPS result is consistent with a passivation mechanism involving the formation a protective sulphur barrier layer it is not conclusive. Conducting an XPS analysis on the surface of a passivated S43000 electrode provided more information.

Figure 4.5(b) shows the XPS sulphur 2p spectrum measured on the surface of an anodically passivated S43000 electrode, 60 minutes at -0.2 $V_{Pt}$, in stirred 93.5 wt.% $H_2SO_4$ at 60°C. The sulphur region exhibits a strong peak at 168.9 eV. The reported binding energy is the adjusted value based on the shift measured in the carbon peak (the reference peak). The adjusted binding energy of the peak is consistent with the binding energy reported in the literature for sulphur bound in a sulphate anion 169.2 eV[111]. The analysis detected no elemental sulphur present on the passivated S43000 electrode. Therefore, assuming that both stainless steels passivate through a similar mechanism, it is unlikely that this mechanism involves the formation of a protective sulphur barrier layer. Furthermore, it is unlikely that the mechanism involves a protective sulphate barrier layer. The grey deposit, believed to be a metal sulphate, that formed during the corrosion of S43000 electrode possessed essentially no protective capability. Conducting an AES analysis on the surface of the passivated S43000 electrode provided more information regarding the passivation mechanism.

Figure 4.6 shows the AES sputter profile of the anodically passivated S43000 electrode surface. The profile shows oxygen and chromium, relative to iron, are significantly enriched at the surface, whereas sulphur is only marginally enriched. Based on the profile,

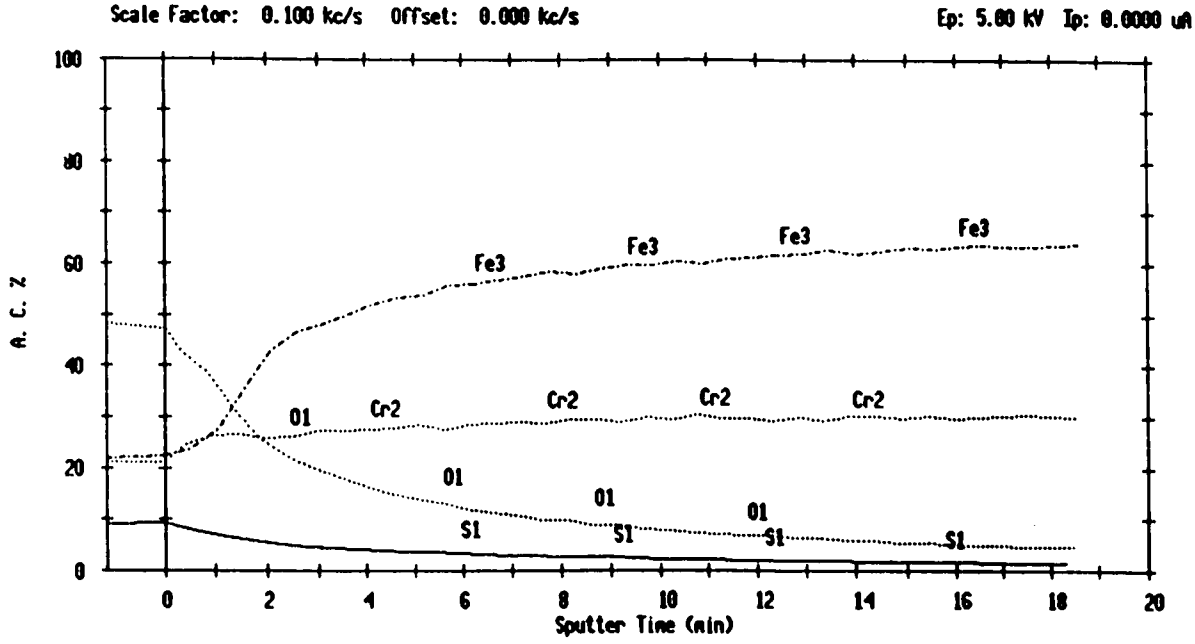


Figure 4.6. AES depth profile of a S43000 electrode after potentiostatic polarization at -0.2 $V_{Pt}$ in 93.5 wt.% $H_2SO_4$ at 60°C for 60 minutes.

the passivated surface consists of a thin chromium-rich oxide film. Anodic passivity of the S43000 electrode involving a chromium-rich oxide film is plausible since chromium anodically passivates in concentrated $H_2SO_4$-$H_2O$ solutions with the formation of a CrOOH film.

### 4.1.6 Summary

Experiments conducted to explore the state of passivity involved studying the corrosion of stainless steels S43000 and S30403 in stirred 93.5 wt.% $H_2SO_4$ at 60°C. The major findings of these experiments may be summarized as follows. Stainless steel alloys containing 17 wt.% chromium do anodically passivate in stirred 93.5 wt.% $H_2SO_4$. Anodic passivity likely involves the formation of a protective, thin, chromium-rich oxide film and not a protective metal sulphate or sulphur barrier layer. The ability of 17 wt.% chromium-stainless steels to spontaneously passivate, albeit periodically, relies on the alloyed nickel; spontaneous passivation does not occur without alloyed nickel. Periodic passivation reduces the weight loss by an order of magnitude.

## 4.2 Influence of Temperature and Stirring on Active-Passive Corrosion

The second step taken to meet the objectives defined above involved clarifying the conditions in which the passive state of S30403 is stable in 93.5 wt.% $H_2SO_4$. The experiments involved exploring the influence of temperature, stirring and presence of

dissolved $O_2$ on the corrosion behaviour of a S30403 RCE. As discussed in Section 2.3, the stability of the passive state is sensitive to both temperature and stirring. Chang[4] found that an increase in either temperature or electrode rotation rate (stirring) decreased the passive state period, resulting in a higher weight loss. Since the passive state is believed to be an oxide film, the influence of the dissolved $O_2$ concentration on the passivation process and the passive state stability needs to be explored. It is possible that a cathodic process involving the reduction of dissolved oxygen provides the necessary driving force and current for anodic passivation and provides the source of oxygen atoms required to form the oxide passive film. The following subsections present and discuss the results of the experiments conducted to explore the influence of temperature, stirring (electrode rotation rate) and the concentration of dissolved $O_2$ respectively.

### 4.2.1 Influence of Temperature on Active-Passive Corrosion

The influence of temperature on the corrosion potential of a S30403 RCE (1000 rpm) in 93.5 wt.% $H_2SO_4$ is shown in Figure 4.7 as a function of time. Potential oscillations, representing active-passive corrosion, occurred at all temperatures studied between 25-80°C. Although not shown on the graph, a potential spike occurred after about 31 hours exposure in the 25°C acid solution. Comparing the behaviour shows temperature has a significant influence on the passive state stability. The period of the oscillation decreased from about 31 hours to 567 s as the temperature increased from 25 to 80°C. As discussed later in Section

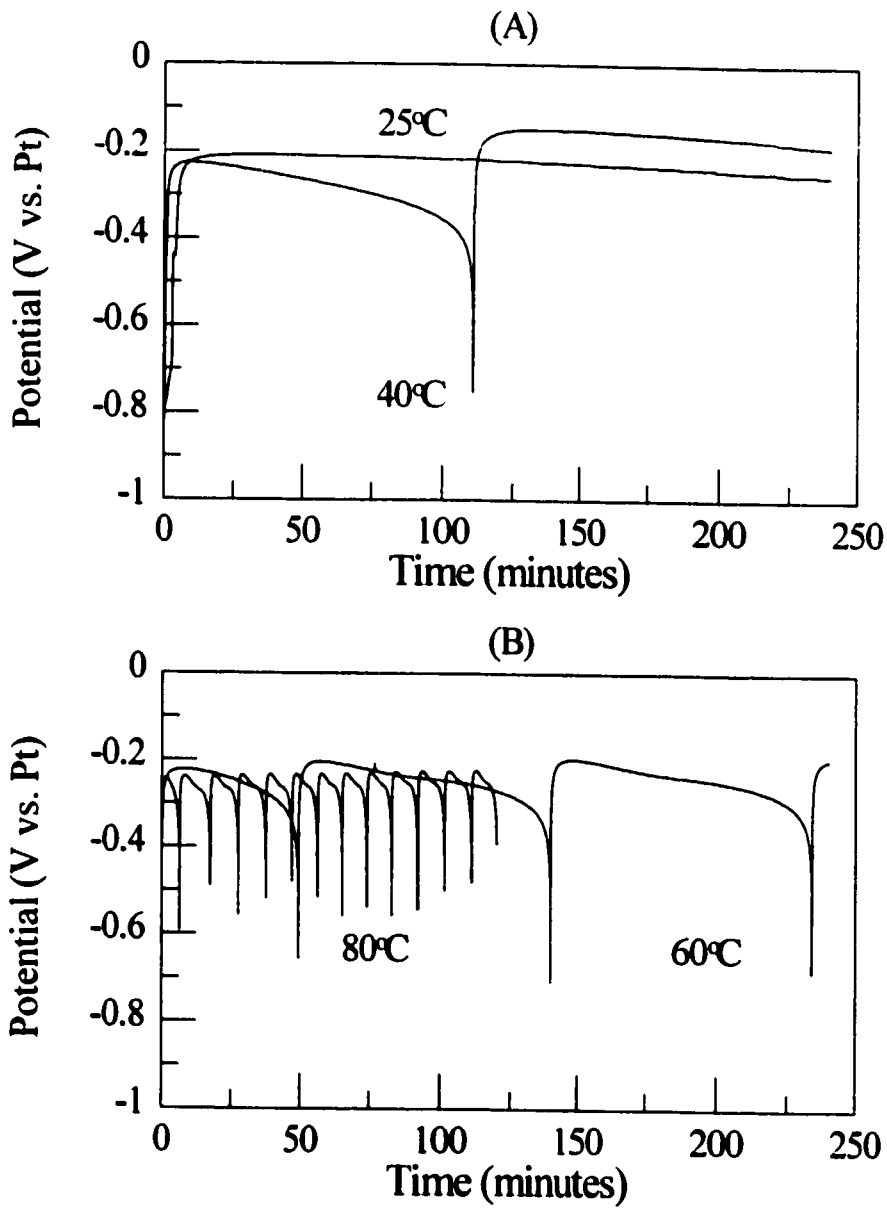


Figure 4.7. Influence of temperature on the corrosion potential of a S30403 RCE (1000 rpm) in 93.5 wt.% $H_2SO_4$ as a function of time immediately after immersion.

6.3.3, the increase in the depassivation tendency, as shown in Figure 4.7, is associated with a decrease in solution viscosity, which occurs with an increase in temperature.

Figure 4.8 shows the effect of temperature on the spike structure. The spike consisted of three distinct stages regardless of temperature: a rapid decrease of potential with time associated with a passive-active transition, a period of slow potential rise with time associated with active state corrosion and a rapid increase in potential with time associated with an active-passive transition. Comparing the behaviour shows that temperature has a strong influence on the active state, the period of the slow potential rise. The active state period decreased from ~600 s (10 min.) to ~ 1 s as the temperature increased from 25 to 80°C. As discussed later in Section 6.3.3, the increase in the passivation tendency, as shown in Figure 4.8, is associated with an increase in temperature and not the associated decrease in solution viscosity.

Table 4.3 shows the influence of temperature on the weight loss of the S30403 RCE (1000 rpm) after 240 minutes exposure in 93.5 wt.% $H_2SO_4$. The weight loss has a complex dependence on temperature; it decreases as the temperature is increased from 25 to 60°C then increases as the temperature is increased from 60-80°C. A more appropriate comparative quantity is the weight loss per spike as the majority of the weight loss occurs during the active state. A shown in Table 4.3, a monotonic decrease in the weight loss per spike occurred as the temperature increased. Further analysis of the weight loss data shows that the rate of weight loss in the active state (weight loss/spike divided by the period of the

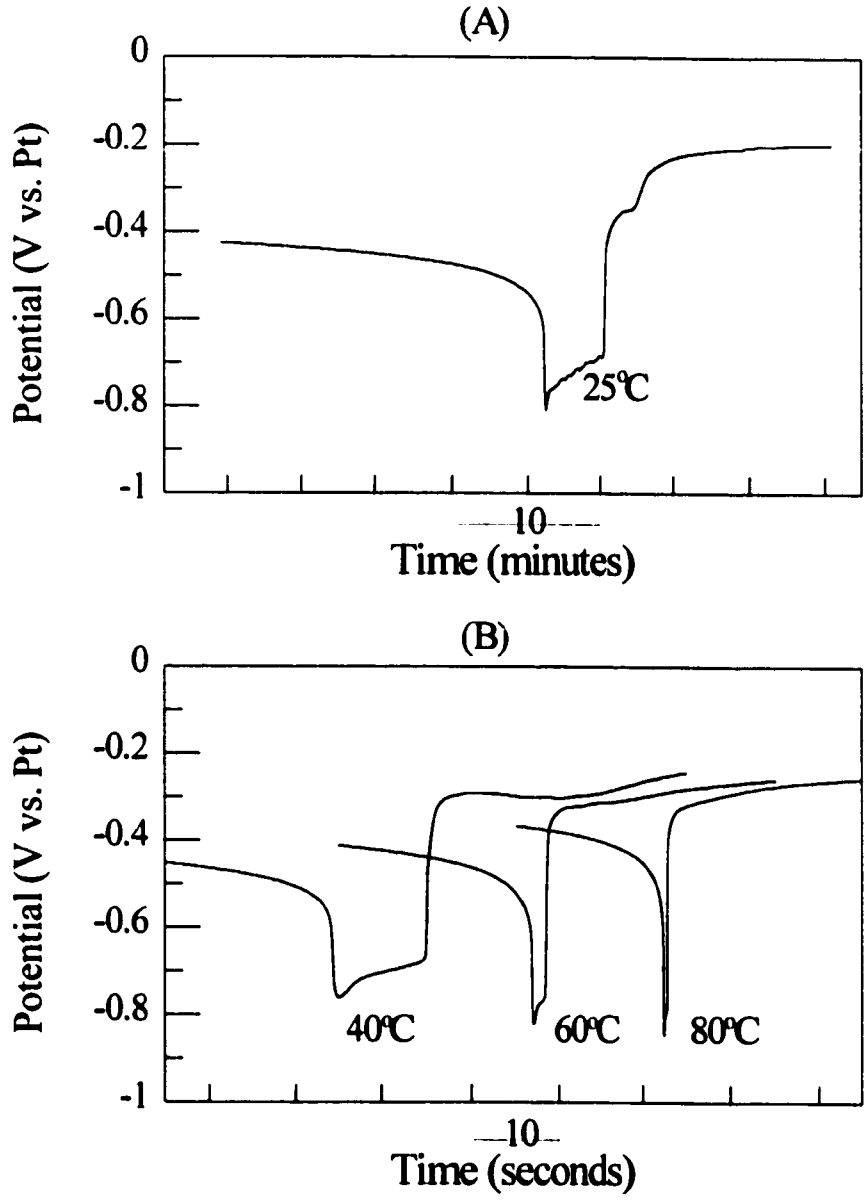


Figure 4.8. Influence of temperature on the corrosion potential of a S30403 RCE (1000 rpm) in 93.5 wt.% $H_2SO_4$ during a potential spike.

spike) increased as the temperature increased. Therefore, the passive state period and the rate/spike determine the overall weight loss of the S30403 electrode during active-passive corrosion.

**Table 4.3.** Influence of Temperature on the Weight Loss of S30403 RCE (1000 rpm) in 93.5 wt.% $H_2SO_4$ at 60°C (after 240 minutes).

| Temperature °C | Weight Loss ($mg/cm^2$) | Weight Loss/Spike ($mg/cm^2/spk$) | Rate/Spike ($\mu g/cm^2/s/spk$) |
|---|---|---|---|
| 25 | .61 | 0.61 | 2 |
| 40 | .57 | 0.29 | 27 |
| 60 | .48 | 0.12 | 60 |
| 80 | 1.10 | 0.08 | 148 |

The dependence of the weight loss/spike on temperature provided further evidence that passivation does not involve the precipitation of a protective metal sulphate film from a supersaturated solution adjacent to the alloy surface. If the passivation process did involve the precipitation of a metal sulphate film, then the weight loss/spike should have increased with increasing temperature since the solubility of metal sulphates increases with temperature in concentrated $H_2SO_4$-$H_2O$ solutions[110]. In fact the weight loss/spike decreased with increasing temperature.

### 4.2.2 Influence of Stirring on Active-Passive Corrosion

Figure 4.9 shows the influence of the rotation rate (stirring) on the corrosion potential of a S30403 RCE in 93.5 wt.% $H_2SO_4$ at 60°C as a function of time. Potential oscillations, representing active-passive corrosion, occurred at all rotation rates studied between 0-2000 rpm. Comparing the behaviour shows the rotation rate has a strong influence on the passive state stability. The period of the oscillations decreased from ~120 to ~50 s as the RCE rotation rate increased from 0 to 2000 rpm. The sensitivity of the passive state period to the rotation rate indicates that the depassivation process is mass transport controlled.

Figure 4.10 shows the influence of the rotation rate on the spike structure. The spike consisted of the three distinct stages previously discussed regardless of the rotation rate. Comparing the behaviour shows the rotation rate has essentially no effect on the active state since the period remained reasonably constant as the rotation rate increased from 0 to 2000 rpm. The results indicate that the passivation process is not mass transport controlled, in contrast to the depassivation process.

Table 4.4 shows the influence of the rotation rate on the weight loss of a S30403 RCE in 93.5 wt.% $H_2SO_4$ at 60°C after 240 minutes exposure. An increase in the rotation rate increased the weight loss, but had essentially no effect on the weight loss per spike or the rate of weight loss per spike. This is consistent with the constant active state period observed regardless of the rotation rate. Therefore, the increased weight loss results from the increased cycle frequency (decreased passive state period) that occurred with an increase in the rotation

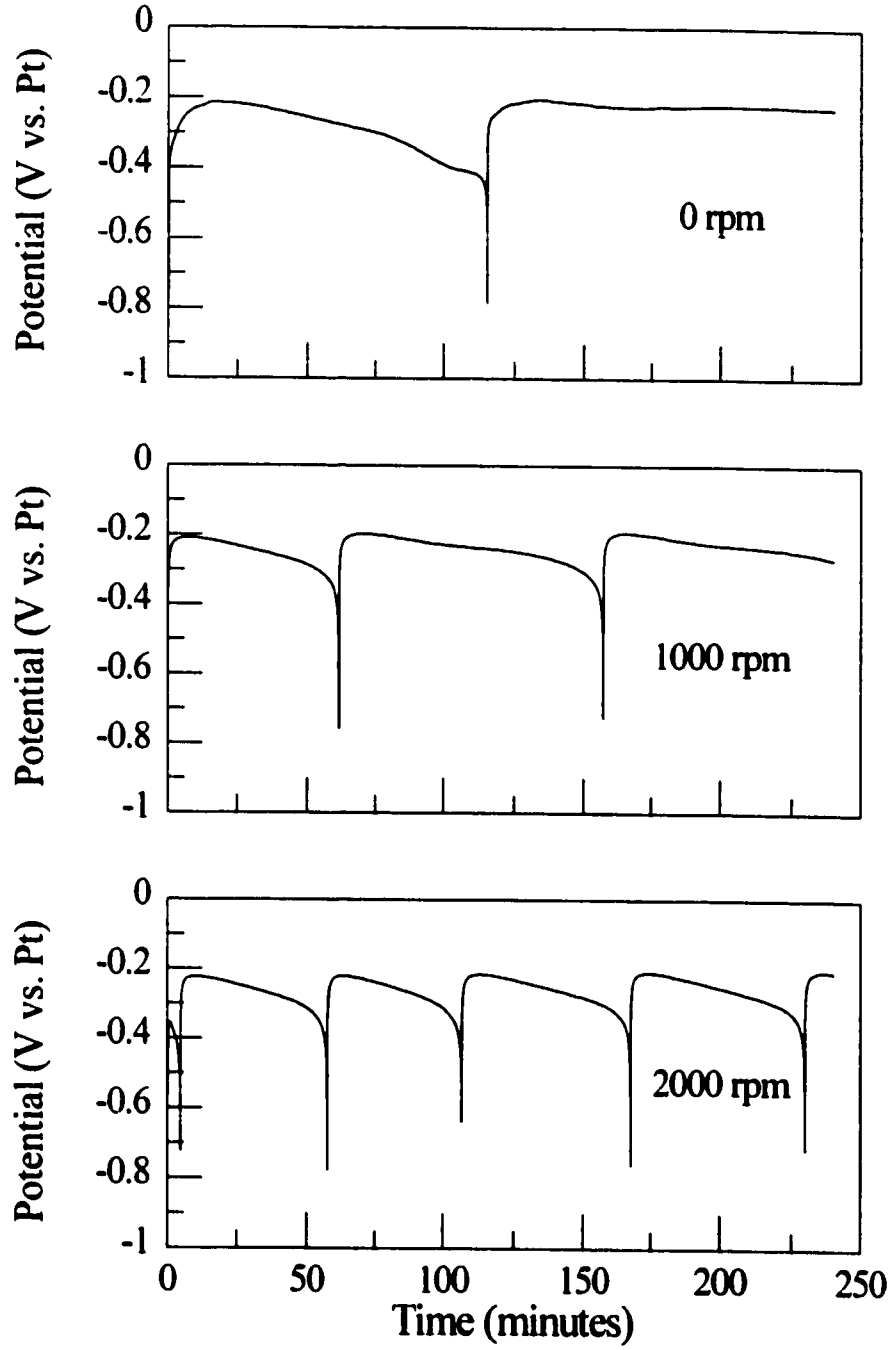


Figure 4.9. Influence of the electrode rotation rate (stirring) on the corrosion potential of a S30403 RCE in 93.5 wt.% $H_2SO_4$ at 60°C as a function of time immediately after immersion.

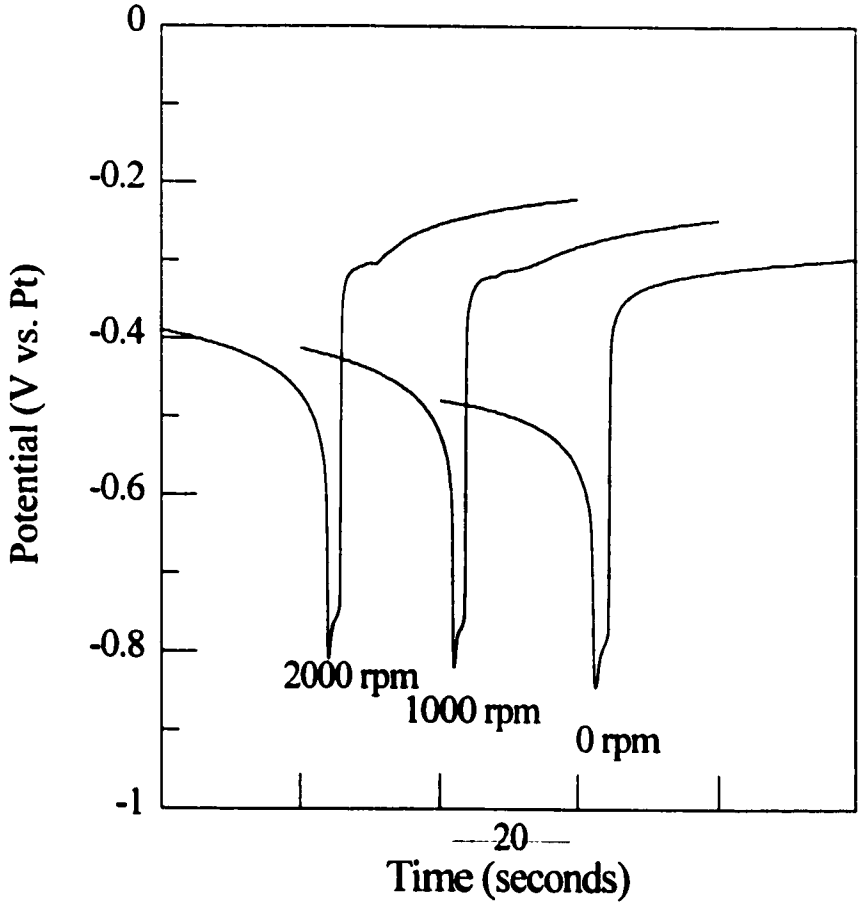


Figure 4.10. Influence of the electrode rotation rate (stirring) on the corrosion potential of a S30403 (RCE) in 93.5 wt.% $H_2SO_4$ at 60°C during a potential spike.

rate. The constant weight loss per spike provided additional evidence that the passivation process does not involve a precipitation of a protective film from a supersaturated solution adjacent to the alloy surface. If passivation did involve the precipitation of a protective film, then the weight loss/spike should have increased with an increase rotation rate in order to counter the enhanced dispersion of corrosion products.

**Table 4.4.** Influence of the Stirring on the Weight Loss of a S30403 RCE in 93.5 wt.% $H_2SO4$ at 60°C (after 240 minutes)

| Rotation Rate (rpm) | Weight Loss ($mg/cm^2$) | Weight Loss/Spike ($mg/cm^2/spk$) | Rate/Spike ($\mu g/cm^2/s/spk$) |
|---|---|---|---|
| 0 | 0.18 | 0.09 | 45 |
| 1000 | 0.48 | 0.12 | 60 |
| 2000 | 0.61 | 0.10 | 50 |

### 4.2.3 Influence of the Dissolved $O_2$ Concentration on Active-Passive Corrosion

It is believed that anodic passivity of S43000 and S30403 in 93.5 wt.% $H_2SO_4$ involves the formation an oxide film. The spontaneous passivation of S30403 requires an oxidizing cathodic reaction capable of providing the necessary driving force and current to anodically passivate the alloy and capable of providing oxygen atoms. As discussed above, the more oxidizing cathodic process may involve the reduction of $H_2SO_4$ molecules to elemental sulphur. Another possible reaction is the reduction of dissolved oxygen.

Oxygen may be reduced, depending on the specific kinetic parameters of the metal-solution system, in acidic solutions according to [4.5][112,113].

$$O_2 + 4H^+ + 4e^- = 2H_2O \qquad [4.5]$$

The solubility of $O_2$ increases from 0.018 to 0.042 g/L at 15.5°C as the $H_2SO_4$ concentration in $H_2SO_4$-$H_2O$ solutions increases from 82 to 95 wt.%[114]. Considering the moderate solubility and the equilibrium redox potential of +1.299 $V_{SHE}$, it is possible the reduction of $O_2$ in concentrated $H_2SO_4$-$H_2O$ mixtures may spontaneously anodically passivate nickel-stainless steel. It is noted that Kuzub *et al.*[68] found potential oscillations for S30400 in deaerated 92.0 wt.% $H_2SO_4$ and concluded that dissolved oxygen had no effect on the active-passive corrosion. Experiments conducted to explore the influence of the dissolved $O_2$ concentration involved comparing and contrasting the corrosion behaviour of a S30403 RCE in as-mixed, aerated and deaerated 93.5 wt.% $H_2SO_4$ at 60°C.

Figure 4.11 shows the influence of dissolved $O_2$ on the corrosion potential of a S30403 RCE (1000 rpm) in 93.5 wt.% $H_2SO_4$ at 60°C as a function of time. Neither aerating or deaerating the acid solution for 30 minutes prior to immersion had a significant effect on the amplitude or period of the potential oscillations measured in the as-mixed acid solution. The period of the potential oscillations increased slightly in the deaerated solution which suggests that the passive state stability is marginally improved without dissolved $O_2$. Studying the influence of the rotation rate showed that the depassivation process is mass

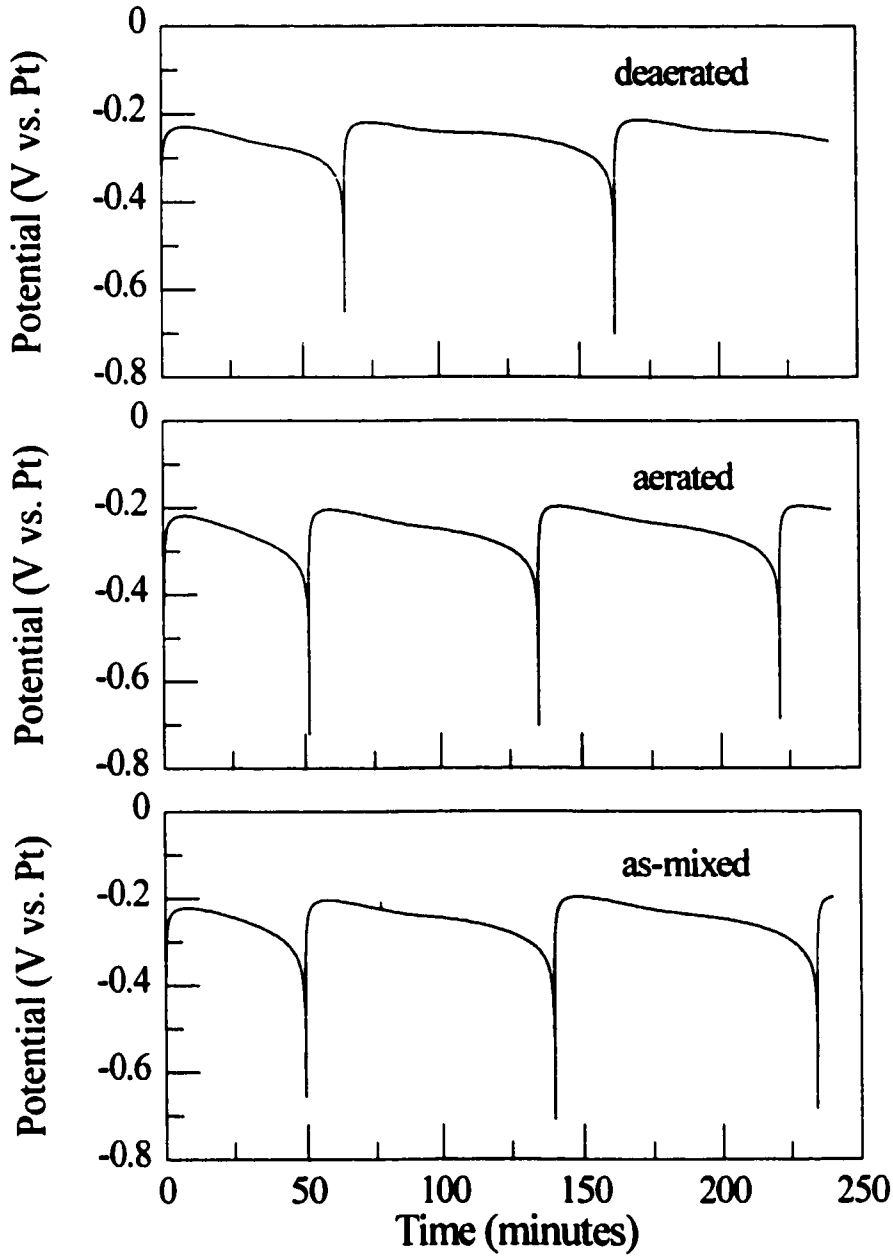


Figure 4.11. Influence of aeration on the corrosion potential of a S30403 RCE (1000 rpm) in 93.5 wt.% $H_2SO_4$ at 60°C as a function of time immediately after immersion.

transport controlled. Therefore, if the $O_2$ reduction is the primary cathodic reaction responsible passivation, then its reduced concentration at the alloy-solution interface in the deaerated solution should decrease the passive state period.

Figure 4.12 shows the influence of dissolved $O_2$ on the spike structure of S30403 in 93.5 wt.% $H_2SO_4$ at 60°C as a function of time. Again, neither aerating or deaerating the solution for 30 minutes prior to immersion had a significant influence on the active state period measured in the as-mixed acid. The results suggest that the spontaneous passivation process does not involve the participation of dissolved $O_2$.

Weight loss measurements provided additional evidence that dissolved oxygen has little effect on the passive state stability and the corresponding active-passive corrosion of S30403. Table 4.5 displays the influence of the dissolved $O_2$ concentration on the weight loss of a S30403 RCE (1000 rpm) in 93.5 wt.% $H_2SO_4$ at 60°C. Neither aerating or deaerating the acid solution had a significant influence on the weight loss, weight loss per spike or the rate per spike. The independence of the weight loss on the dissolved $O_2$ concentration is consistent with the independence of the active and passive state period on the dissolved $O_2$ concentration.

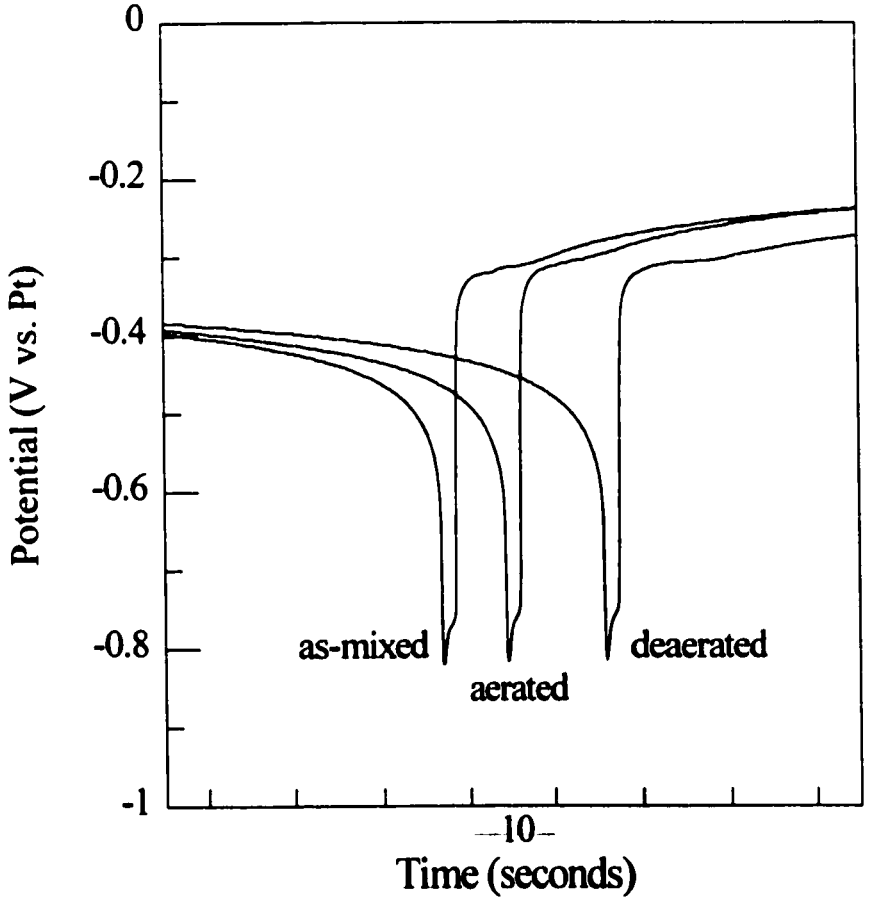


Figure 4.12. Influence of aeration on the corrosion potential of a S30403 RCE (1000 rpm) in 93.5 wt.% $H_2SO_4$ at 60°C during a potential spike.

**Table 4.5.** Influence of the Dissolved $O_2$ Concentration on the Weight Loss of a S30403 RCE (1000 rpm) in 93.5 wt.% $H_2SO_4$ at 60°C (after 240 minutes)

| Acid Condition | Weight Loss ($mg/cm^2$) | Weight Loss/Spike ($mg/cm^2/spk$) | Rate/Spike ($\mu g/cm^2/s/spk.$) |
|---|---|---|---|
| as-mixed | 0.48 | 0.12 | 60 |
| aerated | 0.48 | 0.12 | 60 |
| deaerated | 0.39 | 0.13 | 65 |

### 4.2.4 Summary

Experiments conducted to clarify the conditions in which the passive state is stable involved studying the influence of temperature, stirring (RCE rotation rate) and the dissolved $O_2$ concentration on the active-passive corrosion behaviour of a S30403 RCE. The results confirmed that the passive state stability, quantitatively represented by the passive state period, is dependent on temperature and stirring but is independent of the dissolved $O_2$ concentration. An increase in either temperature or stirring decreases the passive state stability. The weight loss that occurs during active-passive corrosion is a function of the weight loss rate per spike, and the active state period along with the passive state period. Passivation involves a different mechanism than depassivation since only the depassivation process is sensitive to stirring. The non influence of the dissolved $O_2$ concentration indicates that a more oxidizing reaction other than the reduction of dissolved $O_2$ provides the necessary driving force, current and a source of oxygen atoms required to spontaneously passivate the

alloy.

## 4.3. Behaviour of Major Alloying Elements in 93.5 wt.% $H_2SO_4$ at 60°C

A previous study by Hurtado *et al.*[115] showed that examining the electrochemical behaviour of the major alloying elements proved powerful in their attempt to understand the corrosion potential oscillations of a Cu-Ag-Au alloy in 0.5 M NaOH. Therefore, this study involved a similar approach to meet the third objective defined in Section 4.0. The following sections present and discuss the results of the corrosion and anodic polarization measurements respectively made on polycrystalline iron, chromium and nickel electrodes. All experiments reported were conducted in 93.5 wt.% $H_2SO_4$ solutions at 60°C that were mechanically stirred by a glass impeller that was driven by an overhead motor.

### 4.3.1 Corrosion of Iron, Chromium and Nickel in Agitated 93.5 wt.% $H_2SO_4$

Figure 4.13 shows the corrosion potential of the iron, chromium and nickel electrodes in stirred 93.5 wt.% $H_2SO_4$ at 60°C as a function of time. The potential of both the iron and chromium electrodes behaved in a similar manner, attaining a reasonably stable plateau within the first two minutes of exposure, and then remaining at that value. The corrosion potential of the iron electrode stabilized at ~-0.77 $V_{Pt}$, whereas the corrosion potential of chromium electrode stabilized at ~-0.90 $V_{Pt}$. Visible gas evolution occurred from the surface of both metals during the entire test. The gas is believed to be $H_2$ as the corrosion potential

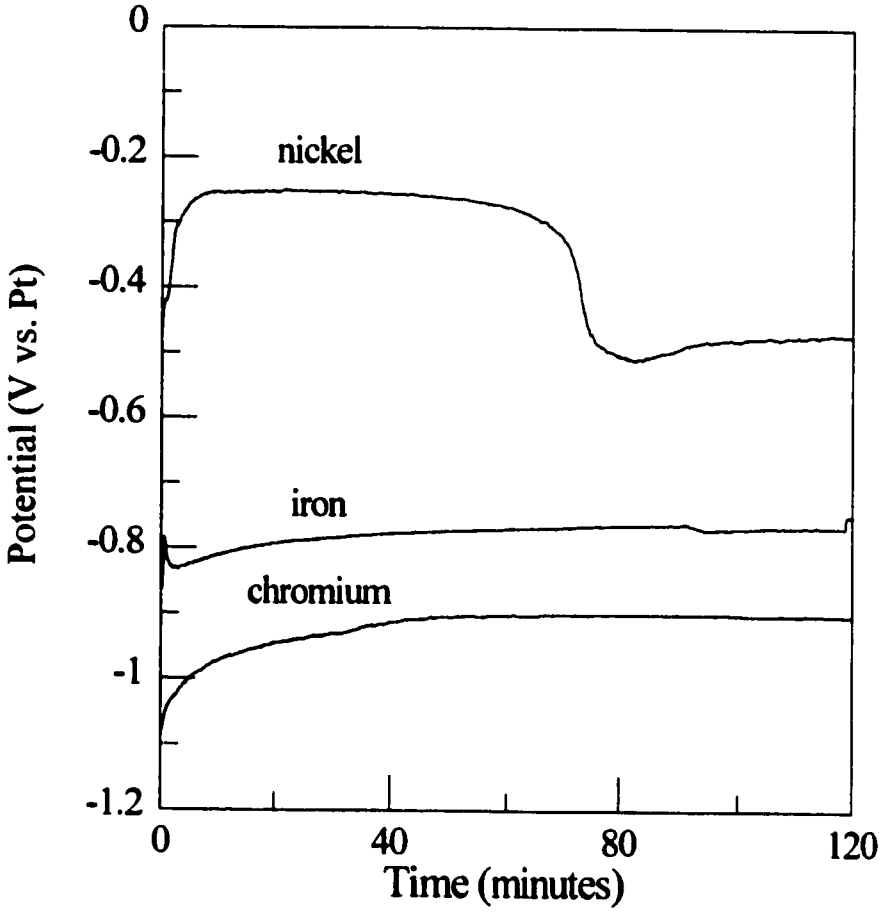


Figure 4.13. Corrosion potential of iron, chromium and nickel electrodes in agitated 93.5 wt.% $H_2SO_4$ at 60°C as a function of time immediately after immersion.

plateaus of both metals electrodes are more negative than the redox potential of the $H_2$ evolution reaction (-0.607 $V_{Pt}$ in 93.5 wt.% $H_2SO_4$ at 25°C).

The corrosion potential behaviour of the nickel electrode is significantly different from that of iron and chromium since it consisted of two plateaus. The first potential plateau occurred at ~-0.25 $V_{Pt}$ and lasted for ~40 minutes. During this time, the majority of the nickel electrode was covered with a black surface deposit. After about 40 minutes the potential decayed relatively quickly to a second, more negative plateau of ~-0.50 $V_{Pt}$ where it remained stable. At the lower potential plateau the nickel electrode had a film free, dull grey surface appearance after 120 minutes exposure. No visible gas evolution occurred from the nickel surface during either of the potential plateaus. Therefore, the cathodic process involved in the corrosion of nickel electrode at either plateau is different than the gas ($H_2$) evolving cathodic process that occurred during the corrosion of both the iron and chromium electrodes.

Table 4.6 shows the weight loss of the three metals electrodes measured after the 120 minutes exposure. A relatively high weight loss occurred for all three metal electrodes. Comparing the data shows that neither the different cathodic processes nor the black surface deposit involved in the corrosion of the nickel electrode had a significant influence on the corrosion resistance of nickel electrode over that of both the iron and chromium electrodes.

**Table 4.6.** Weight Loss of Iron, Chromium and Nickel Electrodes in Agitated 93.5 wt.% $H_2SO_4$ at 60°C (after 120 minutes)

| Metal | Weight Loss ($mg/cm^2$) |
|---|---|
| Iron | 2.14 |
| Chromium | 5.32 |
| Nickel | 2.34 |

### 4.3.2 Anodic Polarization of Iron, Chromium and Nickel

Potentiodynamic anodic polarization scans of the three metals electrodes in agitated 93.5 wt.% $H_2SO_4$ at 60°C provided more information regarding their respective individual corrosion behaviours. Scans were conducted over a potential range corresponding to the potential extremities observed during the potential oscillations of the nickel-stainless steel S30403. For the nickel electrode, one scan was initiated from the more positive corrosion potential plateau and a second from the more negative corrosion plateau.

Figure 4.14 shows the potentiodynamic anodic polarization curves for the three metal electrodes. The anodic polarization of both the iron and nickel electrode consisted of a limiting anodic current (~1 $mA/cm^2$) over the potential range under examination, which for the nickel electrode was independent of the starting potential. The limiting anodic current likely is consistent with the precipitation of a semi-protective sulphate film that is known to form on both iron[84] and nickel[93] in concentrated $H_2SO_4$-$H_2O$ solutions at ambient temperatures. The similar magnitude of the limiting anodic current of the two nickel

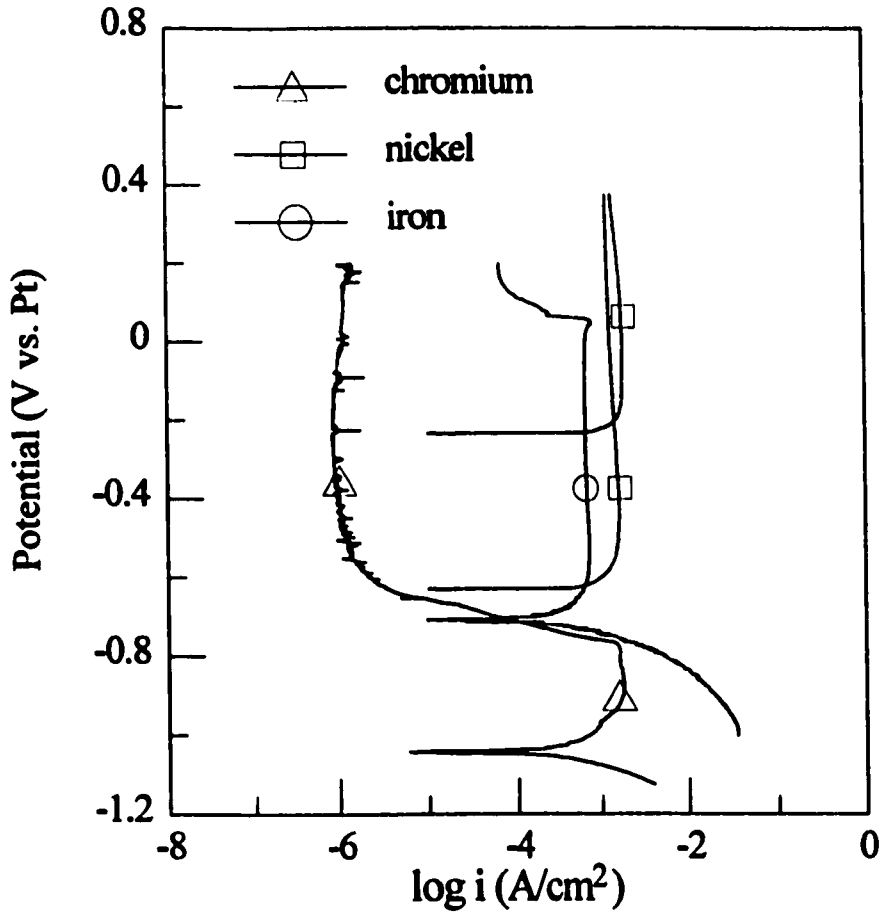


Figure 4.14. Potentiodynamic anodic polarization of iron, chromium and nickel electrodes in agitated 93.5 wt.% $H_2SO_4$ at 60°C. Scan rate = 20 mV/min.

polarization scans indicate the black surface deposit does not possess any additional protective capability.

The anodic polarization of the chromium electrode is significantly different from that of both the iron and nickel electrodes since it possessed an active-passive transition when the potential was made more positive. The anodic polarization behaviour at 60°C is consistent with that reported in the literature for ambient temperatures[96,97,98,99]. Therefore, the anodic passivity displayed by the chromium electrode likely results from a similar solid state formation of CrOOH film[97,98]. The magnitude of the weight loss measured after 120 minutes combined with the anodic polarization behaviour show chromium passivity is not spontaneous in 93.5 wt.% $H_2SO_4$ at 60°C and requires anodic polarization.

Recording the open-circuit potential response of chromium electrode after anodic polarization provided information regarding the stability of the anodic passive film. Figure 4.15 shows the open-circuit potential response as a function of time. The open-circuit potential of the chromium electrode decayed slowly for a period of ~22 minutes before it decayed rapidly and became stable at a potential plateau similar to that observed prior to the anodic polarization measurement. Comparing the potential response with the anodic polarization behaviour shows that the anodically formed passive state is not stable in stirred 93.5 wt.% $H_2SO_4$ at 60°C without anodic polarization. Depassivation of chromium likely occurred as a result of the high solubility of CrOOH passive film. This is plausible considering the high acidity of 93.5 wt.% $H_2SO_4$ since the dissolution of hydrated chromium

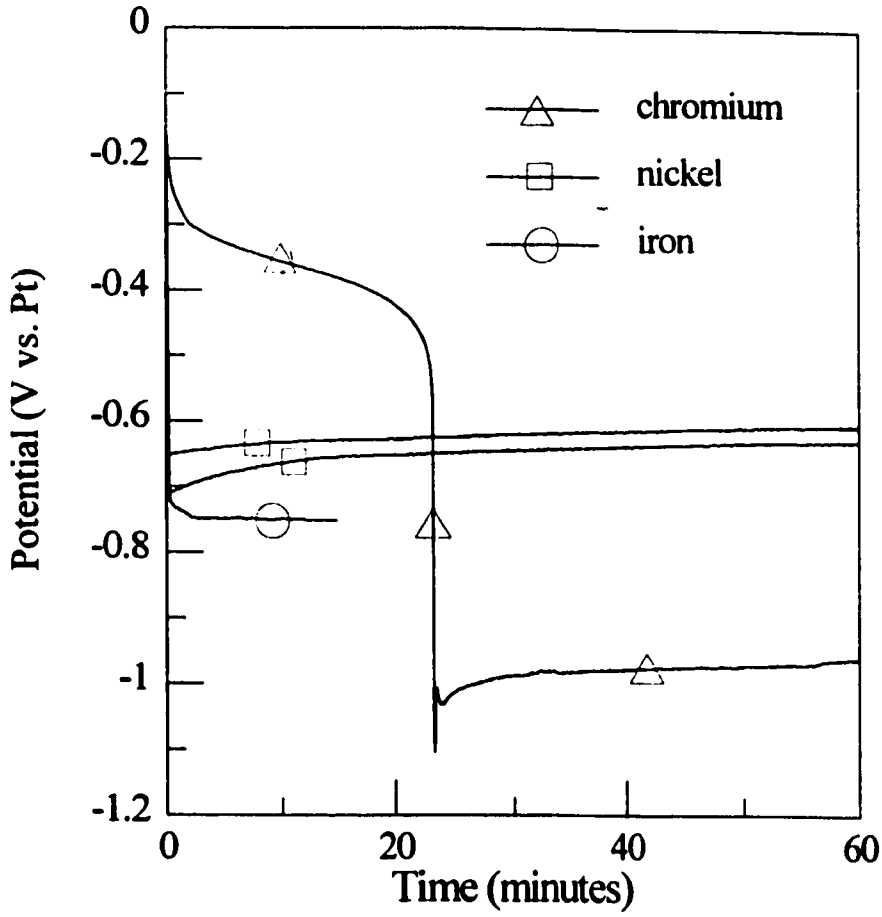


Figure 4.15. Open-circuit potential response after potentiodynamic anodic polarization of iron, chromium and nickel electrodes in agitated 93.5 wt.% $H_2SO_4$ at 60°C.

oxides increases with the proton activity (acidity) in mineral acids such as $H_2SO_4$-$H_2O$ solutions[116].

Superimposed in Figure 4.15 is the open-circuit potential response of the iron and nickel electrode after anodic polarization terminated. The potential of both the iron and nickel electrodes rapidly decayed and became stable within the first few minutes. For the iron electrode, the stable open-circuit potential coincides with its corrosion potential. For the nickel electrode, the stable potential coincides with its more negative corrosion potential plateau, regardless of the initial corrosion potential at which polarization began. Therefore, the precipitated sulphate film on either of the two metals has no influence on the resultant corrosion potential.

### 4.4. Stainless Steel Corrosion Mechanisms

The final step taken to meet the objectives outlined in Section 4.0 involved proposing a tentative explanation of the stainless steel S43000 and S30403 corrosion mechanism in 93.5 wt.% $H_2SO_4$. Proposing a tentative explanation clarified areas that required a more detailed investigation in order to meet the overall objective of the study defined in Section 1.1. The following sections discuss anodic passivity of 17 wt.% chromium-stainless steels, the S43000 corrosion mechanism and the S30403 corrosion mechanism respectively.

### 4.4.1 Anodic Passivity of 17 wt.% Chromium-Stainless Steels

Anodic polarization measurements revealed that stainless steels S43000 and S30403 passivate at anodic potentials in stirred 93.5 wt.% $H_2SO_4$ at 60°C. An AES analysis of the passive surface of a S43000 electrode is consistent with the formation of an oxide passive film; the formation of which likely involves the participation of $H_2SO_4$ molecules as the source of oxygen atoms.

Chromium is the only metal of the three metals studied to show passivity with anodic polarization up to 0.0 $V_{Pt}$. The rather large limiting anodic current of the iron and nickel electrode (~1 $mA/cm^2$) and the much lower passive current of the chromium (~1 $\mu A/cm^2$) electrode suggests chromium plays an active role in the anodic passivation of 17 wt.% chromium-stainless steels. The ability of the 17 wt.% chromium stainless to anodically passivate with the formation of an oxide film steels supports this idea.

Superimposing the anodic polarization behaviour of the chromium electrode with the anodic polarization of the iron and the S43000 electrode, Figure 4.16, provides additional evidence of chromium's role in anodic passivation. If the S43000 electrode is equivalent to the iron electrode alloyed with 17 wt.% chromium then the passive properties of chromium are successfully conferred to an iron-based alloy when alloyed to 17 wt.%.

### 4.4.2 Corrosion Mechanism of S43000

The stainless steel S43000 electrode dissolved in an active state with the evolution

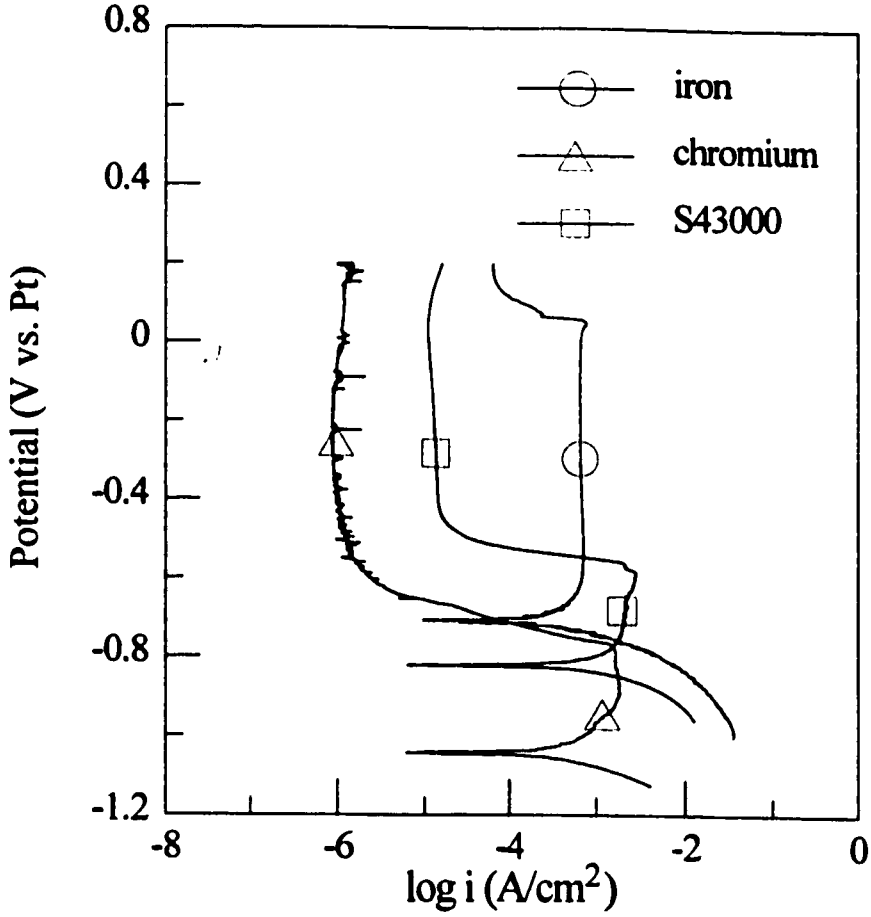


Figure 4.16. Superimposed anodic polarization curves of the iron, chromium and S43000 electrodes in agitated 93.5 wt.% $H_2SO_4$ at 60°C.

of $H_2$ in stirred 93.5 wt.% $H_2SO_4$ at 60°C. Considering that both the iron and chromium electrodes dissolved in an active state which involved the evolution of $H_2$ as the principal cathodic reaction, it is not surprising that the S43000 electrode dissolved with a similar mechanism. Spontaneous passivation of the S43000 electrode did not occur during corrosion since the equilibrium potential for $H_2$ evolution is more negative than the passivation potential.

A previous study by Yau and Streicher[117] found that chromium has a detrimental effect on the corrosion resistance of iron in 1.0 N (~5 wt.%) $H_2SO_4$ at 30-101°C. Alloying iron with 14 wt.% chromium increased the corrosion rate to various degrees depending on the temperature. The effect is more pronounced as the chromium content increased. The increase in corrosion rate with an increase in the chromium content is attributed to the enhanced electrochemical activity which shifts the equilibrium potential of the anodic reaction in the negative direction. The cathodic $H_2$ evolution reaction was found to be independent of the chromium content, that is, the exchange current density ($i_o$) and Tafel slope ($\beta_c$) were essentially constant. Therefore, according to mixed potential theory, the negative shift in the reversible potential shifts the corrosion potential in the negative direction and increases the corrosion current (rate).

It is plausible that the mechanism through which chromium enhances the corrosion of iron reported by Yau and Striecher occurs in stirred 93.5 wt.% $H_2SO_4$ since the primary cathodic reaction is the evolution of $H_2$. Table 4.7 shows the weight loss of the iron and the

S43000 electrode after 120 minutes in stirred 93.5 wt.% $H_2SO_4$ at 60°C. The S43000 electrode has a more negative corrosion potential and a higher weight loss rate than the iron electrode. If the S43000 electrode is equivalent to the iron electrode alloyed with 17 wt.% chromium, then the Yau and Striecher chromium-enhanced corrosion mechanism successfully explains the corrosion of S43000.

**Table 4.7.** Weight Loss Rate and Corrosion Potential of an Iron and a S43000 Electrode in Stirred 93.5 wt.% $H_2SO_4$ at 60°C (after 120 minutes)

| Material | [Cr] wt.% | Weight Loss ($mg/cm^2/hr$) | $E_{corr}$ ($V_{Pt}$) |
|---|---|---|---|
| iron | 0 | 1.07 | -0.750 |
| S43000 | 16.9 | 3.37 | -0.777 |

### 4.4.3 Corrosion Mechanism of S30403

The nickel-stainless steel S30403 dissolved in an active-passive state in stirred 93.5 wt.% $H_2SO_4$ at 25-80°C which is characterized by an oscillating corrosion potential. The ability of the S30403 electrode to spontaneously passivate, albeit periodically, relies on its 7.9 wt.% alloyed nickel content. Measurements conducted on the individual alloying elements show that nickel has a different corrosion mechanism than iron and chromium, one which significantly affects the corrosion potential behaviour but not the magnitude of weight

loss. Superimposing the corrosion potential of the iron, chromium and nickel electrode with a characteristic potential cycle of the S30403 electrode, Figure 4.17, provides more information regarding the nickel-induced, active-passive corrosion state. The more positive potential plateau of the nickel electrode correlates well with the passive state potential maximum of the S30403 electrode. In contrast, the potential plateau of the iron electrode correlates well with the potentials attained during the active state period of the S30403 electrode. The comparison suggests that reactivity of nickel controls the potential during the passive period of the cycle, whereas the reactivity of iron and likely chromium control the potential during the active period of the cycle.

A possible mechanism by which active-passive corrosion of nickel-stainless steel occurs is proposed as follows. Beginning with the active state, iron and chromium atoms dissolve in an active state with $H_2$ evolution as the primary cathodic reaction. The reactivity of nickel results in the formation of a nickel-rich corrosion product, identical to the black corrosion product film formed on pure nickel. The formation of this substance induces a significant anodic polarization which rapidly increases potential of the nickel-stainless steel in the positive direction and establishes the characteristic passive potential plateau in a manner similar as that observed for pure nickel. Passivation is possible as the equilibrium potential of the more oxidizing cathodic process associated with the nickel-rich corrosion product is more positive than the passivation potential and the current is greater than the critical current required for passivation. During the passive potential plateau, the nickel-rich

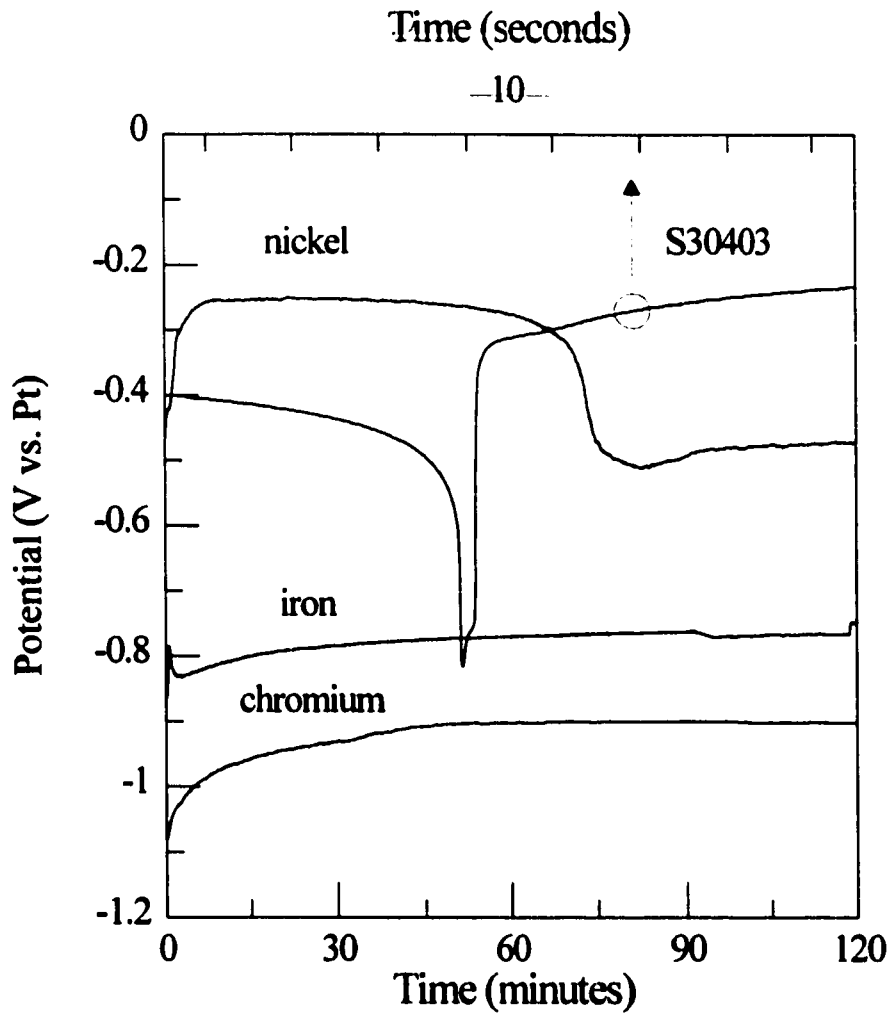


Figure 4.17. Superimposed corrosion potential of iron, chromium, nickel and S30403 (during a potential spike) electrodes in agitated 93.5 wt.% $H_2SO_4$ at 60°C.

corrosion product slowly dissolves which causes the potential to slowly depolarize in a similar manner as that observed for pure nickel. The rapid dissolution of the passive film without anodic polarization coupled with the reactivity of iron and chromium atoms rapidly depolarize the potential to the more negative values observed during the period of the active state. At this point the entire process repeats.

The black surface deposit that formed on the nickel electrode during corrosion is believed to have a strong influence on both the passivation and depassivation processes during active-passive corrosion of the nickel-stainless steel S30403 electrode. Elucidating the mechanism through which the active-passive corrosion occurs required information regarding the composition of the black deposit along with its formation and dissolution mechanism. The review of the literature discussed in Section 2.4 shows that the corrosion mechanism of nickel in concentrated $H_2SO_4$-$H_2O$ solutions is not well-defined and, therefore, needed to be explored in some detail in this study.

If the black deposit has a strong influence on the passivation and depassivation process then the conditions in which the state of passivity is stable determined in Section 4.2 are misleading. Exploring conditions in which the passive state of 17 wt.% chromium-stainless steels is stable in 93.5 wt.% $H_2SO_4$ required information regarding the anodic passive state stability of S43000 as a function of temperature and stirring. The literature discussed in Section 2.3 shows that the anodic passive state stability of Fe-Cr stainless steels is not well-defined and, therefore, needed to be explored in some detail in this study.

## 4.5 Summary

The investigation began by conducting a series of corrosion tests designed to test pre-conceived ideas regarding, the state of stainless steel passivity, the conditions in which it is stable, the role played by the major alloying elements in determining that state and to identify specific areas that require further research. The experimental approach used to meet these objectives involved making weight loss and electrochemical measurements on S43000, S30403, iron, chromium and nickel electrodes in stirred 93.5 wt.% $H_2SO_4$ at 60°C. Testing preconceived ideas regarding the state of passivity involved comparing the corrosion and electrochemical behaviour of a S43000 and S30403 electrode. Testing preconceived ideas regarding the conditions in which the passive state is stable involved exploring the influence of temperature, stirring (RCE rotation rate) and dissolved oxygen on the corrosion behaviour of a S30403 RCE. Testing preconceived ideas regarding the role of the alloying elements in determining passivity involved comparing and contrasting the corrosion and electrochemical behaviour of a iron, chromium and nickel electrode. Identifying areas for further investigation involved establishing a tentative theory that provides a reasonable explanation for all the facts.

The major findings of the results presented and discussed in this chapter may be summarized as follows. Stainless steel alloys containing 17 wt.% chromium anodically passivate in stirred 93.5 wt.% $H_2SO_4$. Anodic passivity likely involves the formation of a protective thin oxide film with the participation of $H_2SO_4$ molecules as the source of oxygen.

The ability of 17 wt.% chromium-stainless steels to spontaneously passivate, albeit periodic, relies on the alloyed nickel; spontaneous passivation does not occur without alloyed nickel. The stability of the spontaneous passivate state is sensitive to temperature and stirring (RCE rotation rate); an increase in either shortens the passive state period and, therefore, the passive state stability. The weight loss during active-passive corrosion is a function of the rate of weight loss in the active state, the period of the active state and the period of the passive state. The ability of alloyed nickel to spontaneously passivate 17 wt.% chromium stainless steel is believed to be related to the formation and subsequent dissolution of a black nickel corrosion deposit. Necessarily associated with this black deposit is a more oxidizing cathodic reaction that provides the driving force and current required to anodically passivate the 17 wt.% chromium stainless steel.

A discussion of the results identified two key areas requiring further investigation. The first area involves the corrosion mechanism of nickel in 93.5 wt.% $H_2SO_4$. The second area involves the influence of temperature and stirring on the anodic passivity of S43000 in 93.5 wt.% $H_2SO_4$. The next chapter, Chapter 5, presents and discusses the results of a more detailed study of the corrosion and electrochemical behaviour of pure nickel in 93.5 wt.% $H_2SO_4$. Experiments conducted to explore the corrosion of S43000 as a function of temperature and stirring are not discussed until Chapter 6. The discussion is better served when discussing the galvanic-passivation theory proposed to explain the active-passive corrosion behaviour of S30403.

# CHAPTER 5

## 5. CORROSION OF NICKEL IN 93.5 wt.% $H_2SO_4$

As shown in Chapter 4, the approach of studying the corrosion and electrochemical behaviour of the major alloying elements proved to be powerful in providing more insight regarding the role of the major alloying elements in imparting corrosion resistance to the nickel-stainless steel S30403. The preliminary experiments conducted indicate that nickel corrodes by a different mechanism in 93.5 wt.% $H_2SO_4$ than that for iron and chromium. The black surface deposit that forms and subsequently dissolves during the corrosion of nickel is believed to play a major role in the passivation and depassivation process involved in the active-passive corrosion of S30403. A better understanding of the corrosion mechanism of nickel is necessary to meet the primary objectives defined in Section 1.1.

The objective of the research presented and discussed in this chapter is to elucidate the corrosion mechanism of nickel in 93.5 wt.% $H_2SO_4$ in order to provide answers to the

following questions:

1. What is the black deposit that forms during the initial stage of nickel corrosion?
2. What is the mechanism through which the black deposit forms and subsequently dissolves during the corrosion of nickel?
3. Does the formation and subsequent dissolution of the black deposit significantly influence the corrosion potential of nickel?
4. Does the formation and subsequent dissolution of the black deposit only occur once during the corrosion of nickel?
5. Does change in temperature and/or stirring affect the rate of formation and/or subsequent dissolution of black deposit?

The experimental approach used to work through the problem involved a long term corrosion test in quiet 93.5 wt.% $H_2SO_4$ at 60°C and a series of short term corrosion tests in stirred 93.5 wt.% $H_2SO_4$ at 50-80°C. The long term test employed immersion, electrochemical and X-ray spectroscopy techniques to characterize the soluble and insoluble anodic and cathodic products that form as a function of time during the corrosion of nickel. The short term test in stirred solutions employed electrochemical techniques using rotating electrodes to characterize the influence of stirring, bulk nickel ion concentration and temperature on the different processes that occur during the corrosion of nickel. The

interpretation of the results led to the development of a mechanistic model that provides a consistent account of the experimental observations.

This chapter is organized into five major sections. The first two sections present the experimental results of corrosion tests conducted in quiet and stirred 93.5 wt.% $H_2SO_4$ at 60°C, respectively. The third section presents the experimental results of the electrochemical test conducted to explore the influence of NiS (the black deposit) on the corrosion potential of nickel in stirred 93.5 wt.% $H_2SO_4$ at 60°C. The fourth section proposes the mechanistic model believed to be responsible for the corrosion of nickel in 93.5 wt.% $H_2SO_4$. The fifth section summarizes the major conclusions drawn from the research conducted in this chapter and their contribution in meeting the objectives of the study as a whole.

## 5.1 Corrosion of Nickel in Quiet 93.5 wt.% $H_2SO_4$ at 60°C

The first step taken to meet the aforementioned objectives involved repeating the corrosion test of nickel in 93.5 wt.% $H_2SO_4$ at 60°C conducted in Section 4.3, but employing additional techniques to characterize the various corrosion products that form. A review of the relevant literature regarding possible soluble and insoluble anodic and cathodic corrosion products provided a better idea of what to expect prior to and, thus, monitor during the corrosion test.

### 5.1.1 Possible Soluble and Insoluble Anodic and Cathodic Products

The review of the literature discussed in Section 2.4 showed that there is limited knowledge regarding actual products that form during the corrosion of nickel in concentrated $H_2SO_4$-$H_2O$ solution. Anodic polarization studies show that nickel atoms anodically dissolve with the formation of soluble ions that subsequently lead to the precipitation of a protective $NiSO_4 \cdot 6H_2O$. Therefore, one soluble anodic product in the corrosion of nickel is nickel ions which may result in the formation of hydrated, but more likely anhydrous, solid nickel sulphate depending on its solubility. The formation of a hydrated film in 15-18 M $H_2SO_4$ seems odd considering that no free water molecules exist in concentrated $H_2SO_4$-$H_2O$ solutions.

No reliable data on the solubility of nickel sulphate in concentrated $H_2SO_4$-$H_2O$ at the temperature of interest were found in the literature. Kendal and Davidson[118] reported that 0.25 mol.% $NiSO_4$ dissolved in 100 wt.% $H_2SO_4$ at ambient temperatures to give a clear yellow solution. Halstead and Lovey[119] found that the $NiSO_4$ solubility depended on concentration and temperature in 70-90 wt.% $H_2SO_4$. The solubility decreased from about 0.47 to 0.24 wt.% as the $H_2SO_4$ concentration increased from 82 to 90 wt.% at 110°C. In 90 wt.% $H_2SO_4$, the solubility increased from about 0.24 to 0.75 wt.% as the temperature increased from 110 to 190°C. Therefore, it is reasonable to expect the formation of $NiSO_4$, due to its moderate solubility, during corrosion of nickel.

Although the cathodic process involved in the corrosion of nickel is not known, a model can be proposed by considering various reduction reactions proposed in the literature. The literature discussed in Section 2.3 indicates that the cathodic process in concentrated $H_2SO_4$-$H_2O$ solutions can include the reduction of $H_2SO_4$ molecules, forming $SO_2$, elemental sulphur and $H_2S$, along with the evolution of hydrogen. According to Banas and Stypula[97], the reaction likely responsible for the more oxidizing redox potential of concentrated $H_2SO_4$-$H_2O$ solutions involves the reduction of $H_2SO_4$ molecules according to,

$$HSO_4^- + 3H^+ + 2e^- = SO_2 + 2H_2O \qquad [5.1]$$

with the formation of $SO_2$ as the reduction product. Assuming that $SO_2$ is a reduction product involved in the corrosion of nickel in 93.5 wt.% $H_2SO_4$, corrosion should initially occur without the gas evolution since $SO_2$ has a moderate solubility in concentrated $H_2SO_4$-$H_2O$ solutions[120]. The solubility of $SO_2$ in 93.5 wt.% $H_2SO_4$ at 60°C, extrapolated from the solubility data of Miles and Carson[120], is ~18 g/l. The dissolved $SO_2$ concentration can be measured analytically *in situ* during corrosion using iodometry. The monograph by Hall[121] gives an excellent description of the procedure to quantitatively measure the dissolved $SO_2$ concentration in concentrated $H_2SO_4$-$H_2O$ solutions.

One of the cathodic processes involved in the active-passive corrosion nickel-stainless steel in concentrated $H_2SO_4$-$H_2O$ solutions is believed to be the reduction of $H_2SO_4$ molecules to elemental sulphur[5,65,68]. Assuming that sulphur is a cathodic product in the

corrosion of nickel in 93.5 wt.% $H_2SO_4$, the reaction should proceed with the formation of a solid yellow deposit since sulphur is insoluble in concentrated $H_2SO_4$-$H_2O$ solutions. Although sulphur is thermodynamically unstable in $H_2SO_4$, dissolving according to,

$$S + 2H_2SO_4 = 3SO_2 + 2H_2O \qquad [5.2]$$

it should remain metastable in 93.5 wt.% $H_2SO_4$ at 60°C as its dissolution is known to proceed slowly at moderate temperatures[49]. Whether it forms an adherent deposit or not during the corrosion of nickel in 93.5 wt.% $H_2SO_4$ at 60°C, sulphur can be collected after the test and analyzed for composition using various X-ray techniques including XPS or XRF.

Along with $SO_2$ and elemental sulphur, the corrosion of copper in 92.6 wt.% $H_2SO_4$ is reported to proceed with the formation of insoluble copper sulphides (CuS and $Cu_2S$)[122]. Therefore, it is reasonable to consider a possible reduction of $H_2SO_4$ molecules leading to the formation of nickel sulphides during the corrosion of nickel in 93.5 wt.% $H_2SO_4$. Assuming that corrosion of nickel in 93.5 wt.% $H_2SO_4$ involves the formation of nickel sulphide(s), the formation of a solid deposit is possible since nickel sulphide apparently has a low solubility in concentrated $H_2SO_4$-$H_2O$ solution. Although no reliable data were reported in the literature for concentrated $H_2SO_4$-$H_2O$ solutions, the solubility of NiS (millerite) is reported to be 0.0094 g/l in 98 wt.% $H_2SO_4$ at 20°C[123]. Whether it forms an adherent deposit or not during the corrosion of nickel in 93.5 wt.% $H_2SO_4$ at 60°C, solid nickel sulphide can be collected after the test and analyzed for composition using various X-

ray techniques including XPS and XRF.

According to the literature, several soluble and insoluble corrosion products are possible during the corrosion of nickel in concentrated $H_2SO_4$-$H_2O$; all of which have been characterized by standard techniques. Therefore, the attempt to characterize the products that form during the corrosion of nickel solutions 93.5 wt. % $H_2SO_4$ at 60°C employed the following similar techniques: iodometry, for *in situ* dissolved $SO_2$ analysis, and x-ray techniques (XPS and XRF), for insoluble product analysis. The test involved a 30 hour immersion of nickel in quiet 93.5 wt. % $H_2SO_4$ at 60°C. The following subsections present and discusses the results of the various measurements made.

### 5.1.2 Influence of Time on the Corrosion of Nickel

Figure 5.1 shows the corrosion potential of nickel in quiet 93.5 wt.% $H_2SO_4$ at 60°C as a function of time. The potential quickly reached a maximum of ~-0.30 $V_{Pt}$ within the first hour of exposure after which it began a two stage decay over a period of about eight hours before stabilizing at ~-0.50 $V_{Pt}$. The two stage decay consisted of an initial slow decay over a period of about 420 minutes (7 hours) followed by a fast decay over a period of about 30 minutes. The potential-time dependence measured in quiet 93.5 wt.% $H_2SO_4$ is consistent with that measured in stirred 93.5 wt.% $H_2SO_4$ (Figure 4.11) with respect to possessing a transition, but the transition time is remarkable shorter in the stirred acid solution. The sensitivity to stirring suggests that the mechanism through which the potential transition

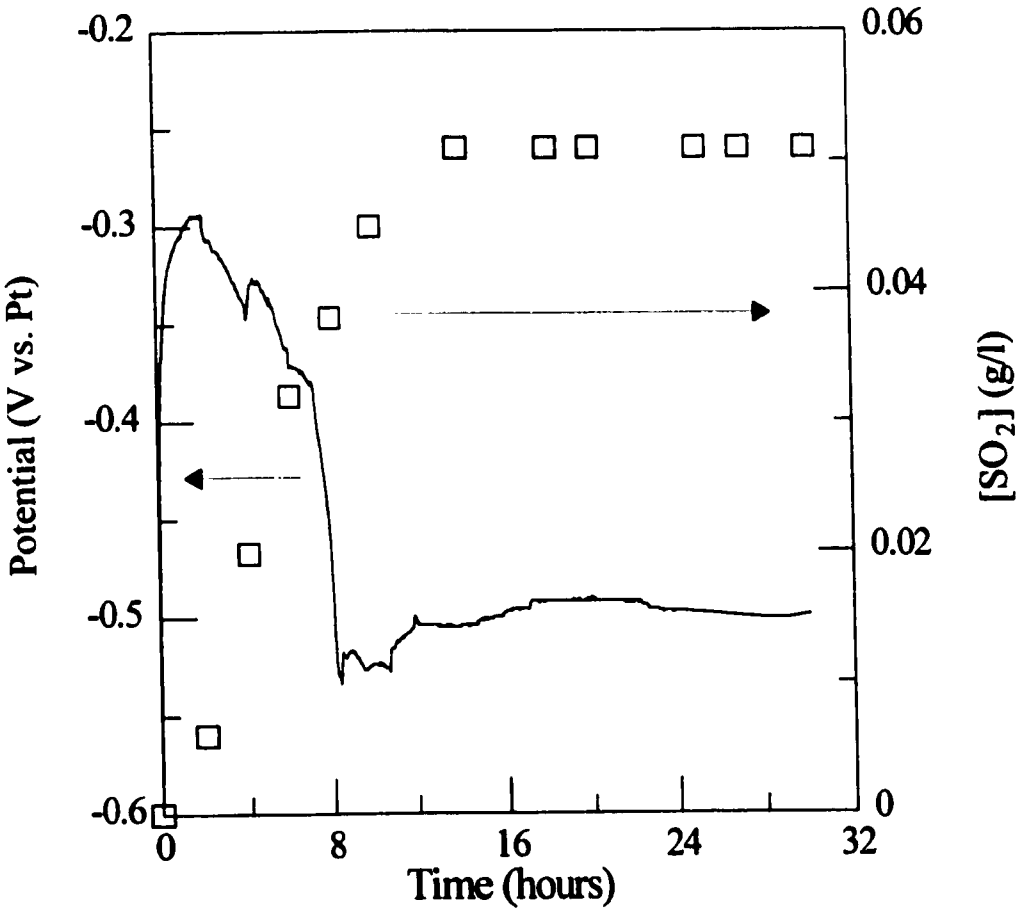


Figure 5.1. Corrosion potential of a nickel electrode and the dissolved $SO_2$ concentration in quiet 93.5 wt.% $H_2SO_4$ at 60°C as a function of time immediately after immersion.

occurs is mass transport controlled.

A solid black deposit formed immediately after immersion and covered the majority of the nickel surface. The black deposit remained on the surface until the potential transition, after which it subsequently dissolved. After the potential transition, the nickel surface had a film-free, dull grey appearance prior to the formation of a stable, yellow surface deposit. Although the acid solution remained homogeneous after the 30 hour exposure, it developed a yellow colour. No visible gas evolution occurred during the corrosion of nickel at either potential plateau, consistent with observations made during the corrosion of nickel in stirred 93.5 wt.% $H_2SO_4$ discussed in Section 4.3. The absence of gas evolution suggests that some cathodic process other than $H_2$ evolution occurred during the corrosion of nickel.

Superimposed on the corrosion potential-time plot in Figure 5.1 is the dissolved $SO_2$ concentration in the acid solution as a function of time during the corrosion of the same nickel electrode in quiet 93.5 wt.% $H_2SO_4$ at 60°C. The $SO_2$ concentration increased linearly with time for a period of 10 hours before it became stable at 0.051 g/l ($2.78\times10^{-3}$ wt.%). As the steady state concentration of 0.051 g/l is significantly lower than the equilibrium solubility of ~18 g/l, it is unlikely that the acid solution became saturated with respect to $SO_2$. When comparing the release of $SO_2$ with the corrosion potential as a function of time it is evident that the release of $SO_2$ occurred during the period prior to the potential transition and not during the period after the transition. Although the presence of $SO_2$ in the acid solution supports a cathodic reaction involving the reduction of $H_2SO_4$ to $SO_2$, it is not

conclusive. It is unclear whether $SO_2$ was produced as a reaction product of nickel corrosion and/or of the black deposit dissolution. For reasons discussed in section 5.4.1, $SO_2$ is believed to be produced as the main cathodic product involved in a galvanic corrosion process taking place at this potential plateau.

The weight loss of the single nickel electrode measured after the 30 hour exposure is 36.6 mg. Such a measurement provides no information regarding the protective nature of either the black or yellow surface. It is possible that the majority of weight loss occurred during the period prior to the potential transition corrosion or during the period after the transition. Making weight loss measurements using multiple nickel coupons as a function of time provided more information in this regard.

Figure 5.2 shows the weight loss of nickel in quiet 93.5 wt.% $H_2SO_4$ at 60°C as a function of time. The curve was constructed by measuring the weight loss of 9 nickel samples, all immersed at approximately the same time in a cell containing 2000 ml acid, but each removed at a different exposure time. The weight loss-time dependence of nickel consisted of an initial, apparent parabolic kinetic stage followed by a linear kinetic stage. All six samples removed during the apparent parabolic stage (10 hours) consisted of an adhered non-continuous black deposit; the adherence decreasing as the exposure time approached 10 hours. The remaining three samples removed during the linear stage were covered with a loosely adherent yellow surface film. Therefore, the weight loss measurements of samples containing the adhered black deposit are misleading since they

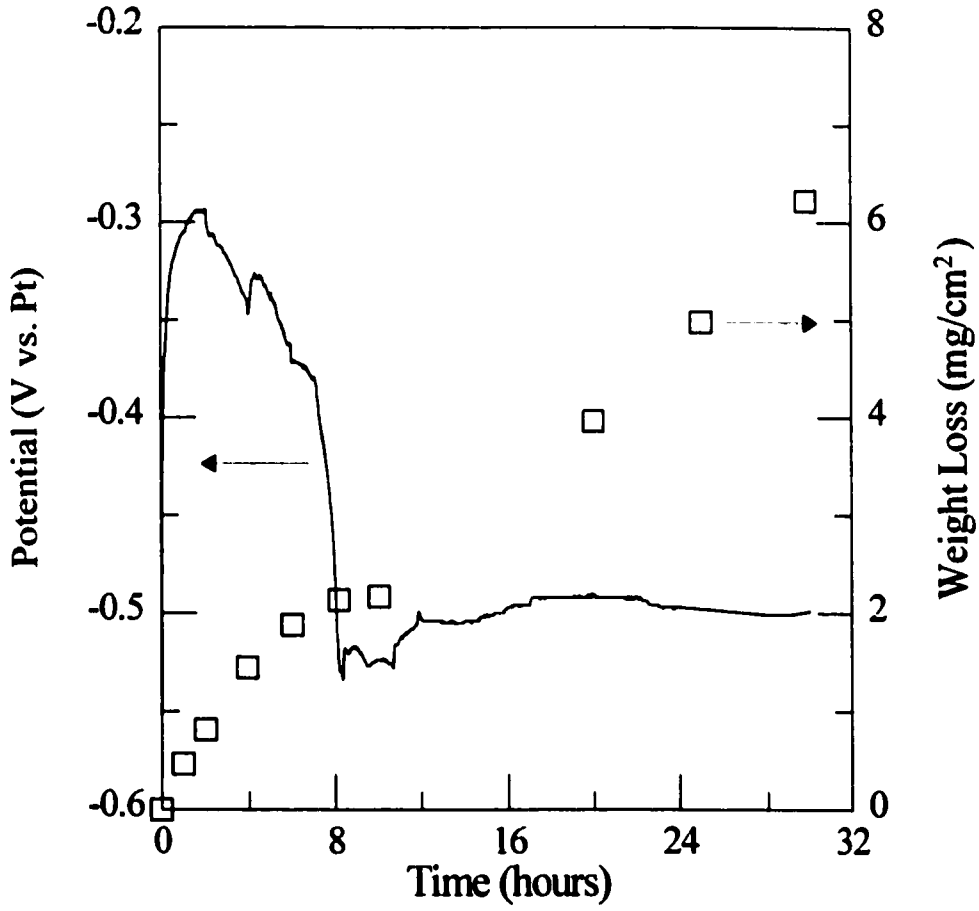


Figure 5.2. Corrosion potential and weight loss of a nickel electrode in quiet 93.5 wt.% $H_2SO_4$ at 60°C as a function of time immediately after immersion.

include the weight gained from the adherent black deposit. Nonetheless, the weight loss data show that neither the black deposit nor the yellow film is protective. In the linear stage, the weight loss of nickel followed,

$$w = 0.20t \qquad [5.3]$$

where w is the weight loss ($mg/cm^2$), 0.20 is the proportionality constant ($mg/cm^2/hr$) and t is time (hr).

When comparing the release of $SO_2$ with the weight-loss as a function as a function of time, it is evident that the corrosion of nickel continues at an appreciable rate despite the absence of further $SO_2$ generation. Therefore, the cathodic reaction involved in the linear stage of corrosion involves the formation of a product(s) other than $SO_2$.

Comparing the measured concentration of dissolved $SO_2$ with an expected concentration calculated from the weight loss of the single nickel electrode after 30 hours exposure provided additional evidence that the cathodic process involved the formation of a product(s) other than $SO_2$. Assuming that the corrosion of the single nickel electrode proceeded according to the reaction sequence,

$$\begin{aligned} &\textit{Anode:} && Ni = Ni^{2+} + 2e^- \\ &\textit{Cathode:} && 2H_2SO_4 + 2e^- = SO_4^{2-} + SO_2 + 2H_2O \\ &\textit{Total:} && Ni + 2H_2SO_4 = NiSO_4 + SO_2 + 2H_2O \end{aligned} \qquad [5.4]$$

where 1 mole of nickel reacted to produce 1 mole of $SO_2$, with a 100% current efficiency, then the $SO_2$ concentration can be calculated from the weight loss using Faraday's Law [4.13]. According to [5.3], the 30 hour weight loss of 36.6 mg corresponds to a theoretical $SO_2$ concentration of 0.160 g/l which is significantly higher than the measured 0.051 g/l and less than the equilibrium solubility 18 g/l. Next, chemical analysis conducted to characterize the elemental composition of the various solid corrosion products demonstrates that other possible reduction products include sulphide ions and elemental sulphur.

### 5.1.3 Solid Corrosion Product Analysis

An XPS analysis conducted on a nickel sample after a 15 minute exposure provided information regarding the strongly adherent non-continuous black deposit. Figure 5.3 shows the sulphur 2p spectrum. The sulphur region possessed a strong peak and shoulder at 161.12 eV and 162.63, respectively, and a small peak at 169.25 eV. Table 5.1 presents a comparison of the binding energies of sulphur in the most probable species that may have appeared in this study with the literature. Based on the comparison, a NiS deposit covered the majority of the nickel surface. The presence of $NiSO_4$ was likely formed by oxidation of the NiS deposit during exposure to the atmosphere prior to the XPS measurement. The most likely source of the sulphide ion is the reduction of $H_2SO_4$ molecules.

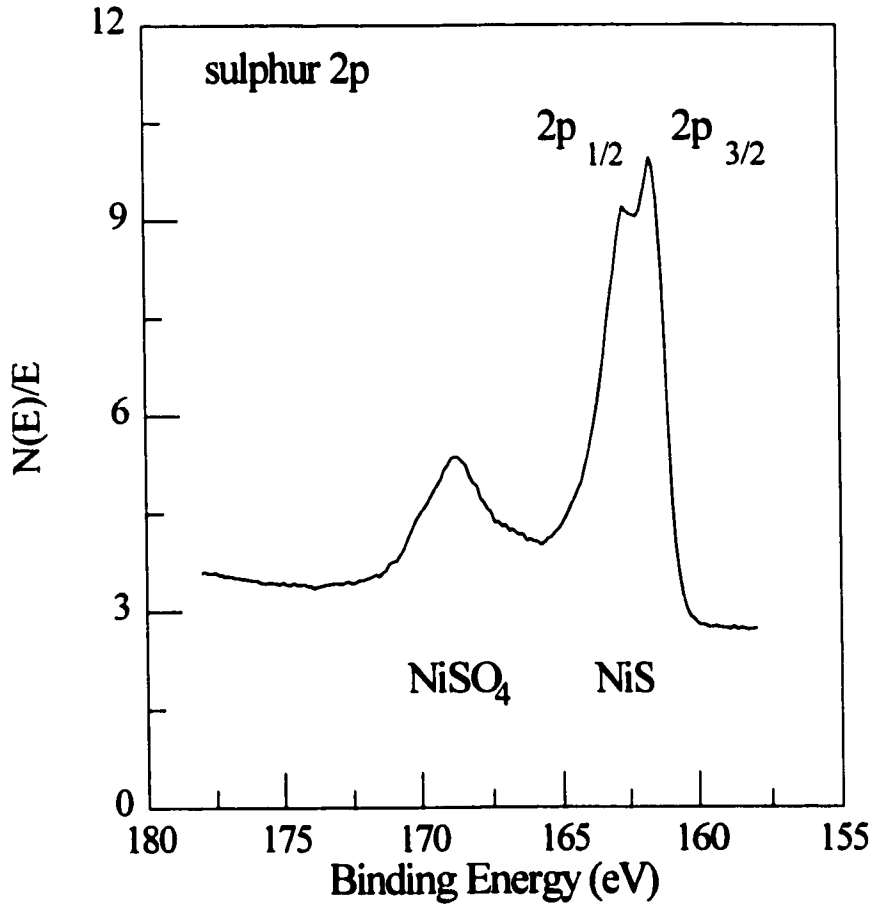


Figure 5.3. XPS sulphur 2p spectra obtained from the surface of a nickel electrode after 15 minutes exposure in quiet 93.5 wt.% $H_2SO_4$ at 60°C.

**Table 5.1.** Binding Energy (B.E.) of Sulphur in Selected Compounds

| Compound | Peak | Measured B.E. (eV) | Literature[113] B.E. (eV) |
|---|---|---|---|
| NiS | $2p_{3/2}$ | 162.12 | 162.2 |
| $NiSO_4$ | 2p | 169.25 | 169.2 |

In anticipation of a subsequent chemical analysis, an attempt was made to collect the loosely adherent yellow film that formed during the 30 hour single nickel electrode corrosion test. The yellow precipitate consisted of a water-soluble component and a water-insoluble component. The soluble component produced a green solution when dissolved in water, consistent with the formation of a hydrated nickel ion ($Ni^{2+}_{aq}$)[124]. The yellow water soluble component is consistent with anhydrous $NiSO_4$. Assuming the $NiSO_4$ solubility in 93.5 wt.% $H_2SO_4$ at 60°C is 0.12 wt.%, extrapolated from the data reported by Halstead and Lovey[119], and nickel dissolved at a rate of 0.24 mg/cm$^2$/hr, then the calculated time required for the acid solution to become saturated with respect to $NiSO_4$ is about 17 hours. Therefore, it is reasonable to postulate that the build up of corrosion products at the metal-solution interface, due to the high solution viscosity, leads to the precipitation of a $NiSO_4$ film from a supersaturated solution at a time much sooner than required to saturate the bulk solution. This is consistent with experimental observation.

The chemical composition of the yellow water insoluble corrosion product was analyzed by XRF. The XRF analysis showed the deposit consisted of >99 wt.% sulphur (S) and <1 wt.% nickel (Ni), Appendix A.2. Based on the analysis, the yellow water insoluble corrosion product is believed to be elemental sulphur. Considering that the steady state corrosion of nickel did not involve the evolution of $SO_2$, the reformation of NiS nor the evolution of $H_2$, it is reasonable to postulate that the cathodic process involved the reduction of $H_2SO_4$ molecules to sulphur.

### 5.1.4 Cathodic Polarization of Platinum - Reduction of 93.5 wt.% $H_2SO_4$

Observations made during the corrosion of nickel suggest that the cathodic process involves a potential-dependent reduction of $H_2SO_4$ molecules; i.e., sulphide ($H_2S$) formation at a potential corresponding to the initial stage of corrosion, $SO_2$ at the more positive potential plateau and sulphur at the more negative, stable potential plateau. A potential-dependent reduction process during the electrolysis of 93.5 wt.% $H_2SO_4$ is not unrealistic considering the electrolysis of fuming $H_2SO_4$ results in the formation of several different potential-dependent reduction products including: $SO_2$, sulphur and $S_2O_3$[51,52,53,54]. Cathodic polarization conducted using an inert platinum disk electrode provided more information in this regard.

Figure 5.4 shows the potentiodynamic cathodic polarization curve of 93.5 wt.% $H_2SO_4$ measured on a rotating platinum disk electrode (500 rpm). Three distinct slopes

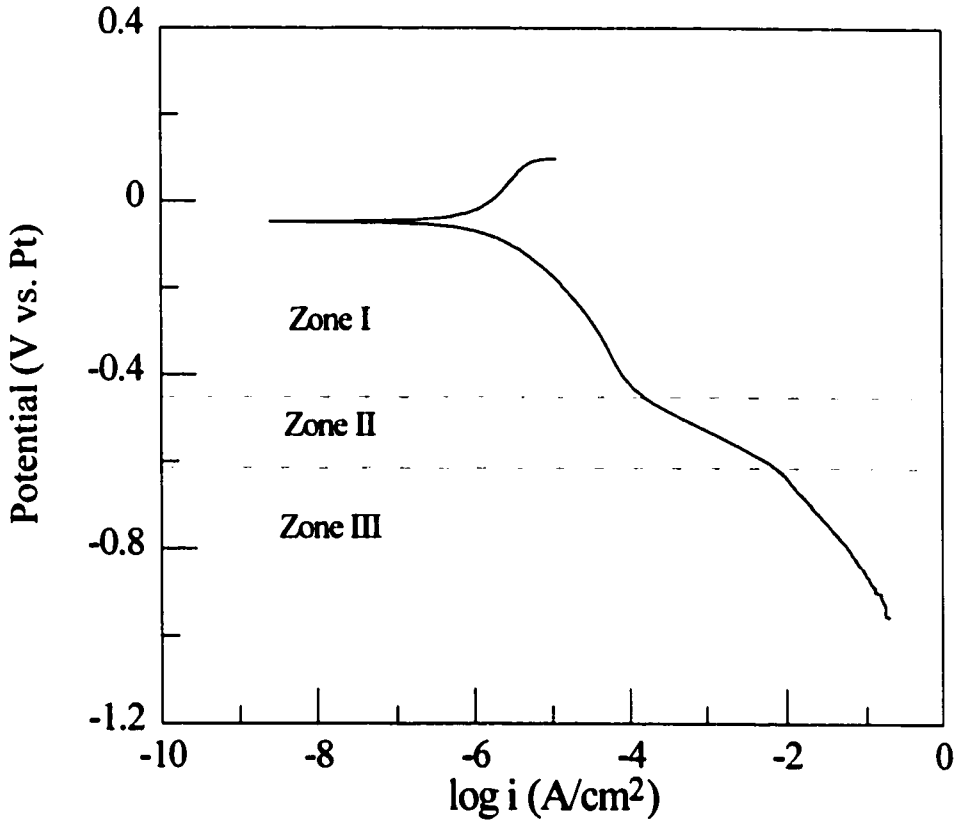


Figure 5.4. Potentiodynamic cathodic polarization of 93.5 wt.% $H_2SO_4$ measured on a platinum RDE (500 rpm rotation). Dashed lines separate the potentials zones possibly representing three different reactions.

[dE/dlog(i)], possibly representing three distinct reactions, occurred as the potential was made more negative. The curve can be separated into the following three potential zones: Zone I where $E \leq -0.42$ $V_{Pt}$, Zone II where $-0.42 \leq E \leq -0.60$ $V_{Pt}$ and Zone III where $E \geq -0.61$ $V_{Pt}$. The only evidence of product formation during the experiment occurred in Zone III. In this zone, gas evolution occurred on the platinum surface along with the formation of a heterogeneous solution adjacent to the electrode surface. By the end of the polarization measurement, the entire solution was cloudy.

The corrosion potential at which $SO_2$ forms during the corrosion of nickel occurs in Zone I of the platinum cathodic polarization curve. Therefore, if $SO_2$ is indeed a product of the cathodic process in this zone then it should be detected in an extended potentiostatic polarization measurement conducted at a potential in this zone. Conducting such an experiment confirmed the electrolytic formation of $SO_2$. The experiment involved measuring the dissolved $SO_2$ generated after polarizing a platinum sheet electrode (46.07 $cm^2$) in quiet 93.5 wt.% $H_2SO_4$ at 60°C (250 ml) at -0.3 $V_{Pt}$ for a 24 hour period. The total charged consumed in the 24 hour potentiostatic polarization test was 316.9 C and the measured dissolved $SO_2$ concentration was 133 ppm by weight. Assuming that the cathodic process consuming the current proceeds with a 100% current efficiency according to,

$$2H_2SO_4 + 2e^- = SO_4^{2-} + SO_2 + 2H_2O \qquad [5.5]$$

then, the corresponding theoretical dissolved $SO_2$ concentration, calculated using Faraday's

Law [4.3], is 115 ppm by weight. The theoretical 115 ppm by weight agrees reasonably well with the measured 133 ppm.

The corrosion potential at which sulphur forms during the corrosion of nickel occurs in Zone II of the platinum cathodic polarization curve. Subsequent potentiodynamic polarization measurements conducted on platinum provided qualitative evidence supporting the formation of sulphur in this zone. The measurements consisted of polarizing the platinum disk electrode to the end of Zone I and II respectively. Observations showed that a yellow, water insoluble, deposit formed on the surface only after polarizing through to the end of Zone II.

The corrosion potential at which NiS forms during the corrosion of nickel occurs in Zone III of the platinum cathodic polarization curve. Therefore, if NiS formation requires the the formation of sulphide as a reduction product then sulphide should be formed as a product in this zone. The evolving gas in Zone III is likely $H_2$, consistent with the observations made in Section 4.1. It is reasonable to consider, however, that another reduction reaction occurs simultaneously. The electrolytic production of sulphide ($H_2S$) may be responsible for the formation of the heterogeneous solution. A simple experiment to explore the reactivity of $H_2S$ with 93.5 wt.% $H_2SO_4$ involved passing the gas through a volume of the acid solution at 60°C. During such a test, the acid solution became cloudy after about 10 minutes. After 90 minutes, the acid solution contained a significant quantity of a yellow, water insoluble, deposit (sulphur) and had a strong $SO_2$ odour. The reaction

products are consistent with the well known reaction[125]:

$$H_2S + H_2SO_4 = SO_2 + S + 2H_2O \quad [5.6]$$

### 5.1.5 Summary

The first step taken to meet the objectives defined in Section 5.0 involved a 30 hour corrosion test of nickel in quiet 93.5 wt.% $H_2SO_4$ at 60°C. A review of relevant literature provided insight into the possible soluble and insoluble products that may form during corrosion. Taking the review into account, the adopted approach involved making electrochemical, iodometric, XPS and XRF measurements to characterize the various corrosion products that form and clarify their influence on the corrosion behaviour.

The results suggest that the corrosion of nickel involves the participation of $H_2SO_4$ molecules that leads to the formation of soluble sulphur dioxide ($SO_2$) and several solid products including nickel sulphide (NiS), nickel sulphate ($NiSO_4$) and elemental sulphur. None of the solid films that form during corrosion are protective when adherent on the surface. Prior to establishing a steady state, the corrosion of nickel involves the formation and subsequent dissolution of a noncontinuous NiS deposit that significantly affects the corrosion potential. The release of $SO_2$ during corrosion occurs only when NiS is present on the surface of nickel.

## 5.2 Corrosion of Nickel in Stirred 93.5 wt.% $H_2SO_4$

The next step taken to meet the objectives defined in Section 5.0 involved studying the corrosion of nickel in stirred 93.5 wt.% $H_2SO_4$ to better understand the stability of NiS. Experiments conducted thus far show that stirring has a marked influence on the potential transition time and thus, the stability of NiS. Anodic polarization measurements conducted in Section 4.4 (Figure 4.12) show that the anodic dissolution of nickel is mass transport controlled regardless of whether NiS is present on the surface. A review of the relevant literature regarding mass transport controlled corrosion provided a better idea of what to expect prior to and, thus, monitor during the corrosion tests.

### 5.2.1 Mass Transport Controlled Corrosion

For any convective mass transfer process the corrosion current density, $i_{corr}$, may be expressed in terms of the Nernst diffusion layer model[126],

$$i_{corr} = nFD\frac{(C_s - C_b)}{\delta} \qquad [5.7]$$

where D is the diffusion coefficient of the rate-limiting species ($cm^2/s$), $\delta$ is the diffusion layer thickness (cm), $C_s$ is the concentration of the species at the surface-solution interface ($mol/cm^3$) and $C_b$ is the concentration of the species in the bulk solution ($mol/cm^3$). The hydrodynamic condition at the metal-solution interface is well defined by carrying out

corrosion measurements on systems such as fluid flow in a pipe and with a rotating disc or cylinder electrode system[127]. For a rotating cylinder electrode, δ in [5.7] may be expressed in terms of the following system parameters[128],

$$\delta = 12.66 d^{0.3} v^{-0.7} D^{0.356} \left(\frac{\eta}{\rho}\right)^{0.344} \qquad [5.8]$$

where d is the diameter (cm), v is the fluid velocity (cm/s), and η is the viscosity (poise) and ρ is the fluid density ($g/cm^3$).

As discussed in Section 2.4, the steady state corrosion of iron in concentrated $H_2SO_4$-$H_2O$ solutions is rate limited by the dissolution of $FeSO_4 \bullet 7H_2O$[87]. The rate determining step is the diffusion of ferrous ions ($Fe^{2+}$) into the bulk solution from the saturated solution at the film-solution interface[86,87]. Rotating cylindrical electrodes showed that the corrosion of iron increases in proportion to velocity (rotation rate) to the nth power where $0.6 < n < 0.8$ in 68 wt.% $H_2SO_4$ depending on temperature[87]. The linear decrease in the corrosion rate of iron with an increase in the bulk ferrous ion ($Fe^{2+}$) concentration demonstrated that the mass transfer of the ferrous ion is the slow step in the corrosion of iron[87].

Employing a rotating cylindrical electrode (RCE) is a powerful technique to explore mass transport controlled corrosion process. The corrosion of nickel is believed to involve the formation of $NiSO_4$ through a dissolution-precipitation mechanism and thus, is likely to have a rate limiting step similar to the corrosion or iron. Therefore, the attempt to better

understand the mass transport controlled corrosion of nickel in 93.5 wt. % $H_2SO_4$ involved studying the corrosion of a rotating nickel cylinder electrode as a function of the rotation rate and the bulk nickel ion concentration. The influence of temperature on the corrosion of nickel in stirred 93.5 wt.% $H_2SO_4$ was also studied since it, along with the stirring, influences the passive state stability of the nickel-stainless steel S30403. The following subsections present and discuss the results of the various measurements made.

### 5.2.2 Influence of Stirring on the Corrosion of Nickel

Figure 5.5 shows the effect of the rotation rate on the corrosion potential of a nickel RCE in 93.5 wt.% $H_2SO_4$ at 60°C as a function of time. Superimposed on the plot is the corrosion potential of the nickel electrode in otherwise quiet 93.5 wt.% $H_2SO_4$ at 60°C measured in Section 5.1.2. The curves show that the rotation rate significantly influences the potential transition time, the maximum potential attained prior to the transition and the steady state potential attained after the transition. An increase in the rotation rate progressively decreased the potential transition time and progressively increased the maximum potential attained. The steady state potential after the transition has a more complex dependence on the rotation rate. An increase in the electrode rotation rate from 0 to 250 rpm increased the potential from ~-0.50 to ~-0.45 $V_{Pt}$ where it remained constant with a further increase in the rotation rate to 500 rpm. An increase in the rotation rate from 500 to 1000 rpm changed the stable potential after the transition from ~-0.50 to ~-0.62 $V_{Pt}$ where

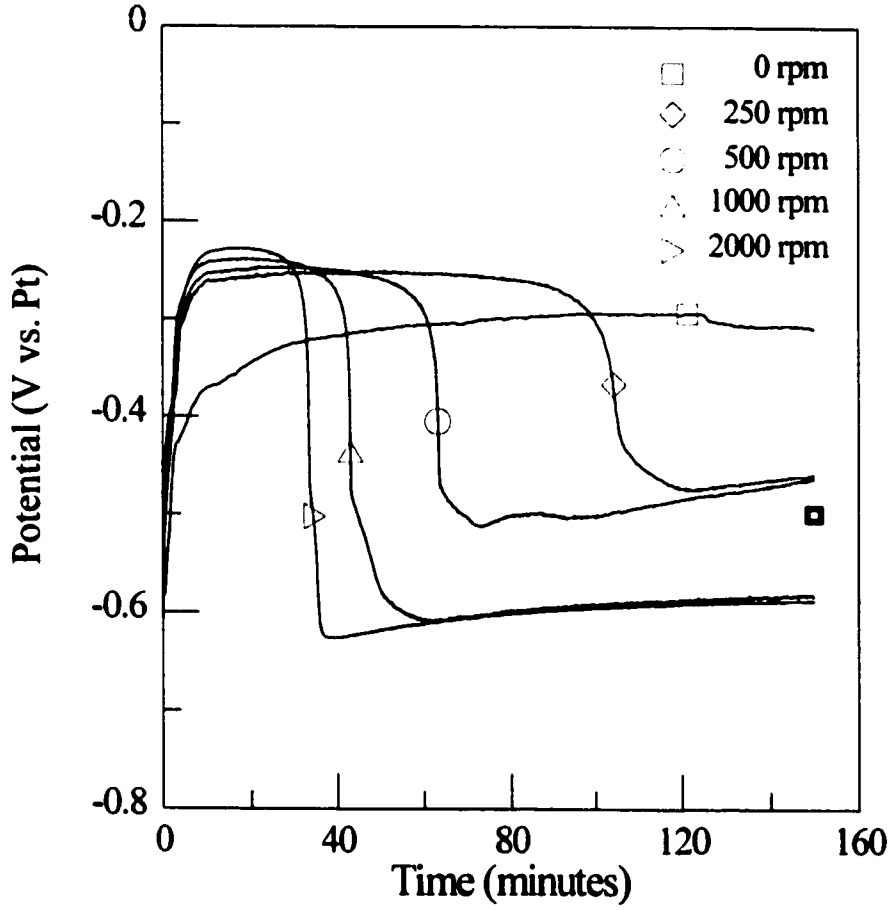


Figure 5.5. Influence of the electrode rotation rate on the corrosion potential of a nickel RCE in 93.5 wt.% $H_2SO_4$ at 60°C as a function of time immediately after immersion (□ represents steady state corrosion potential of nickel electrode at 0 rpm after 30 hours exposure).

it remained constant with a further increase in the rotation rate to 2000 rpm.

Weight loss measurements provided more information regarding the influence of stirring on the corrosion of nickel. Figure 5.6 shows the 15 minute and 150 minute weight losses of a nickel RCE in 93.5 wt.% $H_2SO_4$ at 60°C as a function of the rotation rate. The 15 and 150 minute weight losses increased in proportion to the rotation rate according to,

$$w \propto \omega^{0.41} \qquad [5.9]$$

$$w \propto \omega^{0.78} \qquad [5.10]$$

respectively, where w is the weight loss ($mg/cm^2$) and $\omega$ is the electrode rotation rate (rpm). A proportional dependence of the weight loss on the rotation rate indicates that convective mass transfer is the likely rate limiting step in the corrosion of nickel regardless of whether NiS is present on the surface. A mass transfer rate limiting step is consistent with the limiting anodic current measured during the anodic polarization curve (Figure 4.12).

The sensitivity of the potential transition time to the electrode rotation rate is consistent with the idea that the potential transition is directly related to the dissolution of NiS; the dissolution of which is mass transport controlled. Therefore, the sensitivity can be qualitatively explained by considering the magnitude $\delta$ in [5.7] and [5.8]. According to [5.8], an increase in the electrode rotation rate (fluid velocity) decreases the diffusion layer thickness $\delta$ and, therefore, increases the rate according to [5.7]. The increased NiS dissolution rate requires a shorter time for complete consumption and the corresponding

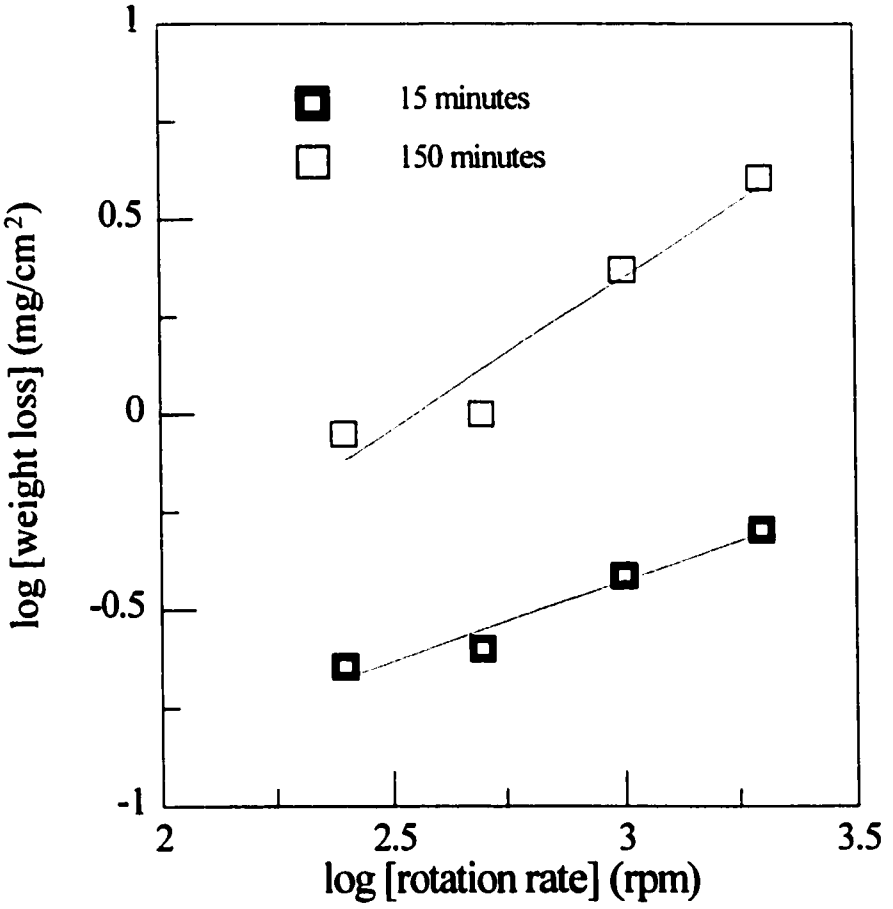


Figure 5.6. Influence of the electrode rotation rate on the 15 minute and 150 minute weight losses of a nickel RCE in 93.5 wt.% $H_2SO_4$ at 60°C.

potential transition.

The sensitivity of the maximum potential attained and the stable potential after the transition to the electrode rotation rate is not well understood. Considering the mixed potential theory, it is plausible that the increase in the electrode rotation rate causes the potential at which the total anodic current balances the total cathodic current to shift in response to a change in the anodic and/or cathodic current. It is also plausible that the maximum potential attained is independent of the rotation rate in stirred solutions and the variance is just experimental uncertainty.

Since the time required for the nickel RCE to reach the maximum potential is essentially independent of the rotation rate in stirred 93.5 wt.% $H_2SO_4$ at 60°C, it is plausible that the NiS formation process is not mass transport controlled. The NiS dissolution process, however, is clearly mass transport controlled, assuming it is directly responsible for the potential transition. The potential transition time of the nickel RCE progressively decreased as the rotation rate increased in stirred 93.5 wt.% $H_2SO_4$ at 60°C.

Experiments conducted to explore the influence of the stirring rate on the corrosion of nickel show that corrosion is mass transport controlled regardless of whether NiS is present on or absent from the surface. Next, experiments to explore the influence of the bulk nickel ion concentration on the corrosion of nickel indicate that the nickel ion is the likely species whose mass transfer is the slow step.

### 5.2.3 Influence of the Bulk Nickel Ion Concentration on the Corrosion of Nickel

The influence of the bulk nickel ion concentration on the corrosion potential and weight loss of a nickel RCE in stirred 93.5 wt.% $H_2SO_4$ at 60°C was explored by dissolving an appropriate weight of reagent grade $NiSO_4 \bullet 6H_2O$ in 93.5 wt.% $H_2SO_4$ to make solutions that contained 0, 250 and 500 ppm by weight nickel ion ($Ni^{2+}$). The maximum dilution resulting from the addition of the water of hydration is 0.09 wt.%. This small change in acid concentration is assumed to have little effect on the resulting corrosion behaviour. Therefore, any change in the corrosion behaviour is assumed to be associated with the change in the concentration of the nickel ion. Dissolved $NiSO_4 \bullet 6H_2O$ in 93.5 wt.% $H_2SO_4$ produced a clear yellow solution regardless of the bulk concentration.

Figure 5.7 shows the influence of the bulk nickel ion concentration on the corrosion potential of a nickel RCE (1000 rpm) in 93.5 wt.% $H_2SO_4$ at 60°C as a function of time. The curves show that the bulk nickel ion concentration influences the potential transition time, the maximum potential attained prior to the transition and the steady state potential attained after the transition. An increase in the bulk concentration from 0 to 500 ppm progressively increased the potential transition time from ~40 to ~150 minutes. An increase in the bulk concentration from 0 to 250 ppm by weight had essentially no effect on the stable potential after the plateau. A further increase in the bulk concentration to 500 ppm by weight, however, increased the stable potential after transition from ~-0.60 to ~-0.45 $V_{Pt}$. It is unclear whether the bulk concentration has an effect on the maximum potential attained since

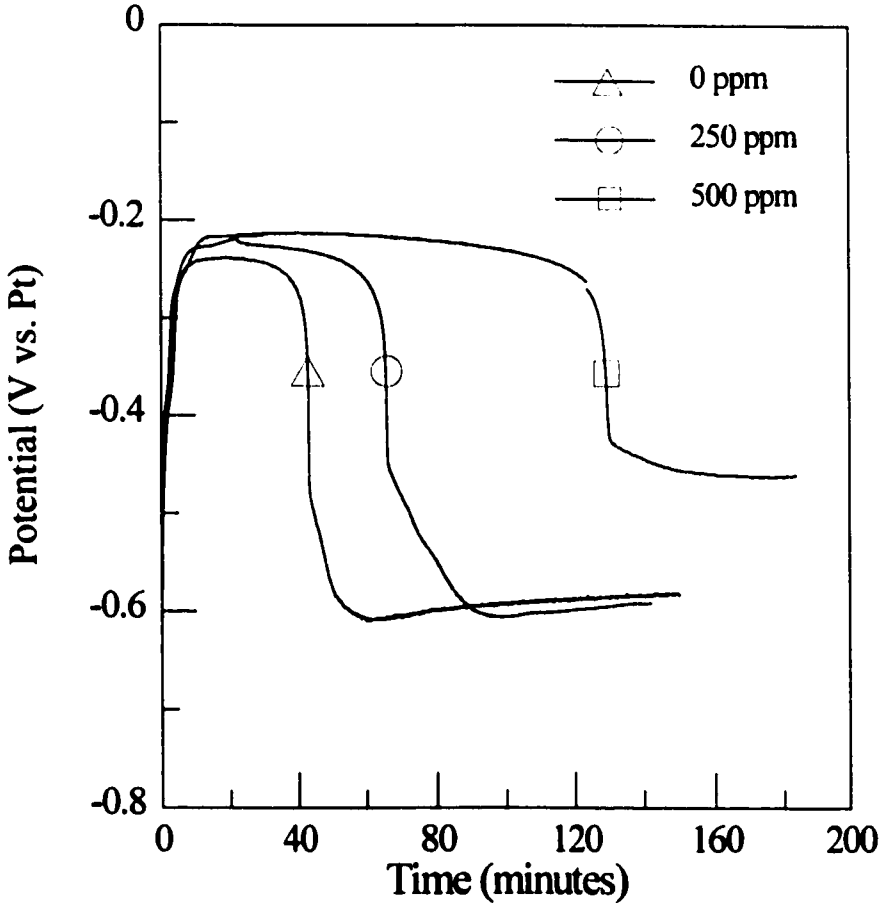


Figure 5.7. Influence of the bulk nickel ion concentration on the corrosion potential of a nickel RCE (1000 rpm) in 93.5 wt.% $H_2SO_4$ at 60°C as a function of time immediately after immersion.

the variance may be just experimental uncertainty. The time required to reach the maximum potential is essentially independent of the bulk nickel ion concentration.

Weight loss measurements after 240 minutes exposure provided more information regarding the influence of the bulk nickel ion concentration on the corrosion of nickel. Figure 5.8 shows the weight loss rate of the nickel RCE as a function of the bulk nickel ion concentration. The weight loss rate decreased linearly with an increase in the bulk nickel ion concentration. The linear dependence suggests that the convective mass transfer of nickel ions is likely the rate-limiting step in the corrosion process.

The sensitivity of the potential transition time to the bulk nickel ion concentration is consistent with the idea that the potential transition is directly related to the dissolution of NiS; the dissolution of which is mass transport controlled. Assuming that the mass transfer of nickel ions is the rate limiting step, the sensitivity can be qualitatively explained by considering the magnitude $C_b$ in [5.7]. An increase in the bulk nickel ion concentration increases $C_b$ therefore, decreases the rate. The decreased NiS dissolution rate requires a longer time for complete consumption and the corresponding potential transition.

An increase in the bulk nickel ion concentration from 250 to 500 ppm has a similar influence on the stable potential after the transition as does a decrease in the electrode rotation rate from 500 to 1000 rpm. The comparison is consistent with a mass transport controlled process that is rate limited by the diffusion of nickel ions. According to [5.7] a decrease in the rate occurs with either an increase in $C_b$ (an increase in the bulk nickel ion

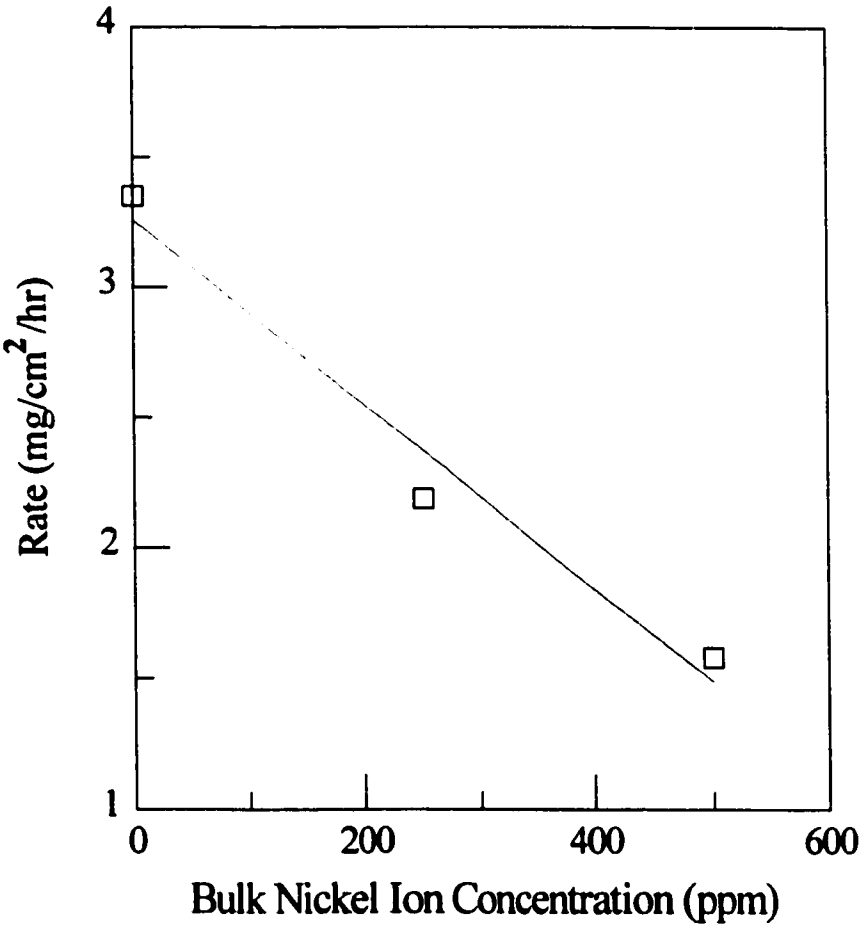


Figure 5.8. Influence of the bulk nickel ion concentration on the average weight loss rate of a nickel RCE (1000 rpm) in 93.5 wt.% $H_2SO_4$ at 60°C.

concentration) or an increase in δ (a decrease in the electrode rotation rate). Therefore, assuming that the potential shift is a response to a change in the anodic current, an increase in the bulk nickel ion concentration or a decrease in the electrode rotation rate shifts the potential the same direction.

### 5.2.4 Influence of Temperature on the Corrosion of Nickel

Along with stirring (acid velocity), another variable of interest in this study is temperature. Experiments conducted to explore the influence of temperature on the corrosion of nickel in stirred 93.5 wt.% $H_2SO_4$ show it has a marked effect which can be explained using the Nernst diffusion layer model.

Figure 5.9 shows the influence of temperature on the corrosion potential of a nickel RCE (1000 rpm) in 93.5 wt.% $H_2SO_4$ as a function of time. A potential transition occurred at all temperatures studied between 50-80°C, indicating that the reactivity leading to the formation and subsequent dissolution of NiS is independent of temperature. The curves show that temperature influences the potential transition time and the steady potential attained after the transition. An increase in temperature from 50 to 80°C decreased the potential transition time from ~125 to ~20 minutes. The potential plateau after the transition progressively increased with an increase in temperature beyond 60°C. A distinct feature not present in other corrosion potential measurements is the shoulder that occurred during the initial potential rise towards the more positive plateau at 50°C.

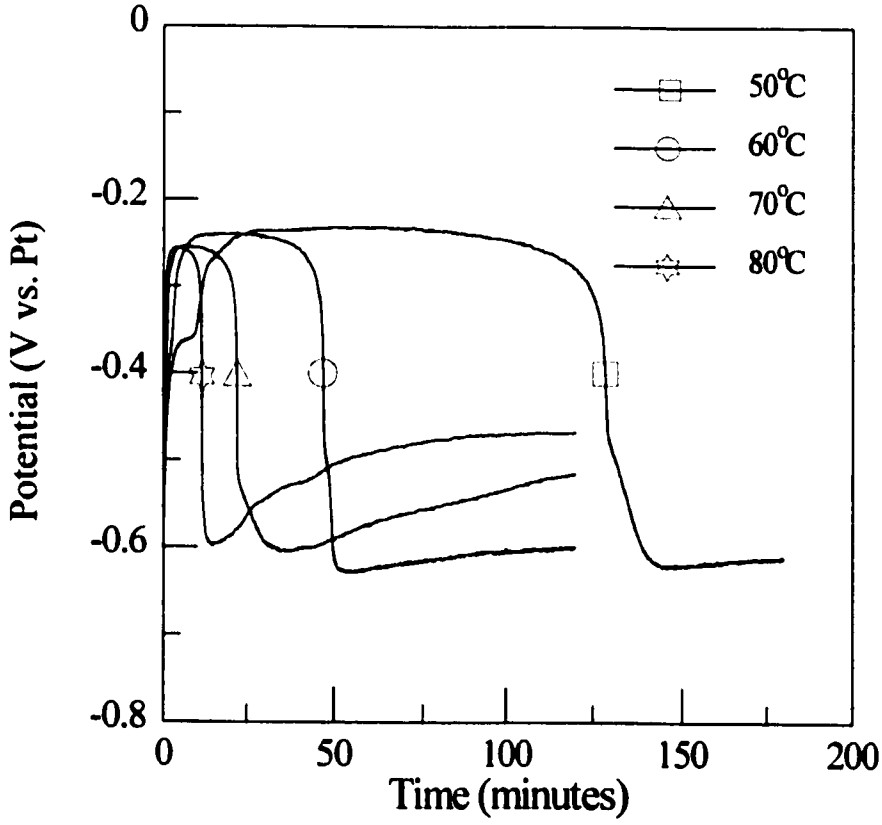


Figure 5.9. Influence of temperature on the corrosion potential of a nickel RCE (1000 rpm in 93.5 wt.% $H_2SO_4$ as a function of time immediately after immersion.

Weight loss measurements provided more information regarding the influence of the bulk nickel ion concentration on the corrosion of nickel. Table 5.2 displays the weight loss of the nickel RCE (1000 rpm) measured in 93.5 wt.% $H_2SO_4$ at 50-80°C. The data show that the weight loss increased as the temperature increased. The dependence of the weight loss on temperature is consistent with a mass transport controlled process with the diffusion of nickel ions as the rate limiting step. Temperature influences $C_s$, D and $\delta$ in [5.7] and according to [5.7] an increase in $C_s$ and D and/or a decrease in $\delta$ increases the corrosion rate. The solubility of $NiSO_4$ in concentrated $H_2SO_4$-$H_2O$ solution increases with increasing temperature[119]. It is assumed that D increases with increasing temperature as diffusion is generally accepted to be a thermally activated process. According to [5.8], $\delta$ is proportional to $\eta^{0.344}$ and thus, decreases with an increase in temperature since the viscosity of 93.5 wt.% $H_2SO_4$ decreases with an increase in temperature[37].

**Table 5.2.** Influence of Temperature on Corrosion of a Nickel RCE (1000 rpm) in 93.5 wt.% $H_2SO_4$

| Temperature °C | Weight Loss mg/cm$^2$ | Time hours | Rate mg/cm$^2$/hr |
|---|---|---|---|
| 50 | 8.13 | 3 | 2.7 |
| 60 | 6.28 | 2 | 3.1 |
| 70 | 6.53 | 2 | 3.3 |
| 80 | 7.59 | 2 | 3.8 |

The sensitivity of the potential transition time to temperature can be explained by the magnitude of the mass transport controlled corrosion rate. The increased mass transport controlled dissolution rate of NiS that occurs with an increase in temperature shortens the time required for complete consumption and the corresponding potential transition. The mechanism through which steady state corrosion potential after the transition became more positive with an increase in temperatures beyond 60°C is likely related to the dependence on both the anodic and cathodic kinetics on temperature.

### 5.2.5 Summary

The second step taken to meet the objectives defined in Section 5.0 involved studying the corrosion of nickel in stirred 93.5 wt.% $H_2SO_4$ to better understand the stability of NiS. A review of the relevant literature regarding mass transport controlled corrosion provided a better idea of what to expect prior to and, thus, monitor during the corrosion tests. Taking the review into account, the adopted approach involved making electrochemical and weight loss measurements on a nickel RCE as a function of the electrode rotation rate, the bulk nickel ion concentration and temperature.

The results show that the corrosion of nickel is a mass transport controlled process regardless of the potential at which corrosion is occurring. The diffusion of nickel ions is the rate limiting step in the process. The Nernst diffusion layer model provides a reasonable account of the influence of the electrode rotation rate, the bulk nickel ion concentration and

temperature on the corrosion of nickel in 93.5 wt.% $H_2SO_4$. The dissolution process of NiS is more sensitive to changes than the formation process regardless of the variable under consideration. The mass transport controlled dissolution of NiS determines its stability.

## 5.3 Influence of NiS on the Corrosion Potential of Nickel in 93.5 wt.% $H_2SO_4$

The final step taken to meet the objectives defined in Section 5.0 involved studying the polarization behaviour of nickel with and without NiS in stirred 93.5 wt.% $H_2SO_4$ to better understand the influence of NiS on the corrosion potential of nickel. A review of the relevant literature regarding mechanisms by which surface deposits influence the potential of metal electrodes provided a better idea of what to expect prior to and, thus, explore during subsequent experiments.

### 5.3.1 Influence of Surface Deposits on Electrode Potential

The electrochemical formation of surface films can occur in a variety of ways. Two extreme processes, however, can be differentiated[129,130]. Formation of a surface film may take place by a dissolution-precipitation process where nucleation of the solid phase occurs in a supersaturated solution adjacent to the metal surface. Here, the anodically-produced cations emerging from the metal are precipitated by another substance in solution, leading to the production and retention of enough solid precipitate at or on the metal to blanket it. Alternatively, formation of a surface film may take place by a solid state process where

nucleation occurs on the metal surface. Here, the anodically-produced cations emerging from the metal are immediately incorporated into the solid phase.

It is a characteristic of noncontinuous films that they exhibit a very low resistance to current flow during corrosion so that the potential at which they grow stays very close to the corrosion potential[129,130]. It is a characteristic of continuous films that they exhibit a significantly higher resistance than noncontinuous films to current flow so that a significant change in the potential is required to continue the reaction[129,130]. Considering that, by inspection, NiS forms a noncontinuous film, some mechanism other than increasing the resistance to current flow is responsible for the significant influence NiS has on the corrosion potential of nickel.

A second mechanism through which a surface deposit can significantly influence the metal potential involves a significant depolarization of a more noble cathodic reaction on the surface of the deposit. Here, the deposit acts as an electrocatalyst. An excellent example is the influence of FeS on the corrosion of iron in contact with sulphur in S-$H_2O$ suspensions[131]. The relatively high electrical conductivity and defect structure of FeS catalyzes the reduction of sulphur to polysulphide[132,133]. The more noble cathodic reaction induces a marked increase in the anodic polarization of the iron dissolution reaction, which is reflected by the marked increase in the corrosion potential of 200 mV[134]. Although it is plausible that NiS acts as an electrocatalyst when formed during the corrosion of nickel in 93.5 wt.% $H_2SO_4$, there is no reasonable explanation of the subsequent dissolution of NiS.

A third mechanism through which a surface deposit can significantly influence the metal potential involves a galvanic interaction between the noncontinuous deposit and the uncovered metal. A galvanic interaction requires an oxidative dissolution of the deposit and an appreciable bulk electronic conductivity. Metal sulphides such as galena (PbS), pyrite ($FeS_2$) and covellite (CuS) oxidatively dissolve in the presence of an oxidant with the formation of a metal cation and elemental sulphur[135,136,137]. The aforementioned metal sulphides are semiconductors and their resistivities are sufficiently low to allow participation in galvanic dissolution couples. Peters *et al.*[138] demonstrated that a galvanic-induced enhanced leaching of galena (PbS) occurs when in electrical contact with pyrite ($FeS_2$). Another excellent example of a galvanic interaction involving mineral sulphides is the enhanced leaching of a chalcopyrite ($CuFeS_2$) bearing material when in electrical contact with pyrite ($FeS_2$)[139].

Considering NiS forms a thick noncontinuous deposit that subsequently dissolves and has no protective capability, a galvanic interaction is the more plausible mechanism responsible for the corrosion potential transition behaviour of nickel in 93.5 wt.% $H_2SO_4$. A galvanic interaction requires that NiS anodically dissolves in 93.5 wt.% $H_2SO_4$. Anodic dissolution of NiS is plausible since $H_2SO_4$ molecules can be cathodically reduced to sulphur-containing species with an oxidation state lower than six[49,50]. A galvanic interaction involving NiS and nickel is possible since the reversible potential $E^o = +0.35\ V_{SHE}$ of the NiS anodic dissolution reaction,

$$NiS = Ni^{2+} + S + 2e^- \quad [5.11]$$

is sufficiently different than the reversible potential $E^o$ = -0.25 $V_{SHE}$, of the nickel anodic dissolution reaction:

$$Ni = Ni^{2+} + 2e^- \quad [5.12]$$

A galvanic interaction actually requires that corrosion potential of the individual materials to be different. Considering the difference in the equilibrium dissolution potentials, it is reasonable to assume that the NiS-$H_2SO_4$ corrosion potential is more noble than the Ni-$H_2SO_4$ corrosion potential. Therefore, during a galvanic interaction, NiS would be the cathodic phase and nickel the anodic phase. From a electronic conduction point of view, NiS is likely capable of sustaining a galvanic interaction with nickel. The bulk electrical resistivity of NiS, 2-4 $\times 10^{-7}$ $\Omega \bullet m$[135], is relatively low and in fact NiS is considered to possess metallic conduction.

Mansfeld *et al.*[140] analyzed the influence of surface area ratio on the galvanic corrosion behaviour in an attempt to provide a more fundamental understanding of galvanic corrosion. An equation relating the galvanic potential to the cathode/anode surface area ratio was derived for each of the following cases: (i) Tafel behaviour, (ii) small polarization and (iii) diffusion control. Any change in the cathode/anode surface ratio ($\theta$) with time is manifested by the change in the galvanic potential with time. For any galvanic corrosion

situation, the galvanic potential is the potential state where the total cathodic current equals the total anodic current and can be determined by superimposing the measured total cathodic polarization curve with the total anodic polarization curve of the system in question.

According to the literature, a galvanic interaction between the noncontinuous NiS deposit and the uncovered metal is the more plausible mechanism responsible for the corrosion potential transition behaviour of nickel in 93.5 wt.% $H_2SO_4$. Therefore, the attempt to better understand this mechanism involved making polarization measurements in 93.5 wt.% $H_2SO_4$ at 60°C. A galvanic couple between NiS and the uncovered nickel metal in the acid solution should establish a mixed potential, in this case a galvanic potential, at a voltage more noble than the corrosion potential of nickel and less noble than the corrosion potential of NiS. The following section presents the polarization measurements and discusses the significance.

### 5.3.2 Polarization Behaviour in 93.5 wt.% $H_2SO_4$ at 60°C

The approach employed to explore a possible galvanic interaction involved measuring the anodic polarization behaviour of a nickel RCE without NiS on its surface and the cathodic polarization behaviour of a NiS(Ni) RCE, NiS grown *in situ* on a nickel RCE, and a platinum RDE. In making such measurements it is assumed that the total anodic current generated in the NiS-Ni galvanic couple is equivalent to the anodic current measured on the nickel RCE and the total cathodic current generated is equivalent to the cathodic

current measured on the NiS(Ni) RCE.

Figure 5.10 superimposes the anodic polarization of a nickel RCE without NiS on its surface with the cathodic polarization of 93.5 wt.% $H_2SO_4$ on platinum RDE and on a nickel RCE with NiS on its surface. The cathodic polarization curve measured on the platinum RDE intersects the anodic polarization curve of the nickel RCE at a potential where $H_2SO_4$ is believed to be reduced to sulphur. Assuming that the rate of the cathodic process (current) on nickel is not higher than that on platinum, the result suggests that the corrosion of nickel without NiS on its surface in 93.5 wt.% $H_2SO_4$ can proceed with the formation of sulphur. This is consistent with the experimental observations made in Section 5.1. The cathodic polarization curve measured on the NiS(Ni) RCE intersects the anodic polarization curve of the nickel RCE at a potential significantly more noble than that of the platinum RDE. The intersection occurs at a potential where $H_2SO_4$ is believed to be reduced to $SO_2$ and therefore, suggests that the corrosion of nickel should proceed with the formation of $SO_2$. This is consistent with experimental observations made in Section 5.1.

Superimposing the cathodic polarization curve of the NiS(Ni) RCE with the anodic polarization curve of the nickel RCE without NiS on its surface for various magnitudes of $\theta$ demonstrates how the galvanic potential ($E_g$) changes during the NiS growth and dissolution, Figure 5.11. The magnitude of $\theta$ is given by,

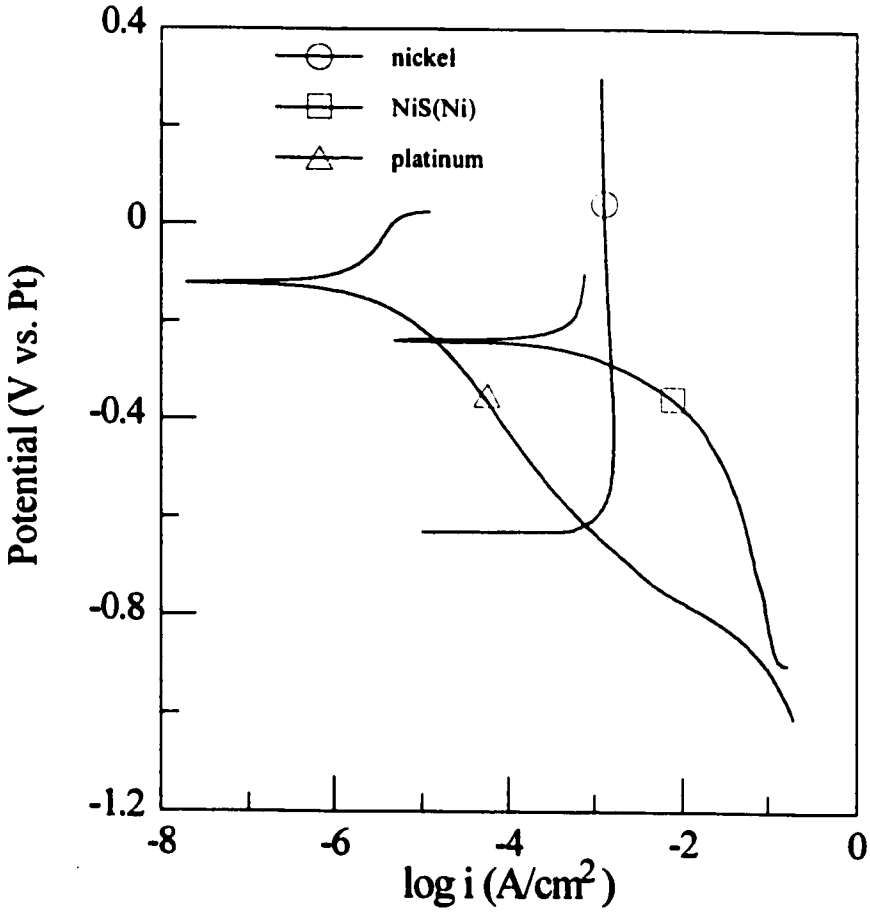


Figure 5.10. Anodic polarization of a nickel RCE (1000 rpm) without NiS superimposed with cathodic polarization of a nickel RCE (1000 rpm) with NiS and a platinum RDE (500 rpm) in 93.5 wt.% $H_2SO_4$ at 60°C. Scan rate = 20 mV/min..

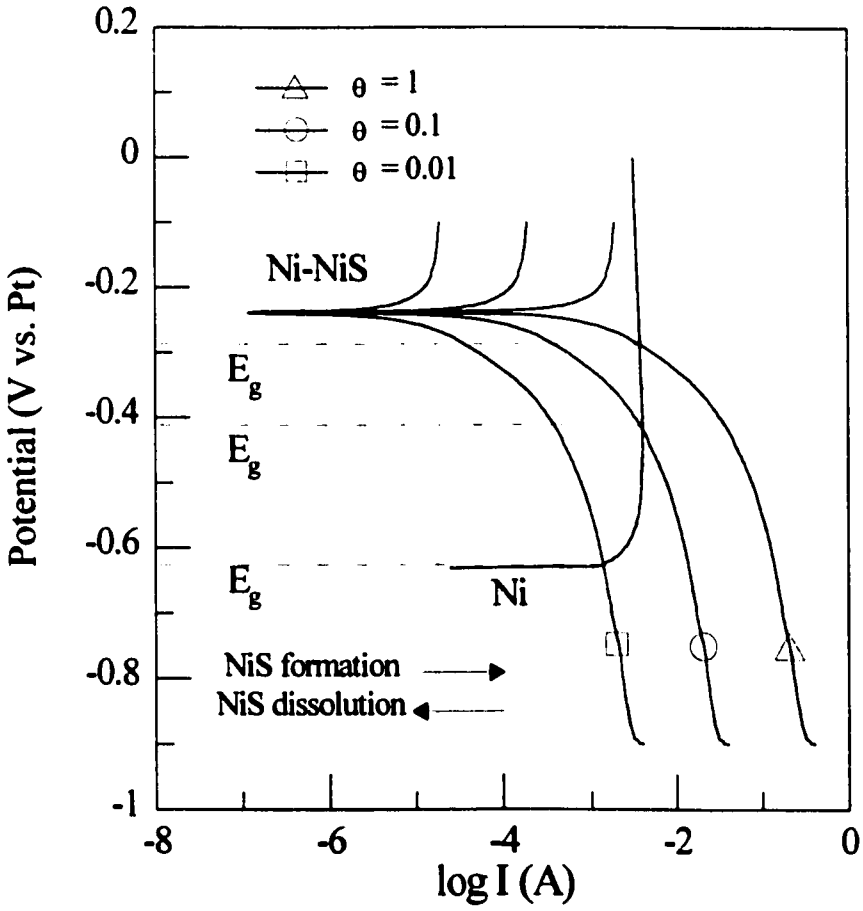


Figure 5.11. Influence of the cathode/anode surface area ratio θ on the galvanic potential of a nickel RCE (1000 rpm) and a NiS(Ni) RCE (1000 rpm) couple in 93.5 wt.% $H_2SO_4$ at 60°C.

$$\theta = \left( \frac{A}{\left( A_o - A \right)} \right) \qquad [5.13]$$

where A is the area covered by the NiS deposit and $A_o$ is the total area of the nickel substrate. As θ is increased from 0.01 to 1, $E_g$ increases from ~-0.62 to -0.28 $V_{Pt}$. The anodic polarization curve, representing the total anodic current at a given potential, is independent of θ since the limiting current arises from the diffusion of $Ni^{2+}$ ions into the bulk from the $NiSO_4$ film-solution interface which is assumed to cover the entire surface and not just the anodic sites.

## 5.4. Corrosion Mechanism of Nickel in 93.5 wt.% $H_2SO_4$

Characterizing the corrosion products that form, exploring the stability of the NiS corrosion deposit and exploring a possible galvanic interaction between NiS and the uncovered metal provided sufficient information to propose a mechanism through which nickel corrodes in 93.5 wt.% $H_2SO_4$. The first subsection to follow presents and discusses the proposed mechanistic model. The second subsection to follow presents and discusses the kinetic model developed to describe the corrosion potential behaviour.

### 5.4.1 Mechanistic Model

A possible mechanism through which nickel corrodes in 93.5 wt.% $H_2SO_4$ is depicted in Figure 5.12. The mechanism consists of the following four stages:

**(a) NiS Formation**

Immediately after immersion, nickel corrodes at a relatively high rate with the formation $H_2S$ according to the following reaction sequence:

$$\begin{aligned} &\textit{Anode:} && 4Ni = 4Ni^{2+} + 8e^- \\ &\textit{Cathode:} && 5H_2SO_4 + 8e^- = 4SO_4^{2-} + H_2S + 4H_2O \\ &\textit{Total:} && 4Ni + 5H_2SO_4 = 4NiSO_4 + H_2S + 4H_2O \end{aligned} \qquad [5.14]$$

Although not measured, the corrosion potential of nickel is more negative than the potential at which $H_2S$ becomes the primary $H_2SO_4$ reduction product. The relatively high reaction rate and solution viscosity results in a rapid build up of $H_2S$ at the metal-solution interface. The cathodic formation of $H_2S$ from the reduction of $H_2SO_4$ molecules provides a source of the required sulphide anions.

Once formed, $H_2S$ provides an alternative reaction path for surface nickel atoms. Thus, during corrosion, nickel atoms can either anodically dissolve with the formation of a

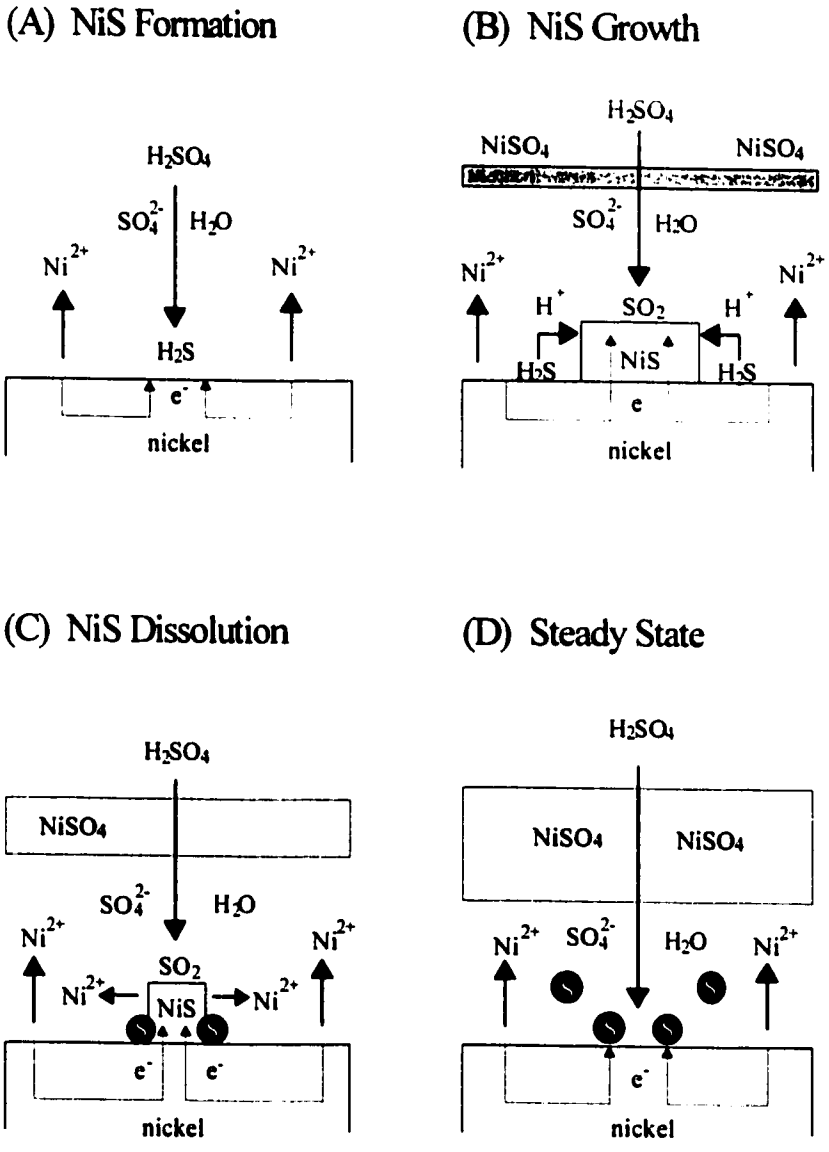


Figure 5.12. Schematic of nickel corrosion mechanism in 93.5 wt.% $H_2SO_4$.

soluble cation according to [5.12] or they can anodically dissolve with the formation of insoluble NiS according to,

$$Ni + H_2S = NiS + 2H^+ + 2e^- \qquad [5.15]$$

which has a reversible potential of -0.270 $V_{SHE}$. Therefore, after the initial formation of $H_2S$, the corrosion of nickel occurs according to the following reaction sequence which makes use of the relation $2H^+ + SO_4^{2-} = H_2SO_4$,

$$\begin{aligned} &\textit{Anode:} && 3Ni = 3Ni^{2+} + 6e^- \\ & && Ni + H_2S = NiS + 2H^+ + 2e^- \\ &\textit{Cathode:} && 5H_2SO_4 + 8e^- = 4SO_4^{2-} + H_2S + 4H_2O \\ &\textit{Total:} && 4Ni + 4H_2SO_4 = 3NiSO_4 + NiS + 4H_2O \end{aligned} \qquad [5.16]$$

resulting in the formation of a NiS surface deposit. The solid state mechanism is consistent with the formation of an initial strongly adhered surface deposit and an initial corrosion potential transient that is essentially independent of the electrode rotation rate.

It is rather difficult to comment on the nucleation process because hetrogeneities may catalyze nucleation, and because of the complexity of the process when hetrogeneities are not involved. It is reasonable to consider, however, that nucleation involves a number of

nuclei one monolayer thick on the nickel surface from which the growth stage commences.

**(b) NiS Growth - Galvanic Polarization Stage**

The growth of NiS following nucleation results in the formation of a thick, noncontinuous film on the surface. The growth of a thick film likely results from the NiS phase being a reasonably good conductor of both ions and electrons. According to Hoar[141], it is the high mobility of electrons and cuprous ions ($Cu^+$) in defective cuprous sulphide that leads to the rapid formation of a ~2000 Å sulphide surface film during the corrosion of copper in polysulphide solutions. The growth of a noncontinuous film likely results from the excess of nickel equivalents dissolving as soluble cations ($Ni^{2+}$) coupled with the limited supply of the reactant $H_2S$ at the metal-solution interface (discussed below).

Once its growth stage commences, NiS establishes a galvanic interaction with the nickel substrate. During the interaction, the cathodic reaction involved in the corrosion of NiS,

$$2H_2SO_4 + 2e^- = SO_4^{2-} + SO_2 + 2H_2O \qquad [5.17]$$

is enhanced on NiS sites, whereas the anodic reactions involved in the dissolution of nickel,

$$Ni = Ni^{2+} + 2e^- \qquad [5.12]$$

$$Ni + H_2S = NiS + 2H^+ + 2e^- \qquad [5.15]$$

are enhanced on nickel sites. The growth of NiS continues despite the discontinued cathode production of $H_2S$ due to the presence of excess $H_2S$ at the metal-solution interface and terminates once reaction [5.15] consumes all the excess $H_2S$. The measured apparent corrosion potential of nickel is now the galvanic potential ($E_g$) of the NiS-Ni couple and is a function of the both the cathodic and anodic kinetic parameters and the cathode/anode surface area ratio ($\theta$).

**(c) NiS Dissolution - Galvanic Depolarization Stage**

The magnitude of $\theta$ at the instant the growth process terminates is relatively large since the noncontinuous NiS film covers the majority of the nickel surface. The large $\theta$ coupled with the high cathodic current for the reduction of $H_2SO_4$ molecules on NiS produce a galvanic situation where the galvanic potential is controlled essentially at the corrosion potential for the oxidative dissolution of NiS. Therefore, the anodic process,

$$NiS = Ni^{2+} + S + 2e^- \qquad [5.18]$$

(with a reversible potential of 0.162 $V_{SHE}$) takes place with a significant rate along with the cathodic process [5.17] on NiS. The significance of these results is that the dissolution of the Ni-NiS galvanic interaction proceeds according to the following reaction sequence:

$$
\begin{aligned}
&\textit{Anode}\,(Ni): && Ni = Ni^{2+} + 2e^- \\
&\textit{Anode}\,(NiS): && NiS = Ni^{2+} + S + 2e^- \\
&\textit{Cathode}\,(NiS): && 2H_2SO_4 + 4e^- = 2SO_4^{2-} + SO_2 + 4H_2O \\
&\textit{Total}: && Ni + NiS + 2H_2SO_4 = 2NiSO_4 + S + SO_2 + 4H_2O
\end{aligned}
\qquad [5.19]
$$

As NiS dissolves during galvanic corrosion, θ decreases and thus, the galvanic potential decreases. Figure 5.11 demonstrates how the galvanic potential $E_g$ changes with θ during the dissolution stage. As θ decreased from 1 to 0.01, $E_g$ decreases from ~-0.28 to -0.62 $V_{Pt}$. Based on the galvanic potential transients measured during the corrosion of nickel, the finite residence time of NiS results from its dissolution rate being significantly slower than its growth rate.

**(d) Steady State Stage**

The galvanic interaction no longer exists once all the NiS dissolves. At this point, the steady state corrosion of nickel occurs, proceeding according to the following reaction sequence:

$$
\begin{aligned}
&\textit{Anode}: && 3Ni = 3Ni^{2+} + 6e^- \\
&\textit{Cathode}: && 4H_2SO_4 + 6e^- = 3SO_4^{2-} + S + 4H_2O \\
&\textit{Total}: && 3Ni + 4H_2SO_4 = 3NiSO_4 + S + 4H_2O
\end{aligned}
\qquad [5.20]
$$

NiS does not reform during the steady state stage since the corrosion potential is more positive than the potential at which $H_2S$ becomes the primary product of the cathodic reaction.

It is possible that the insoluble sulphur deposit formed from the dissolution of NiS sufficiently inhibits the anodic kinetics of nickel so as to induce a small anodic polarization. Adhered sulphur is believed to be responsible for the residual polarization observed after cathodic polarization of platinum in 98 wt.% $H_2SO_4$[4] and 100 wt.% $H_2SO_4$ with 5-20 wt.%[52]. The corrosion potential resulting from the sulphur-induced anodic polarization occurs at a potential state where sulphur is the primary $H_2SO_4$ reduction product.

### 5.4.2 Galvanic Potential Behaviour

According to the galvanic corrosion model, the galvanic potential is a function of $\theta$ which is a function of time. Therefore, by modelling the NiS growth and dissolution kinetics and determining the corresponding galvanic potential transient, the galvanic coupling model can be verified. As pointed out above the exact NiS nucleation and growth mechanism is unknown and is rather difficult to determine experimentally. Nonetheless, an attempt based on the physical situation described below for nickel corrosion in 93.5 wt.% $H_2SO_4$ at 60°C, successfully reproduced the general form of the $E_g$-t dependence and, thus, supported the concept of a galvanic interaction.

As a first approximation, it is reasonable to consider that the growth of NiS is controlled by rate at which nickel atoms anodically dissolve to form NiS according to [5.15]. For the growth of an anodic deposit,

$$\frac{dV}{dt} = \frac{IM}{zF\rho} \qquad [5.21]$$

where V is the volume of the deposit, I is the anodic dissolution current, M is the molecular mass of the deposit, z is the number of electrons transferred per mole of deposit, F is Faraday's constant and ρ is the density of the deposit. Assuming that NiS grows as a hemispherical cap with radius r and height h, a reasonable assumption considering surface energy contributions, on a circular nickel surface with radius $r_o$ (constant), the change in volume at a constant height is governed by the change in radius according to:

$$dV = \pi hrdr \qquad [5.22]$$

When metal dissolution controls the anodic growth rate, the current is given by,

$$I = i(A_o - A) \qquad [5.23]$$

where i is the current density on the uncovered metal surface, $A_o$ is the total metal surface area, $\pi r_o^2$ and A is the area covered by the deposit. Substituting [5.22] and [5.23] into [5.21], integrating and rearranging gives,

$$r^2 = r_o^2 - \exp\left(-\frac{t}{\tau_g}\right) \qquad [5.24]$$

where $r_o$ is the radius of the circular nickel surface and $\tau_g = zF\rho h/2iM$. Figure 5.13(a) shows the fraction $A/A_o$ as a function of $t/\tau_g$.

Considering now the NiS dissolution kinetics, it is reasonable to assume that the rate is controlled by the diffusion of nickel ions ($Ni^{2+}$) ions into solution from the $NiSO_4$ film-solution interface. The anodic polarization behaviour of the nickel RCE and the effect of the electrode rotation rate on the weight loss of a nickel RCE support the assumption of mass transport controlled dissolution. When mass transport controls the dissolution rate, the change in volume with time is given by,

$$\frac{\rho}{M}\frac{dV}{dt} = \frac{DA_o}{\delta}\left(C_s - C_b\right) \qquad [5.25]$$

where all symbols have their previously defined representation. Assuming NiS dissolves as a hemispherical cap of initial radius $r_i$ and constant height h on a circular nickel surface of radius $r_o$ and $C_b = 0$, then substituting [5.22] into [5.25], integrating and rearranging gives,

$$r^2 = r_i^2 - \frac{1}{r_o^2}\frac{t}{\tau_d} \qquad [5.26]$$

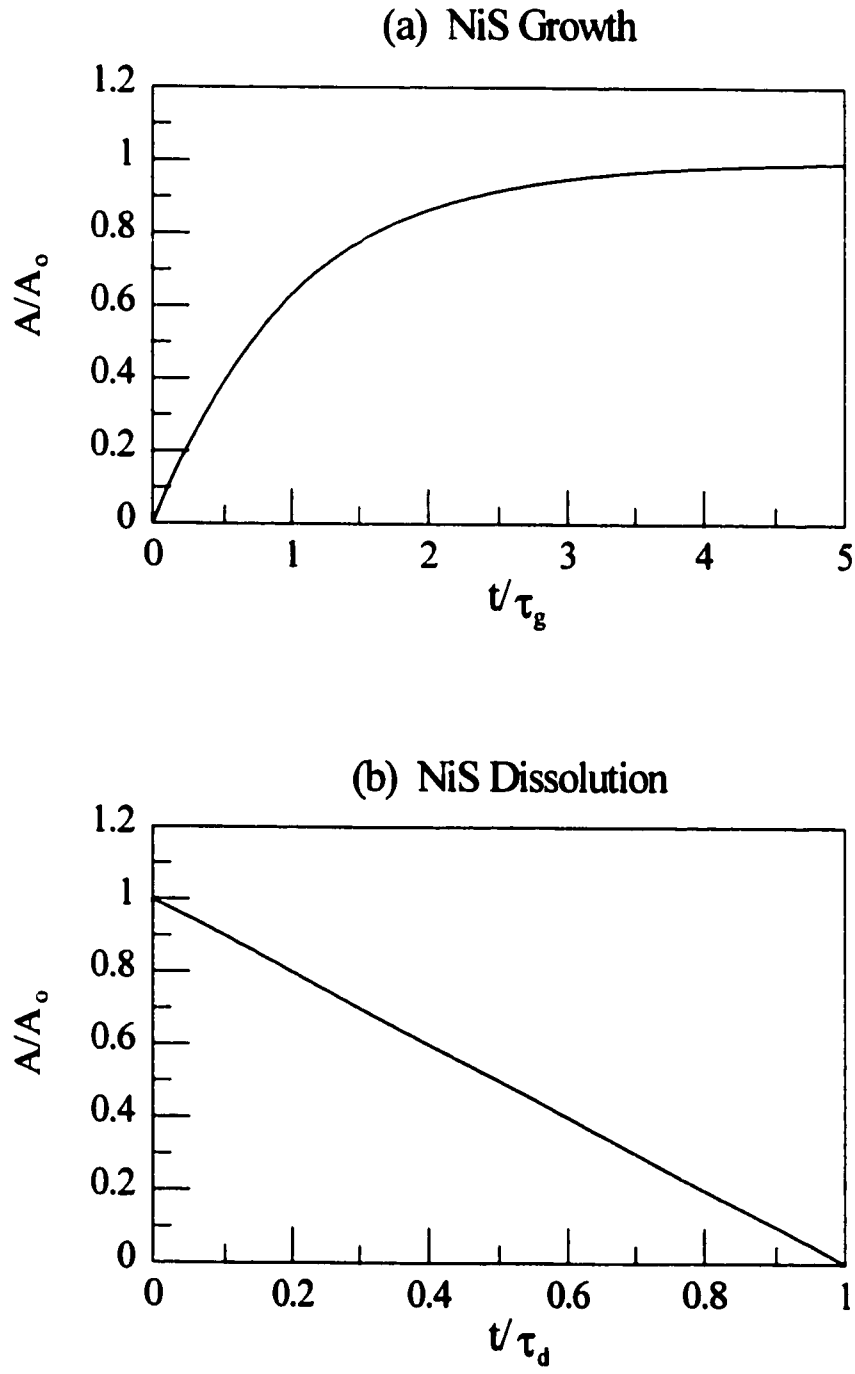


Figure 5.13. Changes in the area covered by NiS. (a) During growth when the metal dissolution controls the rate; (b) During dissolution when convective mass transfer controls the rate.

where $\tau_d = \rho\delta h/DMC_s$. Figure 5.13(b) shows $A/A_o$ as a function of $t/\tau_d$.

The corrosion potential of a nickel RCE when rotated at 1000 rpm in 93.5 wt.% $H_2SO_4$ at 60°C reached a maximum after about 12 minutes exposure and then proceeded to decay, first slowly and then more rapidly, for a period of about 36 minutes before attaining its steady state (Figure 5.5). It is reasonable to consider that the growth of NiS occurred during the initial 12 minute period, whereas the dissolution of NiS occurred during the next 36 minute period. By assuming that the growth rate is significantly higher than the dissolution rate at all times during growth such that the dissolution rate is neglected, then [5.24] determines the $E_g$-t dependence during the initial 12 minutes exposure (NiS growth) and [5.26] determines the $E_g$-t during the next 36 minutes (NiS dissolution). The $E_g$-t dependence corresponding to either [5.24] or [5.26] can be determined graphically using the nickel and NiS(Ni) polarization curves according to the procedure discussed in Section 5.3.3 (Figure 5.11).

It is believed that the NiS deposit forms a noncontinuous film on the surface of nickel and, therefore, $\theta$ attains a maximum value $\theta^m$. Based on the aforementioned assumptions, $\theta$ reaches $\theta^m$ at the point the growth process terminates; after 12 minutes exposure. For the graphical determination of the $E_g$-t dependence, it is assumed that $\theta^m = 3$ which corresponds to a surface coverage, $A/A_o = 0.75$.

Figure 5.14 shows $\theta$, derived from [5.24] and [5.26] using the assumptions described above and the galvanic potential, determined graphically using Figure 5.11, as a function of

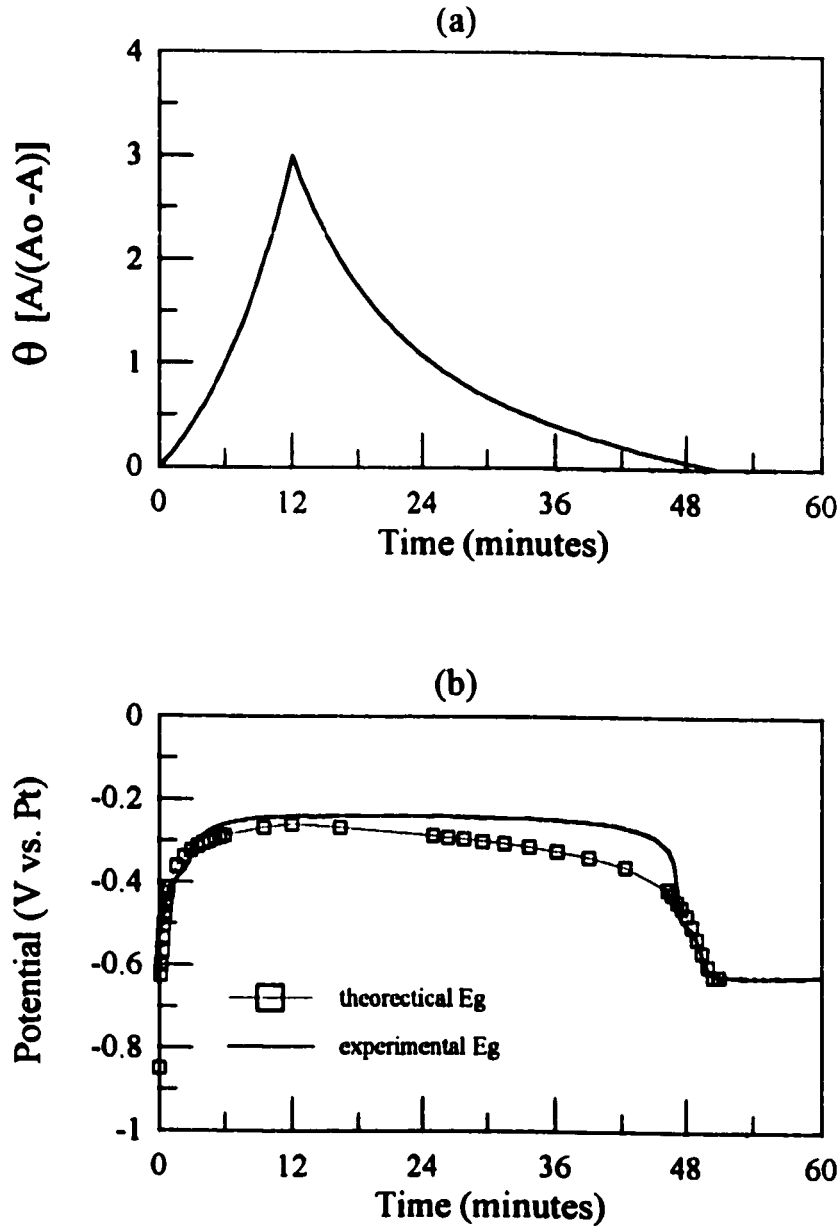


Figure 5.14. Theoretical changes during the growth and dissolution of NiS on a nickel electrode in 93.5 wt.% $H_2SO_4$ at 60°C (1000 rpm). (a) θ as a function of time; (b) NiS-Ni galvanic potential ($E_g$) as a function of time superimposed with measured corrosion potential of a nickel RCE under identical conditions.

time during the growth and subsequent dissolution of the NiS deposit. Superimposed in the $E_g$-t plot is the measured potential transient of nickel when rotated at 1000 rpm in 93.5 wt.% $H_2SO_4$ at 60°C. The theoretical and experimental curves are clearly of the same form, and the agreement is reasonably good except at long times. It appears that the galvanic interaction theory fit the facts reasonably well despite the fact that the exact NiS nucleation and growth process is unknown.

## 5.5. Summary

The research conducted in Chapter 4 showed that a better understanding of the corrosion mechanism of nickel is necessary to meet the primary objectives of the study defined in Section 1.1. The objective of the research presented and discussed in this chapter is to elucidate the corrosion mechanism of nickel in 93.5 wt.% $H_2SO_4$ in order to provide answers to the following questions:

1. What is the black deposit that forms during the initial stage of nickel corrosion?
2. What is the mechanism through which the black deposit forms and subsequently dissolves during the corrosion of nickel?
3. Does the formation and subsequent dissolution of the black deposit significantly influence the corrosion potential of nickel?
4. Does the formation and subsequent dissolution of the black deposit

only occur once during the corrosion of nickel?

5. Does change in temperature and/or stirring affect the rate of formation and/or subsequent dissolution of black deposit?

The experimental approach used to work through the problem involved a long term corrosion test in quiet 93.5 wt.% $H_2SO_4$ at 60°C and a series of short term corrosion tests in stirred 93.5 wt.% $H_2SO_4$ at 60°C. The long term test employed immersion, electrochemical and X-ray spectroscopy techniques to characterize the soluble and insoluble anodic and cathodic products that form as a function of time during the corrosion of nickel. The short term test in stirred solutions employed electrochemical techniques using rotating electrodes to characterize the influence of stirring, bulk nickel ion concentration and temperature on the different processes that occur during the corrosion of nickel. The interpretation of the results lead to the development of a mechanistic model that provides a consistent account of the experimental observations.

It is concluded that corrosion of nickel involves the participation of $H_2SO_4$ molecules that leads to the formation of soluble sulphur dioxide ($SO_2$) and several solid products including nickel sulphide (NiS), nickel sulphate ($NiSO_4$) and elemental sulphur. None of the solid films that form during corrosion are protective. Prior to establishing a steady state, the corrosion of nickel involves the formation and subsequent dissolution of a noncontinuous NiS deposit. When present on the nickel surface, NiS establishes a galvanic interaction with

the uncovered metal, significantly polarizing the nickel anodic dissolution reaction. The anodic dissolution rate of nickel is essentially unaffected during the galvanic-induced polarization since the rate determining step is the convective mass transfer of nickel ions from a precipitated $NiSO_4$ surface film. A theoretical model considering the growth and subsequent dissolution of the NiS deposit and its corresponding galvanic interaction with the uncovered nickel metal can predict the measured corrosion potential response.

At this point the view was formed that a similar galvanic mechanism is responsible for the active-passive corrosion of the nickel-stainless steel S30403. The *in situ* formation of NiS establishes a galvanic interaction with the stainless steel which significantly polarizes the anodic reaction. Stainless steel passivity is achieved with a sufficient surface coverage of NiS. As the galvanic interaction is only temporary as a result of the subsequent dissolution of NiS, depassivation occurs as the passive film is not stable without sufficient anodic polarization.

The next chapter, Chapter 6, presents and discusses the results of experiments conducted to explore a galvanic interaction between NiS(Ni) and stainless steel S43000. The results demonstrate the ability of this galvanic couple to anodically passivate S43000 in those conditions where the active-passive corrosion of the nickel-stainless steel S30403 occurs. Modelling the active-passive behaviour using a NiS-S43000 galvanic couple provides a reasonable explanation of the active-passive behaviour and, thus, meets the objectives identified in Section 1.1.

# CHAPTER 6

## 6. GALVANIC PASSIVATION OF STAINLESS STEEL

The two areas requiring further research identified in Section 4.4.3 are the conditions in which the anodic passive state of 17 wt.% chromium-stainless steels is stable and the role of alloyed nickel in determining that state. The conditions of stability identified for S30403 (Section 4.2) are misleading since the formation and subsequent dissolution of nickel-rich corrosion product is believed to play a major role in the passivation and depassivation process respectively. Experiments conducted in Chapter 5 show that the nickel-rich corrosion product in question is NiS. The objectives of the research presented and discussed in this chapter are to clarify the conditions in which passivity (chromium-rich oxide surface film) is stable and to clarify the role of alloyed nickel in promoting spontaneous passivation and subsequent depassivation.

The experimental approach adopted to meet these objectives involved modelling the active-passive corrosion of S30403 in concentrated $H_2SO_4$-$H_2O$ solutions with a NiS(Ni)-S43000 galvanic couple. In particular, the approach involved demonstrating a galvanic-induced anodic passivation of S43000 by NiS(Ni), confirming galvanic passivation conditions are satisfied for S43000 and nickel as a function of temperature, stirring (electrode rotation rate) and $H_2SO_4$ concentration. The model was then used to explain the influence of temperature, stirring and $H_2SO_4$ concentration on the active-passive corrosion of S30403.

This chapter is organized into five major sections. The first section presents the results of the tests conducted comparing and contrasting the corrosion behaviour of a S43000 electrode with and without a NiS(Ni) galvanic interaction in 93.5 wt.% $H_2SO_4$ at 60°C. The second section presents the results of the anodic polarization measurements made on a S43000 RCE as a function of temperature and stirring in 93.5 wt.% $H_2SO_4$. The third section presents the galvanic passivation model proposed to explain the active-passive corrosion of S30403 in 93.5 wt.% $H_2SO_4$. The fourth section presents the results of the tests conducted on nickel, S43000 and S30403 electrodes in 90 and 96.4 wt.% $H_2SO_4$ at 60°C. The fifth section summarizes the major conclusions drawn from the research conducted.

## 6.1 NiS(Ni)-S43000 Galvanic Couple in 93.5 wt.% $H_2SO_4$

The first step taken to meet the objectives defined above involved demonstrating the ability of NiS, grown *in situ* on nickel, to anodically passivate a 17 wt.% chromium-stainless

steel during a galvanic interaction in 93.5 wt.% $H_2SO_4$ at 60°C. The following subsections present and discuss the results of the experiments conducted.

### 6.1.1 NiS(Ni) Galvanic-Induced Passivation of S43000

The first experiment consisted of making a periodic external electrical contact between a S43000 electrode with a NiS(Ni) electrode (NiS formed *in situ* on a nickel electrode) both of equal surface area (2.95 $cm^2$). Connecting the two external electrodes leads with a copper wire provided an external electrical contact. Figure 6.1 shows the potential of the S43000 electrode during the periodic galvanic coupling experiment in 93.5 wt.% $H_2SO_4$ at 60°C as a function of time. The potential quickly became stable at ~-0.82 $V_{Pt}$ during the first 15 minutes exposure prior to electrical contact. Immediately after establishing electrical contact with the NiS(Ni) electrode, the corrosion potential of the S43000 electrode increased rapidly from ~- 0.82 $V_{Pt}$ to ~- 0.25 $V_{Pt}$ where it remained stable. Upon removing the electrical contact after 15 minutes, the potential decreased rapidly from ~-0.25 $V_{Pt}$ and quickly became stable at ~0.82 $V_{Pt}$. An identical potential response occurred during subsequent coupling for a period of 30 and 60 minutes respectively.

The basic concepts of the potential response during the galvanic couple can be understood by considering the form and the relative positions of the anode and cathode polarization curves of the S43000 and NiS(Ni) electrodes respectively in 93.5 wt.% $H_2SO_4$ at 60°C, Figure 6.2. The curves showed that for electrodes of equal surface area:

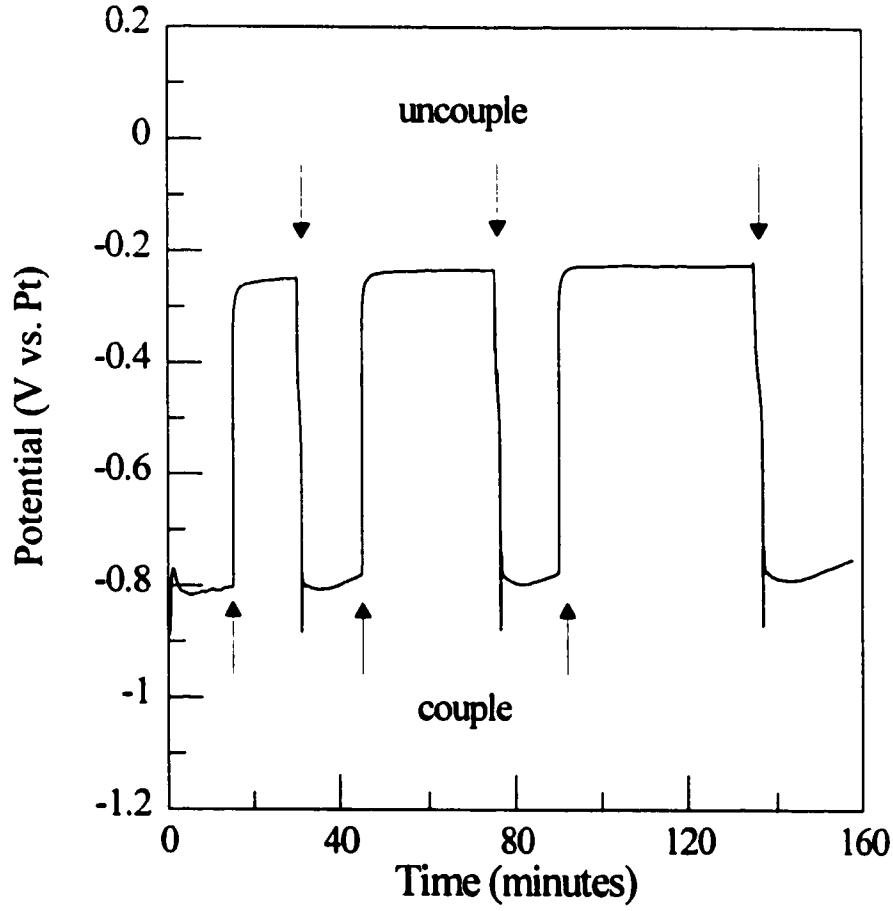


Figure 6.1. Influence of periodic NiS(Ni) galvanic couple on corrosion potential of a S43000 electrode in quiet 93.5 wt.% $H_2SO_4$ at 60°C immediately after immersion.

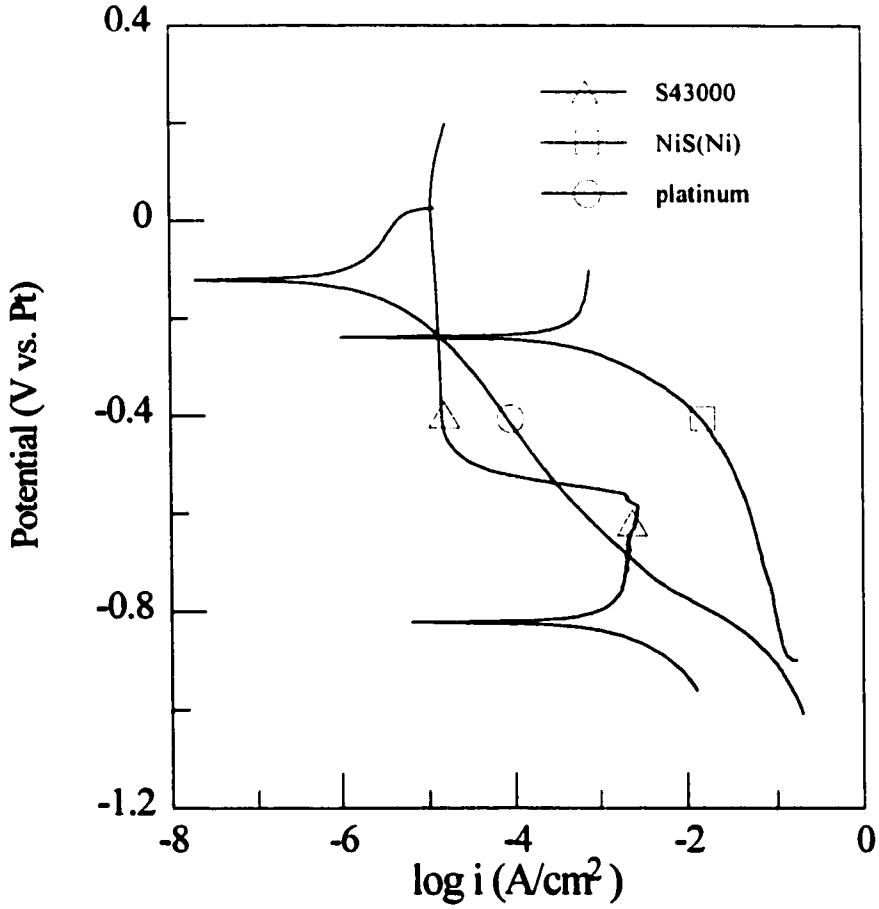


Figure 6.2. Superimposed potentiodynamic anodic polarization of a S43000 electrode and cathodic polarization of a platinum and NiS(Ni) electrode in quiet 93.5 wt.% $H_2SO_4$ at 60°C. Scan rate = 20 mV/min.

1. The corrosion potential of NiS(Ni) is more noble than the passivation potential of S43000.
2. The cathodic current of NiS(Ni) is greater than the critical passivation current of S43000.
3. The galvanic potential occurs at a potential close to the corrosion potential of NiS(Ni).

According to the potential response in Figure 6.1, a galvanic passivation of the S43000 electrode occurred when electrically coupled to the NiS(Ni) electrode of an equal surface area. Rapid passivation occurred upon making electrical contract and rapid depassivation occurred upon removing electrical contact.

According to Figure 6.2, the NiS(Ni) galvanic-induced passivation of the S43000 electrode occurs only when the cathodic current on the NiS(Ni) electrode is greater than the critical passivation current of the S43000 electrode and, therefore, depends on the cathode/anode surface area ratio, $\theta$. In this case the cathode area is the area of the NiS(Ni) electrode and the anode area is the area of the S43000 electrode. Figure 6.3 shows the effect of $\theta$ on the ability of the NiS(Ni) electrode to anodically passivate the S43000 electrode. According to Figure 6.3, galvanic passivation of the S43000 electrode occurs when $\theta \geq \theta^*$ (~0.05), the critical cathode/anode surface area ratio required for galvanic passivation.

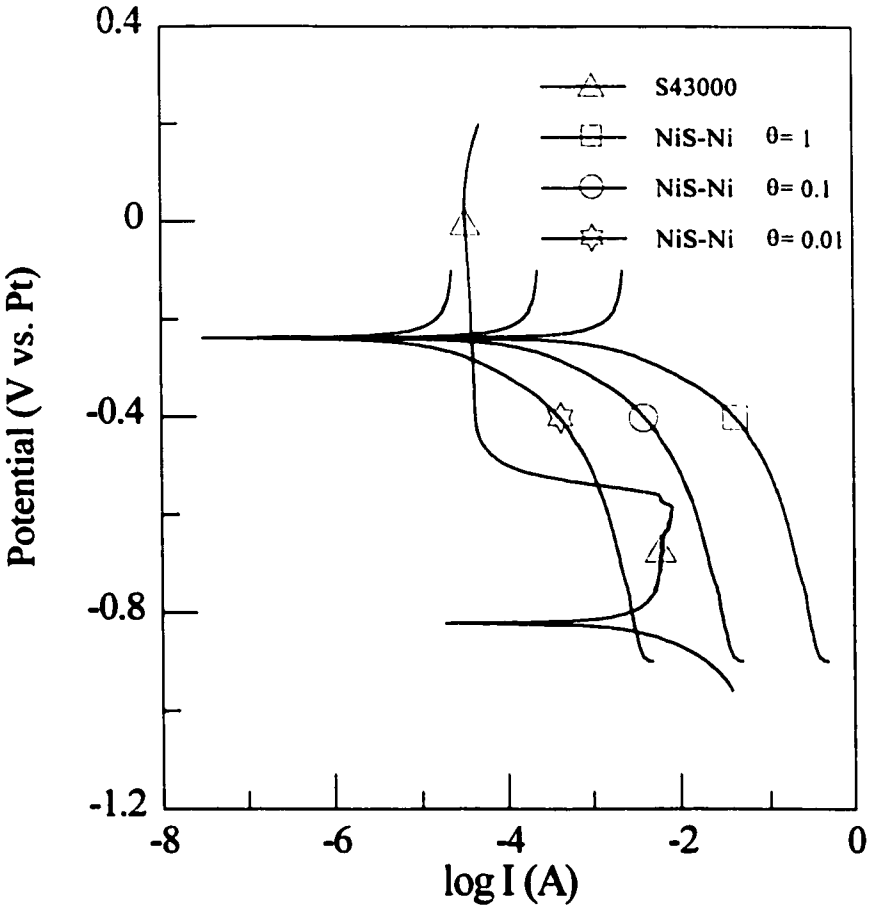


Figure 6.3. Influence of θ ($A_{NiS(N)i}/A_{S43000}$) on the galvanic passivation of a S43000 electrode by a NiS(Ni) electrode in quiet 93.5 wt.% $H_2SO_4$ at 60°C.

### 6.1.2 Modelling the Active-Passive Corrosion of S30403

The next experiment involved measuring the corrosion behaviour of a NiS(Ni)-S43000 galvanic couple in stirred 93.5 wt.% $H_2SO_4$ at 60°C to demonstrate its ability to reproduce the active-passive corrosion behaviour of S30403 under identical conditions. Modelling the active-passive corrosion behaviour of S30403 using a NiS(Ni)-S43000 galvanic couple involved making the following modifications:

1. Adjusting the NiS(Ni)-S43000 surface area ratio $\theta$ to make it more representative to that which occurs during the corrosion of S30403.
2. Coupling the two electrodes prior to the immersion of the nickel electrode to ensure that the galvanic interaction starts instantaneously with the nucleation and growth of NiS.
3. Rotating the NiS(Ni) electrode to promote the dissolution of NiS and thus, *in situ* depassivation of the S43000 electrode.

As a first approximation it is reasonable to calculate $\theta$ using the stoichiometry of S30403. This involves assuming that the surface consists of 8 wt.% nickel and that the area covered by the NiS deposit equals the stoichiometric area of the surface nickel atoms. The calculated stoichiometric magnitude of $\theta$ for S30403 is 0.081 which is greater than the predicted critical value of 0.05 required for the NiS(Ni) induced galvanic passivation of S43000. Employing a flag shaped S43000 electrode with a 36.13 $cm^2$ surface area and nickel RCE with a 2.95 $cm^2$ surface area achieved the required $\theta$ of 0.081. The flag shaped S43000

electrode, 4.25 $cm^2$ base with a 0.6 x 15 cm rectangular stem, was prepared from a 0.1 cm thick sheet. A heat shrink PTFE tube was used to mask the stem to ensure exposure of only the square base.

Figure 6.4 shows the potential of the S43000 electrode during the modified galvanic coupling experiment in 93.5 wt.% $H_2SO_4$ at 60°C as a function of time. A rapid increase in potential from ~-0.90 to ~-0.27 $V_{Pt}$ occurred upon immersion of the pre-coupled nickel electrode. The rapid increase in potential coincided with the formation of NiS on the nickel electrode. After reaching ~-0.25 $V_{Pt}$, the potential remained stable for a period of ~40 minutes before it decayed rapidly and became stable ~-0.70 $V_{Pt}$. The rapid decrease in potential coincided with the dissolution of NiS on the nickel electrode.

Comparing the galvanic potential response in Figure 6.4 with the oscillatory corrosion potential of S30403, Figure 4.1, shows that the NiS(Ni)-S43000 galvanic couple essentially reproduced the potential features of one cycle. Both curves show the following:

1. A rapid increase of potential in the positive direction.
2. A slow decrease of potential in the negative direction from a maximum of ~-0.25 $V_{Pt}$ for a finite period.
3. A rapid decrease in potential following the period of the slow decrease.

The NiS(Ni)-S43000 galvanic interaction did not produce potential oscillations since the galvanic potential stabilized at ~-0.70 $V_{Pt}$ after the transition. After its dissolution, NiS did

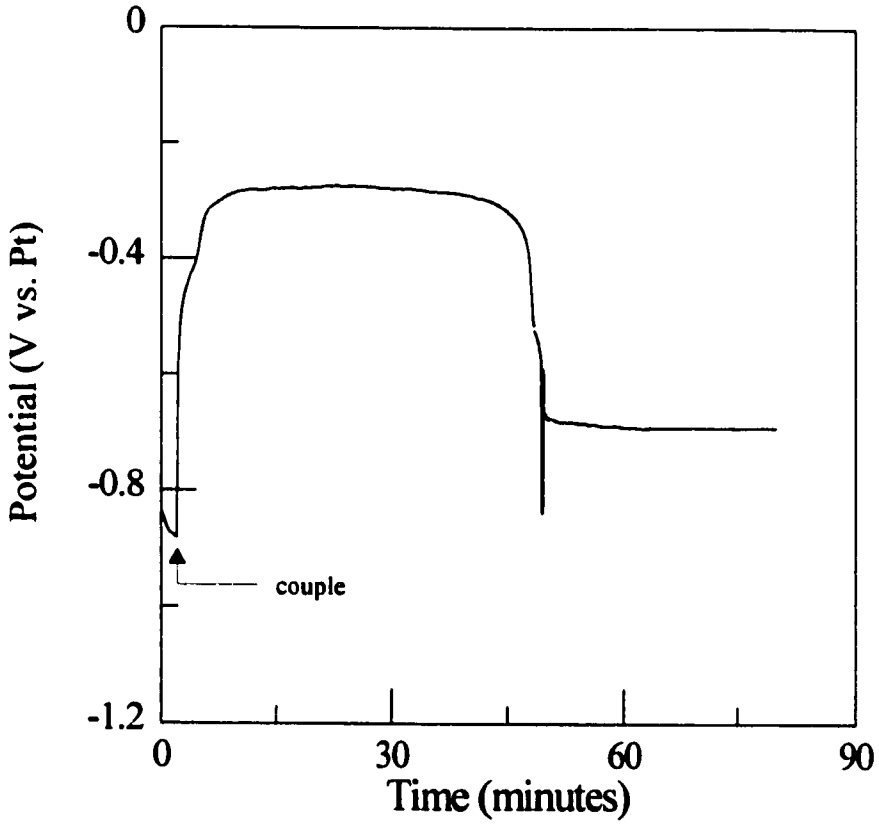


Figure 6.4. Influence of a NiS(Ni) RCE (1000 rpm) galvanic couple on the corrosion potential of a S43000 electrode (0rpm) in 93.5 wt.% $H_2SO_4$ at 60°C. $\theta$ = 0.081

not reform on the nickel electrode despite the galvanic potential decaying to a potential more negative than the potential at which $H_2S$ becomes the primary $H_2SO_4$ reduction product (Section 5.3). Furthermore, the passive state period of the S43000 electrode produced during the galvanic interaction, ~50 minutes, is significantly lower than the passive state period of the S30403 RCE, ~90 minutes, under identical conditions. The lack of a cyclic galvanic potential response and the difference in the passive state period are likely a consequence of the IR potential drop introduced by employing separate electrodes to reproduce the anodic and cathodic reactions occurring simultaneously on a single electrode.

Weight loss measurements provided additional evidence that anodic passivation of the S43000 electrode occurred during a galvanic interaction with a NiS(Ni) RCE with $\theta$ = 0.081. Table 6.1 shows the four hour weight loss data of the S43000 electrode with and without a NiS(Ni) galvanic couple. Galvanic coupling with a NiS(Ni) RCE decreased the weight loss by two orders of magnitude. Furthermore, the four hour weight loss measured during corrosion in the galvanic-induced passivated state, 0.03 mg/cm$^2$, corresponds well with the calculated four hour weight loss of 0.05 mg/cm$^2$ using the passive state current of 13.61 $\mu$A/cm$^2$ obtained from the anodic polarization curve.

The NiS(Ni)-S43000 galvanic coupling experiments conducted demonstrate the ability of a NiS(Ni) electrode to galvanically passivate a S43000 electrode in 93.5 wt.% $H_2SO_4$ at 60°C. Comparing and contrasting the galvanic corrosion behaviour of the couple with the active-passive corrosion behaviour of S30403 under identical conditions shows that

the couple is successful in reproducing the major features of a single active-passive cycle.

**Table 6.1.** Influence of a NiS(Ni) Galvanic Interaction on the Weight Loss (4 hour) of a S43000 Electrode (0 rpm) in 93.5 wt.% $H_2SO_4$ at 60°C

| NiS(Ni) Galvanic Couple | Weight Loss ($mg/cm^2$) |
|---|---|
| With | 0.03 |
| Without | 3.69 |

## 6.2 Influence of Temperature and Stirring on the Anodic Behaviour of S43000

Active-passive corrosion of S30403 occurred at all temperatures and electrode rotation rates studied in 93.5 wt.% $H_2SO_4$. For a galvanic interaction between NiS, formed *in situ* from the corrosion of the 8 wt.% nickel component, and the Fe-17 wt.%Cr base alloy to be responsible for the active-passive corrosion, several conditions for each material must be satisfied. Conditions for NiS include the following:

1. *In situ* formation during active state corrosion of nickel component.
2. Sufficient growth to anodically passivate the Fe-17 wt.%Cr base alloy.
3. *In situ* dissolution during passive state corrosion.

Conditions for the Fe-17wt.%Cr base alloy include the following:

1. Active state corrosion in open-circuit condition.
2. Passivation with anodic polarization.
3. Depassivation without anodic polarization .

Experiments discussed in Chapter 5 demonstrate that conditions 1 and 3 for NiS are satisfied for all temperatures and electrode rotation rates where the active-passive corrosion of S30403 occurred. Galvanic coupling experiments discussed in Section 6.1 demonstrate that condition 2 for NiS is satisfied for 60°C and there is no reason to believe otherwise for lower temperatures. Next, experiments conducted to explore the anodic behaviour of a S43000 RCE show that conditions 1 to 3 are satisfied for the Fe-17wt.%Cr base alloy in all solution environments where the active-passive corrosion of S30403 occurred.

### 6.2.1 Influence of Temperature on the Anodic Behaviour of S43000

Figure 6.5 shows the influence of temperature on the potentiodynamic anodic polarization of a S43000 RCE (1000 rpm) in 93.5 wt.% $H_2SO_4$. An active to passive transition occurred with increasing anodic polarization at each temperature studied. Increasing the temperature increased both the limiting active ($i_l$) and limiting passive ($i_p$) anodic current density. The results indicate that passivity of the S43000 RCE at 1000 rpm rotation is not spontaneous and requires anodic polarization at all temperatures studied

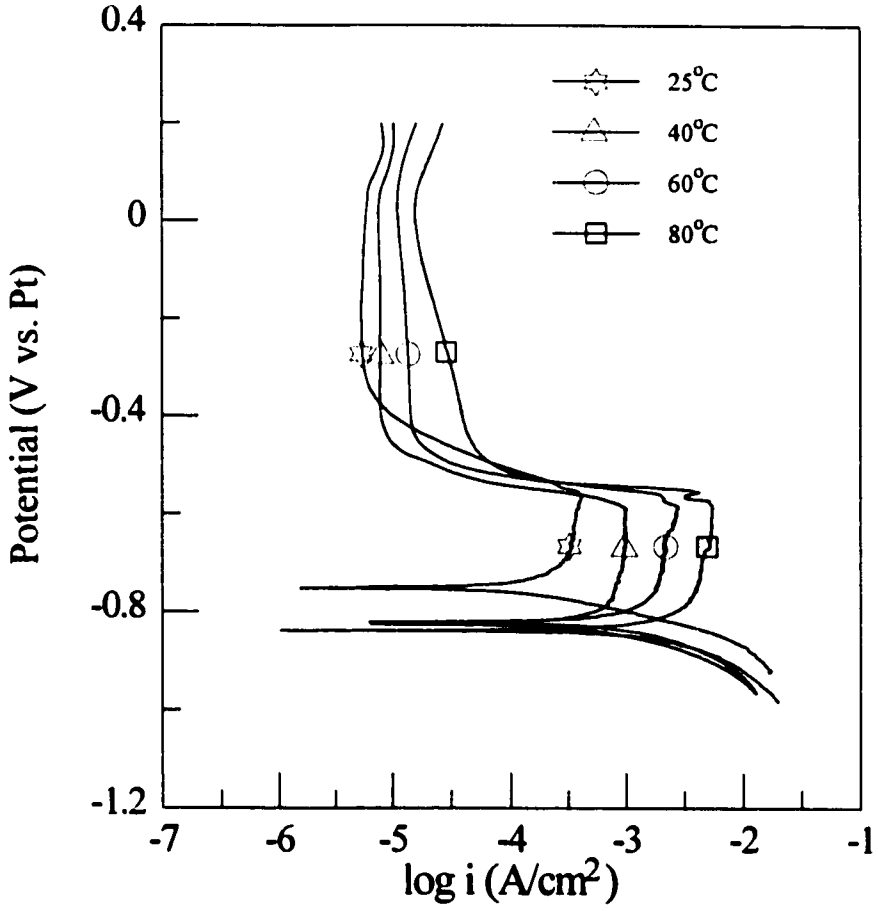


Figure 6.5. Influence of temperature on the potentiodynamic anodic polarization of a S43000 RCE (1000 rpm) in 93.5 wt.% $H_2SO_4$. Scan rate = 20 mV/min.

between 25-80°C.

Weight loss measurements conducted to explore the corrosion of the S43000 RCE under open-circuit conditions show that passivity is not spontaneous. Table 6.2 shows the effect of influence of temperature on weight loss of the S43000 RCE measured after 240 hours exposure in 93.5 wt.% $H_2SO_4$. Included in the Table 6.2 are the limiting active and passive state current densities taken from the anodic polarization curves. Converting the measured weight loss to a current density and comparing with the measured current densities suggest that the S43000 RCE corrodes in an active state regardless of temperature.

**Table 6.2.** Influence of Temperature on the Corrosion of a S43000 RCE (1000 rpm) in 93.5 wt.% $H_2SO_4$

| Temp. °C | Wt. Loss mg/cm$^2$ | Rate mg/cm$^2$/hr | Calculated i mA/cm$^2$ | $i_l$ mA/cm$^2$ | $i_p$ mA/cm$^2$ |
|---|---|---|---|---|---|
| 25 | 7.66 | 1.91 | 2.03 | 0.36 | $6.28\times10^{-3}$ |
| 40 | 7.73 | 1.93 | 2.05 | 0.88 | $8.46\times10^{-3}$ |
| 60 | 13.49 | 3.37 | 3.57 | 2.20 | $1.35\times10^{-2}$ |
| 80 | 28.41 | 7.10 | 7.52 | 4.58 | $2.61\times10^{-2}$ |

The limiting anodic current (corrosion rate) that occurs prior to the active-passive transition is believed to result from the precipitation of a metal sulphate film at the alloy-solution interface. Similar to the corrosion of iron and nickel in concentrated $H_2SO_4$-$H_2O$,

the rate limiting step during anodic dissolution is likely the diffusion of metal cations from the film-solution interface into the bulk solution. Section 5.2 provides a detailed discussion of the effect of temperature on corrosion when mass transfer is the rate limiting step.

The anodic polarization curves and the weight loss data show that the galvanic passivation conditions 1 and 2 are satisfied for the Fe-17wt.%Cr base alloy in stirred 93.5 wt.% $H_2SO_4$ at all temperatures between 25-80°C. Recording the open-circuit potential response of S43000 after potentiodynamic anodic polarization shows that the galvanic passivation condition 3 for the Fe-17wt.%Cr base alloy is also satisfied. Figure 6.6 shows the open-circuit potential response of the S43000 RCE as a function of time for the various temperatures. Each potential transient had an arrest that occurred at a potential in the active-passive transition region of the respective anodic polarization curve, the period of which decreased with an increase in temperature. After the arrest, the potential rapidly decayed and became stable at a potential similar to the corrosion potential of the anodic polarization curve, regardless of temperature between 40-80°C. The results indicate that anodic passivity at temperatures between 40-80°C is not stable without anodic polarization and its breakdown is thermally activated. The potential transient at 25°C was not recorded beyond 60 minutes.

### 6.2.2 Influence of Stirring on the Anodic Behaviour of S43000

Figure 6.7 shows the effect of the stirring (RCE rotation rate) on the potentiodynamic anodic polarization behaviour of a S43000 RCE in 93.5 wt.% $H_2SO_4$ at 60°C. An active-

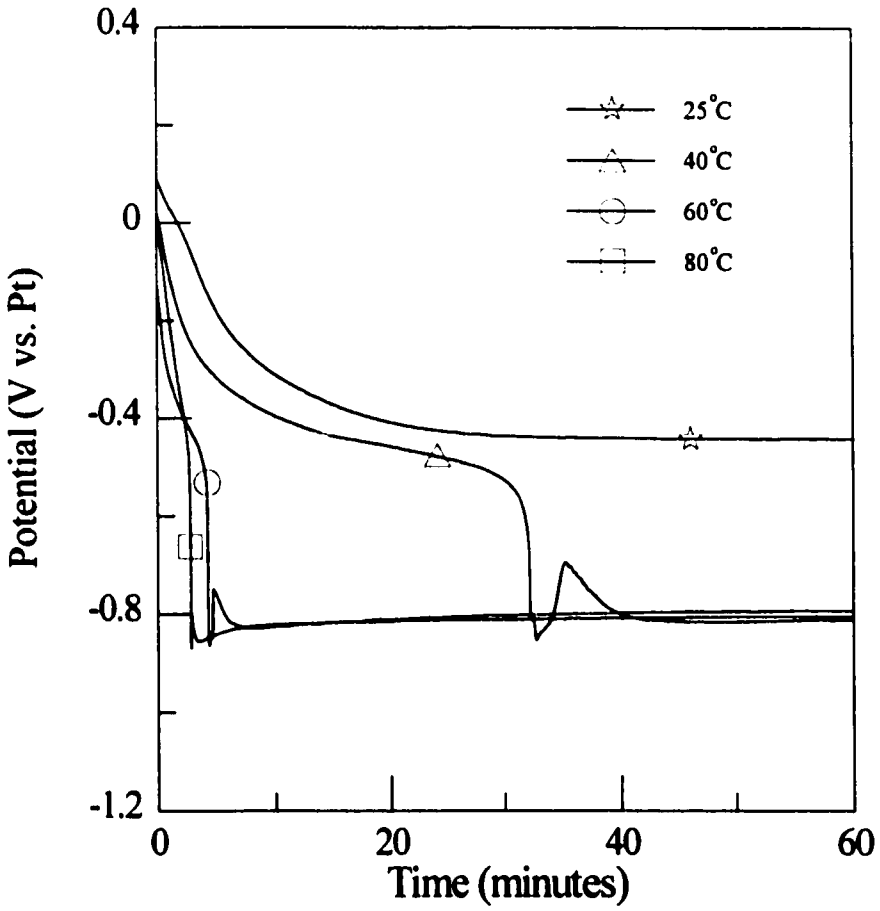


Figure 6.6. Influence of temperature on the open-circuit potential response of a S43000 RCE (1000 rpm) after potentiodynamic anodic polarization in 93.5 wt.% $H_2SO_4$.

passive transition occurred with increasing anodic polarization at each rotation rate studied. Increasing the rotation rate increased the limiting active anodic current but had practically no effect on the limiting passive anodic current. The rotation-independent passive anodic current provides additional support that anodic passivity of 17 wt.% chromium-stainless steels involves the solid-state film formation of a protective surface film The results suggest that passivity of the S43000 RCE is not spontaneous and requires anodic polarization at all electrode rotation rates studied between 0-2000 rpm.

Weight loss measurements conducted to explore corrosion of the S43000 RCE under open-circuit conditions show that passivity is not spontaneous. Table 6.3 shows the influence of stirring (RCE rotation rate) on weight loss of the S43000 RCE measured after 240 hours exposure in 93.5 wt.% $H_2SO_4$. Included in the Table 6.3 are the limiting active and passive state current densities taken from the respective anodic polarization curves. Converting the measured weight loss to a current density and comparing with the measured current densities shows that the S43000 RCE corrodes in an active state. The rotation-dependent weight loss, under open-circuit conditions, along with the rotation-dependent limiting active anodic current suggest a mass transport-controlled corrosion in the active state. Similar to the corrosion of iron and nickel in concentrated $H_2SO_4$-$H_2O$, the rate limiting step during anodic dissolution is likely the diffusion of metal cations from a precipitated metal sulphate film-solution interface into the bulk solution. Section 5.2 provides a detailed discussion of the effect of stirring on corrosion when mass transfer is the

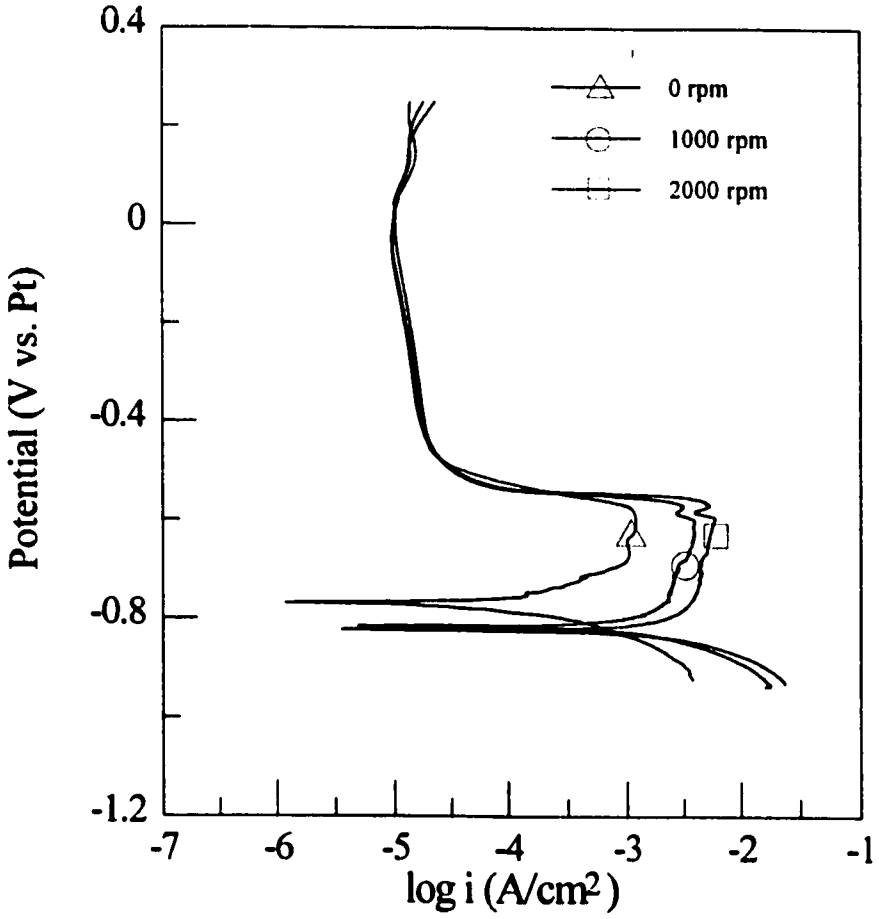


Figure 6.7. Influence of the electrode rotation rate on the potentiodynamic anodic polarization of a S43000 RCE in 93.5 wt.% $H_2SO_4$ at 60°C. Scan rate = 20 mV/min.

rate limiting step.

**Table 6.3.** Influence of Stirring on the Corrosion of a S43000 RCE in 93.5 wt.% $H_2SO_4$ at 60°C

| Rotation rpm | Wt. Loss $mg/cm^2$ | Rate $mg/cm^2/hr$ | i $mA/cm^2$ | $i_l$ $mA/cm^2$ | $i_p$ $mA/cm^2$ |
|---|---|---|---|---|---|
| 0 | 3.69 | 0.92 | 0.98 | 0.20 | $1.37\times10^{-2}$ |
| 1000 | 13.49 | 3.37 | 3.57 | 2.20 | $1.35\times10^{-2}$ |

The anodic polarization curve and the weight loss data show that the galvanic passivation conditions 1 and 2 are satisfied for the Fe-17wt.%Cr base alloy at all rotation rates between 0-2000 rpm in 93.5 wt.% $H_2SO_4$ at 60°C. Recording the open-circuit potential response of the S43000 RCE after potentiostatic anodic polarization shows that the galvanic passivation condition 3 for the Fe-17wt.%Cr base alloy is also satisfied. Figure 6.8 shows the open-circuit potential response as a function of time for the various electrode rotation rates. Rotation had practically no effect on the potential decay kinetics. The potential decreased rapidly within the first three minutes and became stable at a potential which, according to the respective anodic polarization curve, corresponds to the active state. The results suggest that anodic passivity is not stable without anodic polarization regardless of the electrode rotation rate and its breakdown is insensitive to rotation.

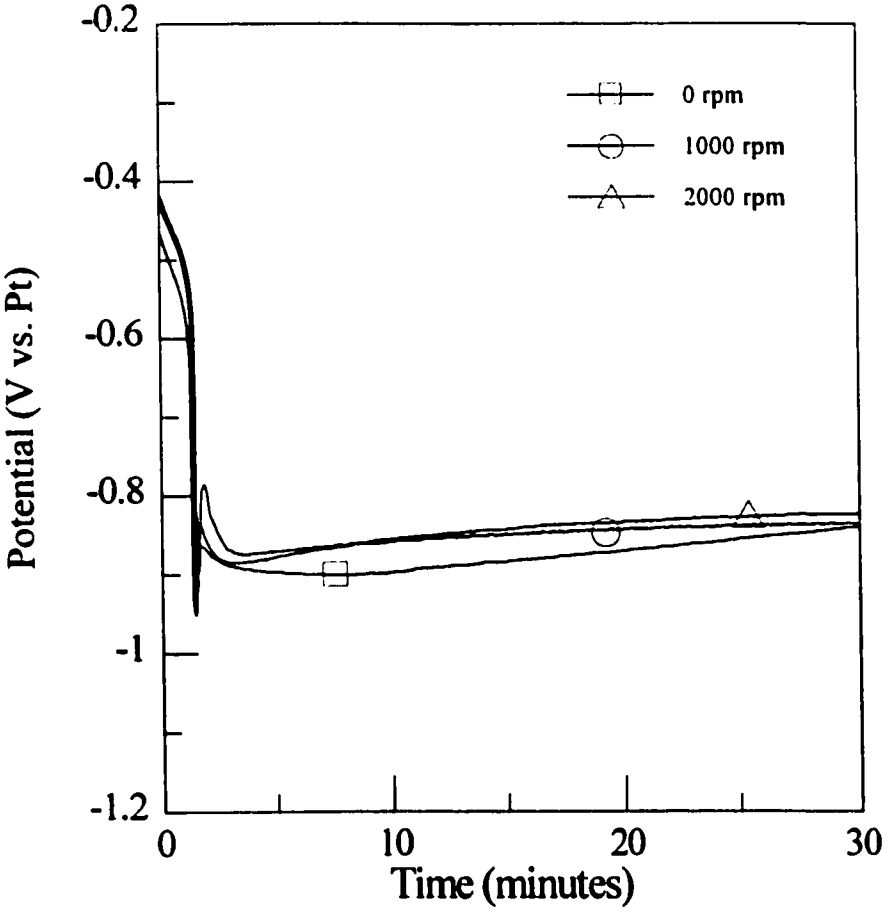


Figure 6.8. Influence of the electrode rotation rate on the open-circuit potential response of a S43000 RCE after potentiostatic polarization to -0.2 $V_{Pt}$ for 60 minutes in 93.5 wt.% $H_2SO_4$ at 60°C.

## 6.3 Active-Passive Corrosion Mechanism of S30403 in 93.5 wt.% $H_2SO_4$

Experiments conducted thus far demonstrated that the major conditions necessary for a galvanic-induced passivation of S43000 by coupling with NiS, formed *in situ* on nickel, are satisfied in 93.5 wt.% $H_2SO_4$ at 25-80°C and 0-2000 rpm rotation. The active-passive corrosion of S30403 is believed to occur through a similar mechanism; a galvanic-induced passivation of the Fe-17wt.%Cr base alloy by coupling with NiS, formed *in situ* during the anodic dissolution of the 8 wt.% nickel component. The following subsections present the proposed mechanistic model, a kinetic model describing the corresponding $E_g$-t dependence and a discussion using the proposed model to explain the influence of temperature and stirring respectively on the active-passive corrosion behaviour.

### 6.3.1 Mechanistic Model

Figure 6.9 depicts the corrosion mechanism of S30403 in 93.5 wt.% $H_2SO_4$ and consists of the following four stages.

#### (a) Active State Corrosion - NiS Formation

Beginning with the active state, iron and chromium atoms anodically dissolve with the cathodic formation of $H_2$ according to the reaction sequence,

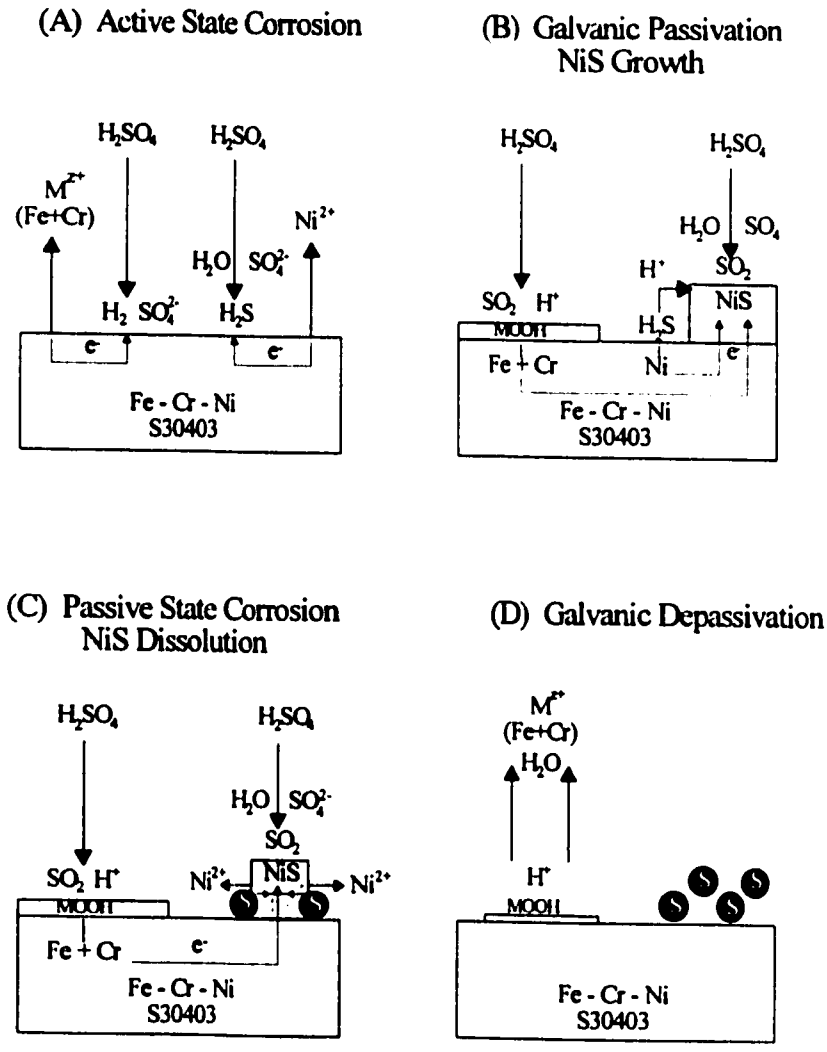


Figure 6.9. Schematic of the S30403 corrosion mechanism in 93.5 wt.% $H_2SO_4$

$$\begin{aligned} &\textit{Anode:} && xM = xM^{n+} + xne^- \\ &\textit{Cathode:} && yH_2SO_4 + 2ye^- = yH_2 + ySO_4^{2-} \\ &\textit{Total:} && xM + yH_2SO_4 = M_y(SO_4)_x + yH_2 \end{aligned} \qquad [6.1]$$

where M represents both iron and chromium atoms. Similar to pure nickel, nickel atoms anodically dissolve with the cathodic formation of $H_2S$ according to the following reaction sequence:

$$\begin{aligned} &\textit{Anode:} && 4Ni = 4Ni^{2+} + 8e^- \\ &\textit{Cathode:} && 5H_2SO_4 + 8e^- = 4SO_4^{2-} + H_2S + 4H_2O \\ &\textit{Total:} && 4Ni + 5H_2SO_4 = 4NiSO_4 + H_2S + 4H_2O \end{aligned} \qquad [6.2]$$

The relatively high reaction rate and solution viscosity result in the rapid build up of dissolved $H_2S$ in the boundary layer. Once present in the boundary layer, $H_2S$ provides an alternative reaction path for the surface nickel atoms. As a result, nickel atoms can either anodically dissolve as soluble cations according to,

$$Ni = Ni^{2+} + 2e^- \qquad [6.3]$$

or they can anodically dissolve as cations which are directly incorporated into an insoluble

NiS deposit according to the following reaction:

$$Ni + H_2S = NiS + 2H^+ + 2e^- \qquad [6.4]$$

Therefore, after the initial formation of $H_2S$, the anodic dissolution of the nickel atoms occurs according to the following reaction sequence which makes use of the relation $2H^+ + SO_4^{2-} = H_2SO_4$,,

$$\begin{aligned} &\textit{Anode:} && 3Ni = 3Ni^{2+} + 6e^- \\ & && Ni + H_2S = NiS + 2H^+ + 2e^- \\ &\textit{Cathode:} && 5H_2SO_4 + 8e^- = 4SO_4^{2-} + H_2S + 4H_2O \\ &\textit{Total:} && 4Ni + 5H_2SO_4 = 3NiSO_4 + NiS + 4H_2O \end{aligned} \qquad [6.5]$$

resulting in the solid state formation of a NiS surface deposit. Although the exact mechanism is unknown, the nucleation and growth of NiS on the alloy surface is believed to involve the nucleation of a number of nuclei one monolayer thick from which the growth stage commences.

The corrosion of S30403 occurs at a potential where the total cathodic current balances the total anodic current. In this state, the corrosion potential is more negative than the passivating potential of the alloy, the equilibrium potential of $H_2$ evolution and the

potential at which $H_2S$ becomes the primary $H_2SO_4$ reduction product.

**(b) Galvanic Passivation - NiS Growth**

Once its growth stage commences, NiS establishes a galvanic interaction with the base alloy. During the interaction, the cathodic reaction involved in the oxidative dissolution of NiS,

$$2H_2SO_4 + 2e^- = SO_4^{2-} + SO_2 + 4H_2O \qquad [6.6]$$

is enhanced on the growing NiS deposit, whereas the anodic reactions involved in the oxidative dissolution of the alloy,

$$M = M^{n+} + ne^- \qquad [6.7]$$

$$Ni + H_2S = NiS + 2H^+ + 2e^- \qquad [6.4]$$

where M represents iron, chromium and nickel atoms, are enhanced on the uncovered alloy surface. The growth of NiS continues despite the discontinued cathodic formation of $H_2S$ due to the presence of excess $H_2S$ dissolved in the boundary layer.

The corrosion potential is now a galvanic potential that increases as $\theta$ increases during the growth of the NiS deposit. When $\theta > \theta^*$, the critical cathode/anode surface area ratio required for galvanic passivation, the cathodic current generated in the galvanic couple is sufficient to anodically passivate the base alloy. Sufficient corrosion of the 8 wt.% nickel

component according to [6.2] and [6.4] occurs in the active state such that when the NiS growth process terminates, $\theta$ is > $\theta^*$.

Anodic passivation of the base alloy likely involves the solid state formation of an oxide-type film, according to,

$$M + H_2SO_4 = M(HSO_4)_{ad} + H^+ + e^- \quad [6.9]$$

$$M(HSO_4)_{ad} = MOOH + SO_2 \quad [6.10]$$

where M represents chromium atoms and possibly iron atoms similar to that proposed for chromium in concentrated $H_2SO_4$-$H_2O$ solutions[97,98]. As a consequence of the high corrosion current density of NiS in 93.5 wt.% $H_2SO_4$, the galvanic-induced anodic passivation occurs at a relatively low $\theta$, which results in the protective oxide film covering the majority of the alloy surface.

**(c) Passive State Corrosion - NiS Dissolution**

The high corrosion current density of NiS in 93.5 wt.% $H_2SO_4$ produces a situation where the galvanic potential is controlled essentially at the corrosion potential for the oxidative dissolution of NiS. Therefore, the anodic process,

$$NiS = Ni^{2+} + S + 2e^- \quad [6.11]$$

takes place with a significant rate along with the cathodic process [6.6] on NiS. As a

consequence, the anodic process of the galvanic couple in the passive state consists of the oxidative dissolution of metals atoms in the alloy according to [6.7] and the oxidative dissolution of NiS according to [6.11]. The cathodic process of the galvanic couple involves the reduction of $H_2SO_4$ molecules according to [6.6]. As NiS dissolves during galvanic corrosion, $\theta$ decreases and therefore, the galvanic potential decreases. The galvanic-induced anodic passivation of the base alloy remains stable along as $\theta > \theta^*$.

**(d) Depassivation**

Once the condition $\theta < \theta^*$ is met, the cathodic current on NiS is no longer sufficient to stabilize the anodic passive state of the base alloy. Without sufficient current (anodic polarization) the protective oxide film rapidly dissolves, likely according the following:

$$MeOOH + 3H^+ = Me^{3+} + 2H_2O \qquad [6.12]$$

As the passive film rapidly dissolves, the galvanic potential decreases rapidly. Complete dissolution of the protective oxide film restores the active state. Here, the film-free reactivity of the iron, chromium and nickel components reestablishes the alloy's initial corrosion potential. At this point the entire process repeats.

### 6.3.2 Galvanic Potential Behaviour

According to the galvanic interaction model, the galvanic potential ($E_g$) is a function

of θ which is a function of time. Therefore, by modelling the NiS growth and dissolution kinetics and the corresponding θ-t dependence, the $E_g$-t dependence can be determined graphically from representative polarization curves. The galvanic passivation model can then be verified by comparing this calculated $E_g$-t dependence with the cyclic $E_{corr}$-t dependence of S30403. As pointed out above, the exact nucleation and growth mechanism is unknown and is rather difficult to determine experimentally. Nonetheless, an attempt based on the physical situation described below for the active-passive corrosion of S30403 in 93.5 wt.% $H_2SO_4$ at 60°C successfully reproduced the general cyclic form of the $E_g$-t dependence including the spike structure.

The physical situation describing the NiS growth and dissolution processes is identical to that presented in Section 5.4.2. There, it is assumed that NiS grows and dissolves as a hemispherical cap with radius r and a constant height h. For convenience, only the resultant equations describing the time dependence of the cap radius during growth and dissolution are presented here. The time dependence of the cap radius during growth is given by,

$$r^2 = r_o^2 - \exp\left(-\frac{t}{\tau_g}\right) \qquad [6.13]$$

where $r_o$ is the radius of the circular alloy surface and $\tau_g = zF\rho h/2iM$. The time dependence of the cap radius during dissolution is given by,

$$r^2 = r_i^2 - r_o^2 \frac{t}{\tau_d} \qquad [6.14]$$

where $r_i$ is the initial radius and $\tau_d = \rho\delta h/DMC_s$.

As discussed in Chapter 4, active state corrosion of S30403 occurs during the potential spikes and passive state corrosion occurs during the period between the spikes. In 93.5 wt.% $H_2SO_4$ at 60°C the active state period of the S30403 RCE, when rotated at 1000 rpm, is about 2 seconds, whereas the passive state period is about 90 minutes. It is reasonable to consider that the growth of NiS occurs during the 2 second active state period, whereas the dissolution of NiS occurs during the subsequent 90 minute passive state period. If the growth rate is significantly higher than the dissolution rate at all times during growth such that the dissolution rate is neglected, then [6.13] determines the θ-t dependence during the 2 second active state (NiS growth) and [6.14] determines the θ-t during the 90 minutes passive state (NiS dissolution).

It is believed that the NiS deposit forms a noncontinuous film on the surface of S30403 and, therefore, θ attains a maximum value $\theta^m$. Based on the aforementioned assumptions, θ reaches $\theta^m$ at the point the growth process terminates; after the 2 second active state period. For the determination of the θ-t dependence, it is assumed that $\theta^m$ = 0.081 which corresponds to a surface coverage, $A/A_o$ = 0.075. The corresponding $E_g$-t dependence is determined graphically using representative polarization curves. If the total

cathodic current in the couple is equivalent to the cathodic current measured on a NiS(Ni) electrode as a function of potential and the total anodic current in the couple is equivalent to anodic current on a S43000 electrode as a function of potential, then Figure 6.3 can used to graphically determine the $E_g$-$\theta$ dependence.

Figure 6.10(a) shows the $\theta$-t dependence during growth and subsequent dissolution of the NiS hemispherical cap deposit derived from [6.13] and [6.14] using the assumptions described above. Figure 6.10(b) shows the corresponding calculated $E_g$-t dependence incorporating the $E_g$-$\theta$ dependence determined graphically using Figure 6.3. Superimposed in the $E_g$-t plot is the measured corrosion potential of a S30403 RCE (1000 rpm) in 93.5 wt.% $H_2SO_4$ at 60°C. The calculated and experimental curves are clearly of the same form, and the agreement is reasonably good.

Figure 6.11 shows the calculated $E_g$-t dependence during a potential spike on a much finer time scale. Superimposed in Figure 6.12 is the measured corrosion potential of a S30403 RCE (1000 rpm) in 93.5 wt.% $H_2SO_4$ at 60°C during a potential spike. The galvanic passivation model is successful in reproducing the three distinct stages of a potential spike: passive-active transition, the finite active state period and the active-passive transition.

### 6.3.3 Influence of Temperature and Stirring on Active-Passive Corrosion

According to the galvanic passivation model, any parameter affecting $d\theta/dt$ during the active state and/or passive state corrosion changes the corresponding period and, thus,

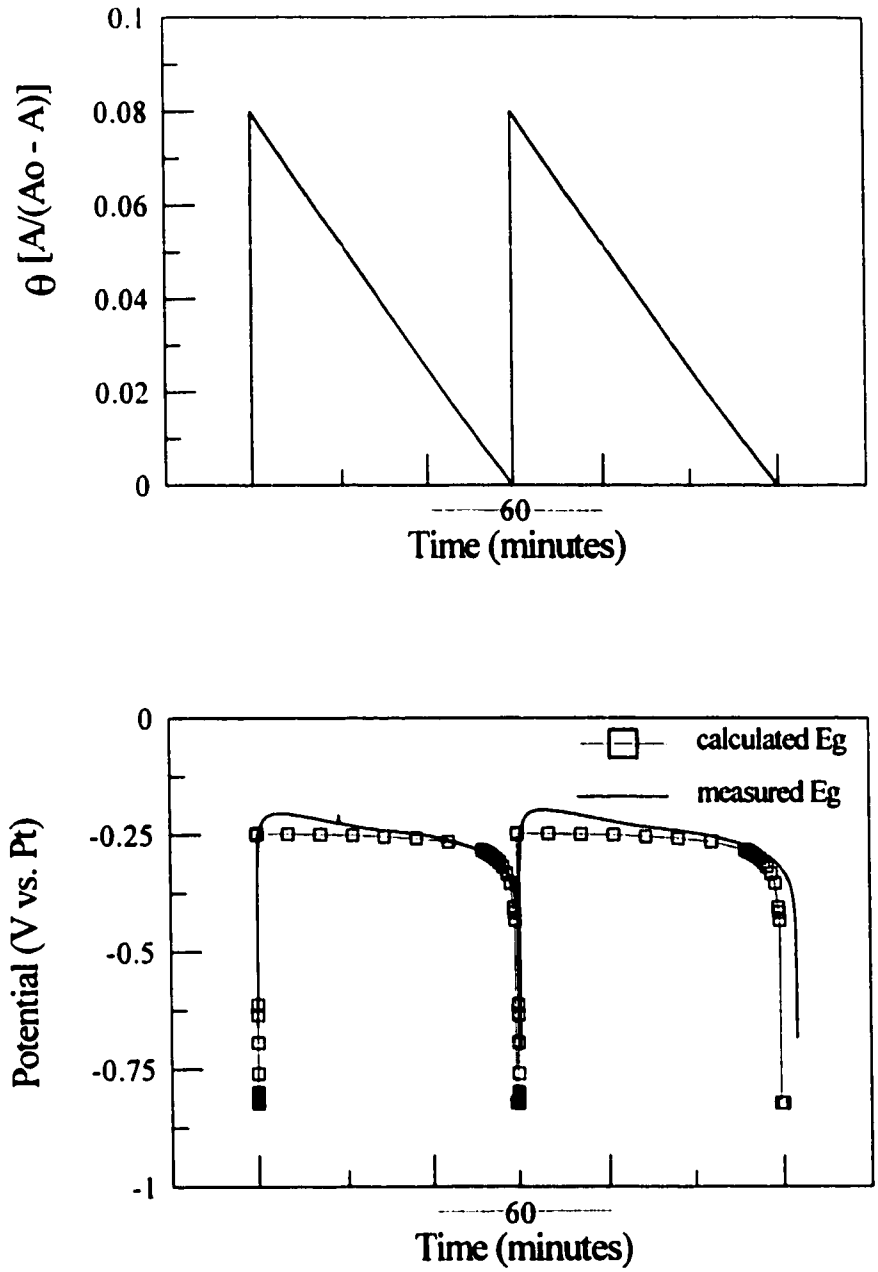


Figure 6.10. Theoretical changes during the growth and dissolution of NiS on a S30403 RCE (1000 rpm) electrode in 93.5 wt.% $H_2SO_4$ at 60°C. (a) θ as a function of time; (b) NiS(Ni)-UNS S43000 galvanic potential ($E_g$) as a function of time superimposed with the measured corrosion potential of a S30403 RCE (1000 rpm) in 93.5 wt.% $H_2SO_4$ at 60°C.

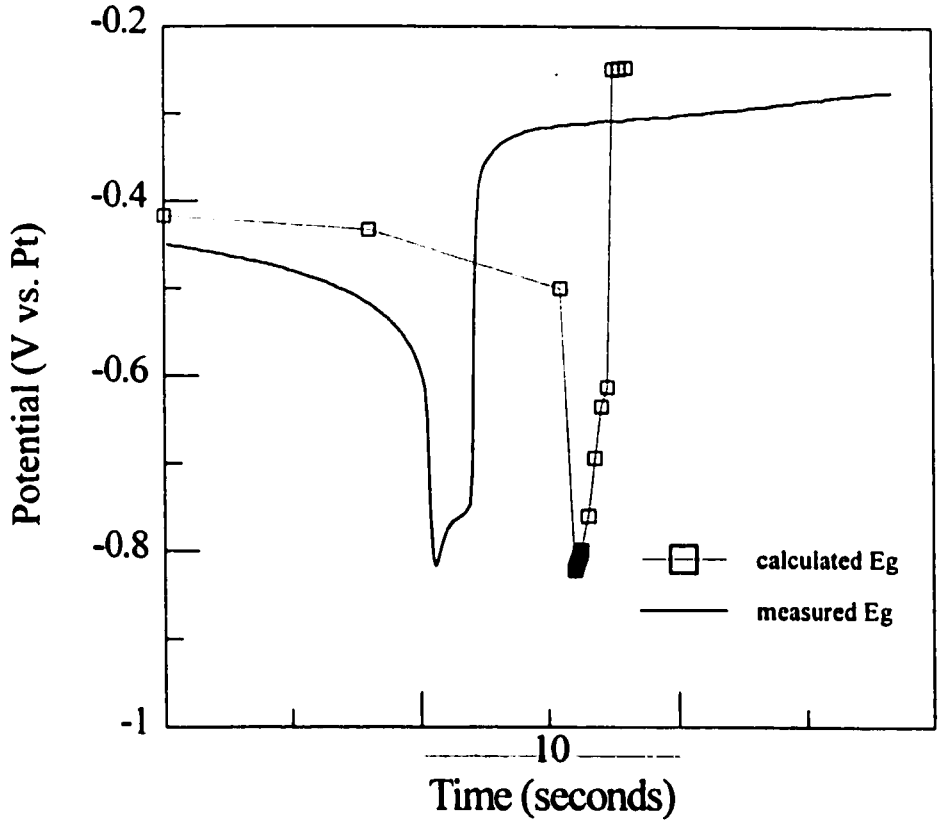


Figure 6.11. NiS(Ni)-S43000 galvanic potential ($E_g$) as a function of time during a potential spike superimposed with the measured corrosion potential of a S30403 RCE (1000 rpm) during a potential spike in 93.5 wt.% $H_2SO_4$ at 60°C.

changes the weight loss per cycle. Experiments conducted in Section 4.2 show that the active-passive corrosion of S30403 is sensitive to temperature and stirring (RCE rotation rate). The following discussion shows that the galvanic passivation model provides an explanation for each effect.

In the active state, $d\theta/dt$ is believed to be controlled by the rate at which nickel atoms anodically dissolve to form NiS. Based on the kinetic model described above, the time constant for such a growth process is inversely proportional to the anodic dissolution rate i: $\tau_g = zF\rho h/2iM$. Any variable which affects i changes the magnitude of the time constant and, thus, $d\theta/dt$. As i is under activation control, it is sensitive to temperature but insensitive to the electrode rotation rate. Therefore, according to the model, the active state period is sensitive to temperature but insensitive to the electrode rotation rate. An increase in temperature increases the magnitude of i which reduces the time constant and, thus, decreases the time required for $\theta$ to reach $\theta^*$. This is consistent with the results presented in Section 4.2.

In the passive state, $d\theta/dt$ is believed to be controlled by the rate at which nickel atoms diffuse into solution from the solution from a precipitated metal sulphate film-solution interface. Based on the kinetic modelling described above, the time constant for such a dissolution process is directly proportional to $\delta$ and inversely proportional to the D and $C_s$: $\tau_d = \rho\delta h/DMC_s$. Any variable which affects $\delta$, D and/or $C_s$ changes the magnitude of the time constant and, thus, $d\theta/dt$. Experiments conducted in Section 4.2 show the passive

state period decreases with an increase in temperature and the electrode rotation rate. An increase in temperature increases $C_s$, and likely simultaneously increases D and decreases $\delta$. All such changes reduce the time constant and, thus, decrease the time required for $\theta$ to reach $\theta^*$. An increase in the electrode rotation rate decreases $\delta$ which reduces the time constant and, thus, the time required for $\theta$ to reach $\theta^*$.

## 6.4 Model Validation - Influence of the $[H_2SO_4]$

Thus far, this study has analyzed only two variables known to affect the corrosion resistance of stainless steel in concentrated $H_2SO_4$-$H_2O$ solutions: temperature and stirring (RCE rotation rate). Another significant variable known to affect the corrosion resistance in concentrated $H_2SO_4$-$H_2O$ solutions is the $H_2SO_4$ concentration, $[H_2SO_4]$. Studying the influence of $[H_2SO_4]$ on the corrosion behaviour of a S30403 RCE provided an opportunity to test the validity of the galvanic passivation model. Testing the validity involved explaining the influence of $[H_2SO_4]$ on the active passive corrosion of S30403 within the context of galvanic passivation. This required recording the influence of $[H_2SO_4]$ on the corrosion behaviour of a nickel RCE and the anodic behaviour of a S43000 RCE. The following subsections present and discuss the results of the various experiments conducted.

### 6.4.1 Influence of $[H_2SO_4]$ on the Corrosion Behaviour of S30403

Figures 6.12 and 6.13 show the influence of $[H_2SO_4]$ on the corrosion potential of a

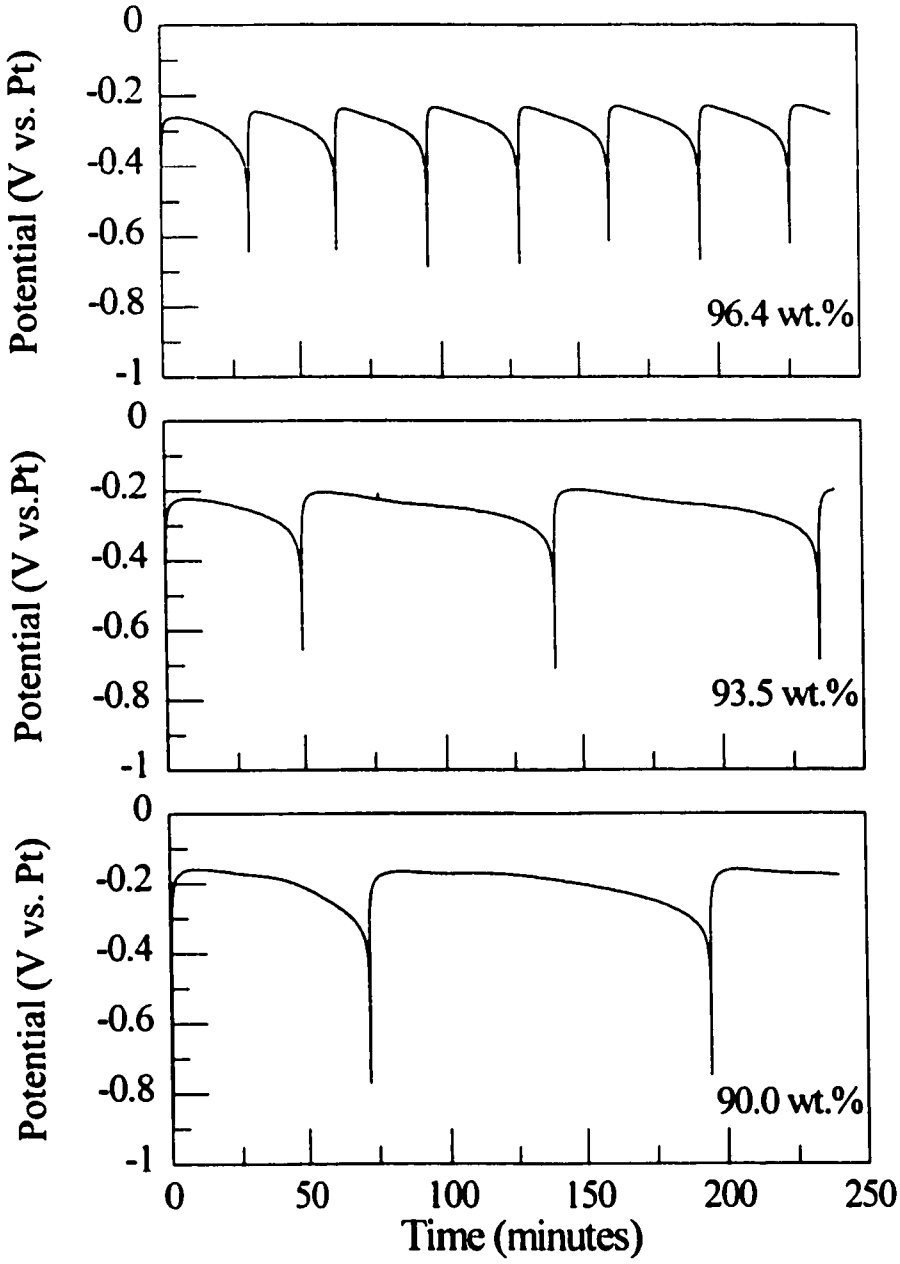


Figure 6.12. Influence of $[H_2SO_4]$ on the corrosion potential of a S30403 RCE (1000 rpm) at 60°C as a function of time immediately after immersion.

S30403 RCE (1000 rpm) at 60°C as a function of time. Potential oscillations (Figure 6.10) and, thus, active-passive corrosion occurred in each $H_2SO_4$-$H_2O$ solution studied between 90.0-96.4 wt.%. An increase in the [$H_2SO_4$] from 90.0 to 96.4 wt.% decreased the passive state period from ~122 to ~32 minutes. The potential spike (Figure 6.11) consisted of the characteristic three distinct stages regardless of [$H_2SO_4$]: passive-active transition, active state corrosion and the active-passive transition. An increase in [$H_2SO_4$] from 90.0 to 96.4 wt.% decreased the active state period from 5.6 to 1.2 seconds.

Table 6.4 shows the influence of [$H_2SO_4$] on the weight loss of the S30403 RCE at 60°C. The weight loss has a complex dependence on [$H_2SO_4$]; first decreasing then increasing with an increase in [$H_2SO_4$]. The weight loss per spike decreased as [$H_2SO_4$] increased, consistent with a shorter active state period. The enhanced corrosion of S30403 at lower [$H_2SO_4$] likely results from the increased active-passive frequency despite a decrease in the weight loss per spike.

**Table 6.4.** Influence of [$H_2SO_4$] on the Weight Loss of a S30403 RCE (1000 rpm)at 60°C after 4 hours exposure.

| [$H_2SO_4$] wt.% | Weight Loss ($mg/cm^2$) | Weight Loss/Spike ($mg/cm^2$) |
|---|---|---|
| 90.0 | 0.73 | 0.24 |
| 93.5 | 0.45 | 0.11 |
| 96.4 | 0.61 | 0.08 |

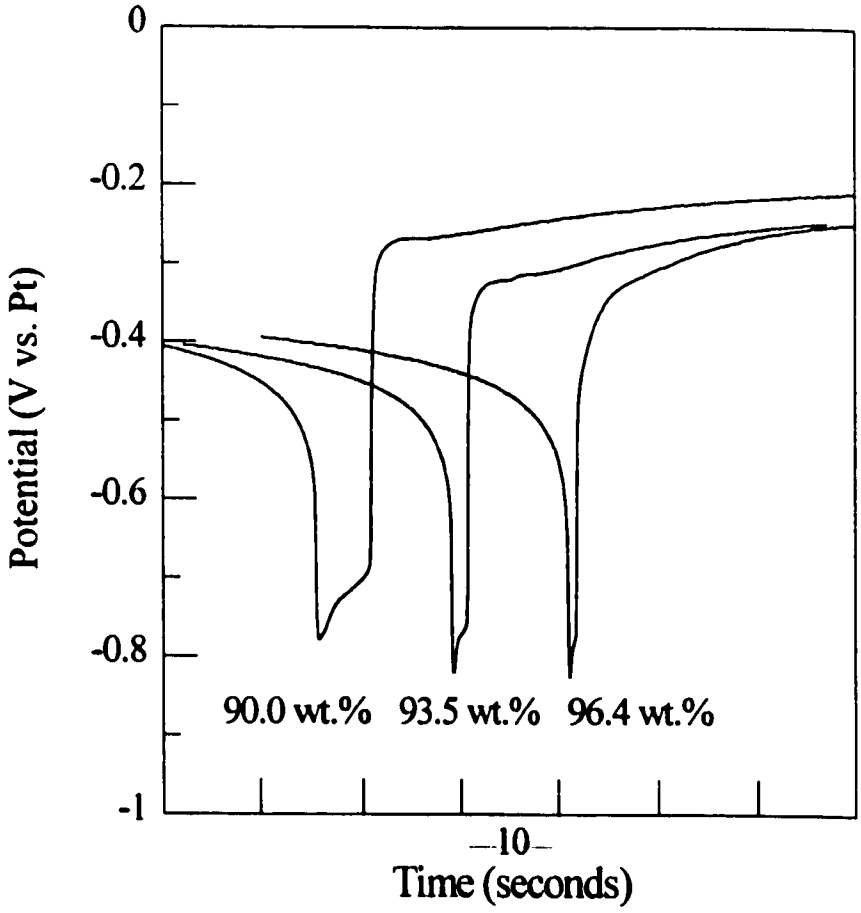


Figure 6.13. Influence of $[H_2SO_4]$ on the corrosion potential of a S30403 RCE (1000 rpm) at 60°C during a potential spike.

Extending the galvanic passivation model to account for the active-passive corrosion of the S30403 RCE (1000 rpm) in 90 and 96.4 wt.% $H_2SO_4$ requires the conditions for NiS and the Fe-17wt.%Cr base alloy identified earlier in Section 6.2 be satisfied. Anodic polarization measurements conducted on a S4300 RCE (1000 rpm) demonstrate that the conditions are satisfied in 90 and 96.4 wt.% $H_2SO_4$. Potential measurements conducted on a nickel RCE demonstrate that the conditions are satisfied in 90 and 96.4 wt.% $H_2SO_4$.

### 6.4.2 Influence of [$H_2SO_4$] on the Anodic Behaviour of S43000

Figure 6.14 shows the influence of [$H_2SO_4$] on the potentiodynamic anodic polarization of a S43000 RCE (1000 rpm) at 60°C. The anodic polarization curves show two important features:

1. The S43000 RCE dissolves in an active state under open-circuit conditions regardless of [$H_2SO_4$].
2. The S43000 RCE passivates with sufficient anodic polarization regardless of [$H_2SO_4$].

An increase in [$H_2SO_4$] decreased the limiting active anodic current, decreased the passivation potential and had reasonably no effect on the passive current density.

If the limiting active anodic current is controlled by the mass transport of metal ions from the surface of a precipitated metal sulphate film, then the decrease in the limiting current with an increase in [$H_2SO_4$] is related to the metal sulphate solubility. The solubility

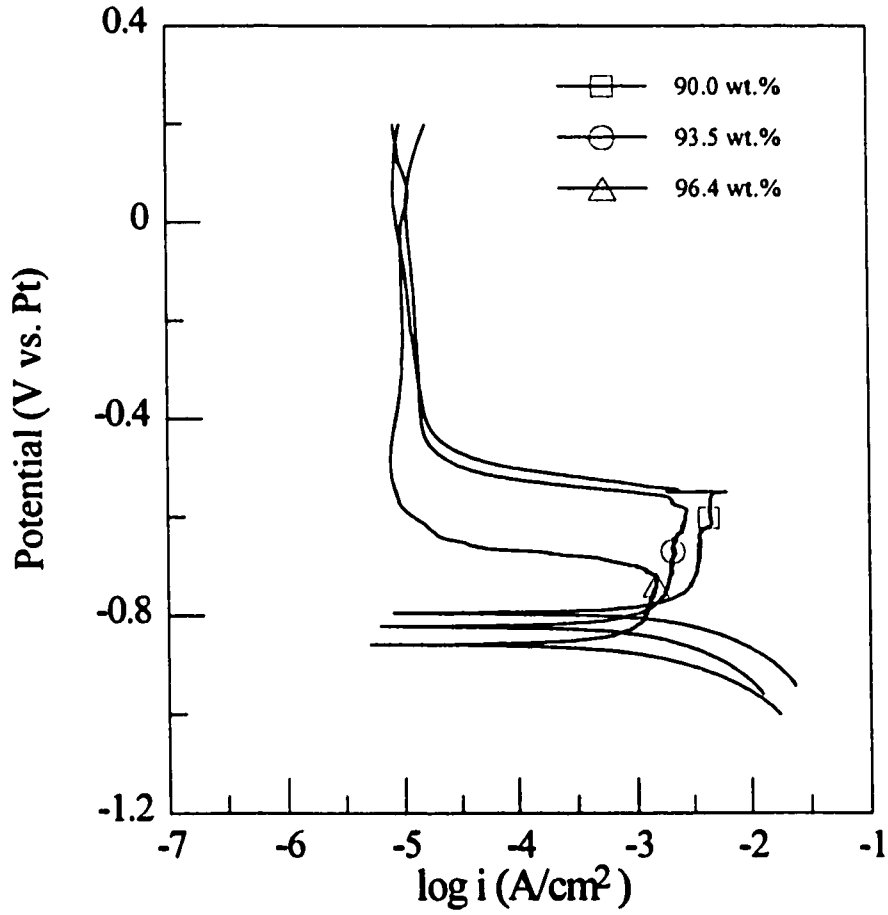


Figure 6.14. Influence of $[H_2SO_4]$ on the potentiodynamic anodic polarization of a S43000 RCE (1000 rpm) at 60°C. Scan rate = 20 mV/min.

of $FeSO_4$ decreases as the $[H_2SO_4]$ increases in concentrated $H_2SO_4$-$H_2O$ solutions[109]. According to the Nernst diffusion model [5.10] discussed in Section 5.2, a decrease in the metal sulphate solubility decreases the corrosion rate (current).

If the anodic passivation reaction occurs according to [6.9] and [6.10], then the dependence of the passivation potential on $[H_2SO_4]$ is given by the corresponding Nernst equation,

$$E_p = E^o + \frac{RT}{nF}\ln\left(\frac{a_{H_2SO_4}}{a_{H^+}}\right) \qquad [6.15]$$

where $E_p$ is the passivation potential, $E^o$ is the standard potential, R is the gas constant, T is temperature, F is Faraday's constant, n is the number of electrons involved in the half cell reaction, $a_{H2SO4}$ is the activity of $H_2SO_4$ molecules and $a_{H+}$ is the activity of the proton. A dependence of the passivation potential on $[H_2SO_4]$ provides further evidence of a mechanism involving a solid state reaction.

Figure 6.15 shows the influence of $[H_2SO_4]$ on the open-circuit potential response of the S43000 RCE (1000 rpm) after the potentiostatic polarization at -0.2 $V_{Pt}$ for 60 minutes at 60°C. Immediately after polarization stopped, the potential decayed slowly to a state of ~-0.5 $V_{Pt}$, after which it decayed rapidly and became stable at ~-0.85 $V_{Pt}$. The potential response shows that passivity is not stable and requires anodic polarization regardless of the

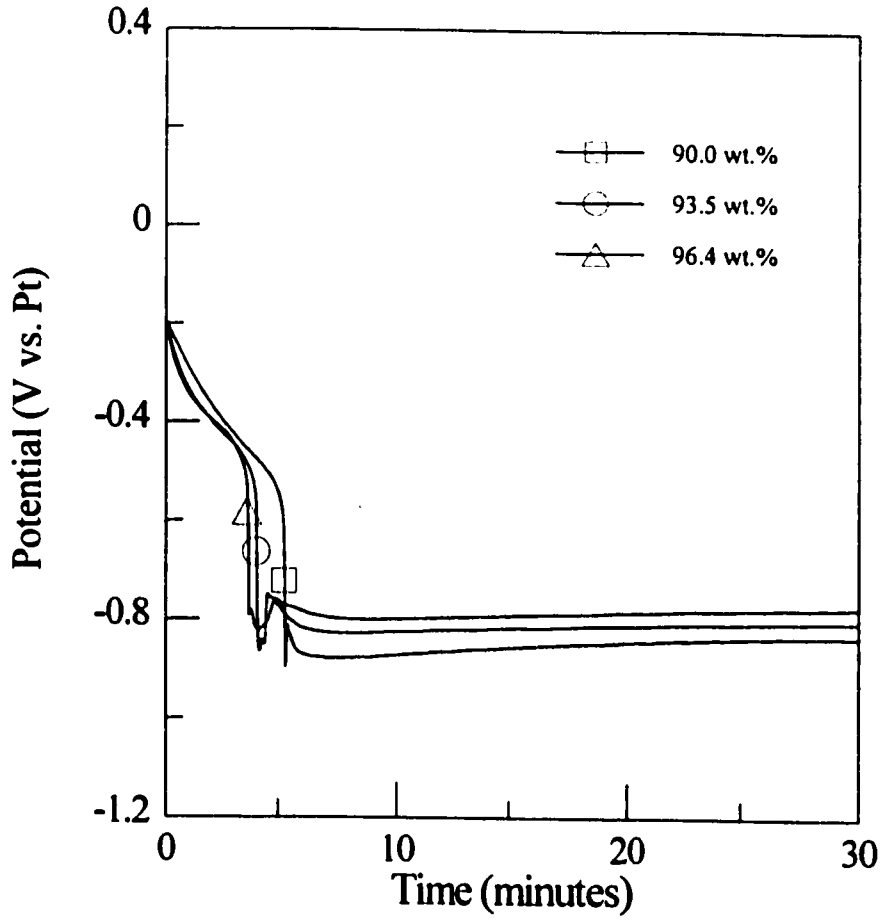


Figure 6.15. Influence of $[H_2SO_4]$ on the open-circuit potential response of a S43000 RCE (1000 rpm) after potentiostatic polarization to -0.2 $V_{Pt}$ for 60 minutes at 60°C.

$[H_2SO_4]$.

### 6.4.3 Influence of $[H_2SO_4]$ on the Corrosion Behaviour of Nickel

Figure 6.16 shows the influence of $[H_2SO_4]$ on the corrosion potential of a nickel RCE (1000 rpm) at 60°C as a function of time. A potential transition from an initial, more positive potential plateau occurred in each $[H_2SO_4]$ studied. An increase in $[H_2SO_4]$ shortened the time at which the potential transition occurred. A black deposit formed on the surface within the first few minutes which subsequently dissolved as the potential decayed towards a more negative plateau. The observations indicate that NiS forms as a corrosion product in 90 and 96.4 along with 93.5 wt.% $H_2SO_4$ and establishes a galvanic interaction with the base metal during its limited stability.

**Table 6.5.** Influence of $[H_2SO_4]$ on Weight Loss of a Nickel RCE (1000 rpm) at 60°C

| $[H_2SO_4]$ (wt.%) | Exposure Time (minutes) | Weight Loss ($mg/cm^2$) |
|---|---|---|
| 90.0 | 150 | 13.2 |
| 93.5 | 120 | 6.5 |
| 96.4 | 120 | 3.6 |

Measurements conducted in Chapter 5 show that the potential transition results from the mass transport controlled dissolution of NiS. Any variable that increases the mass

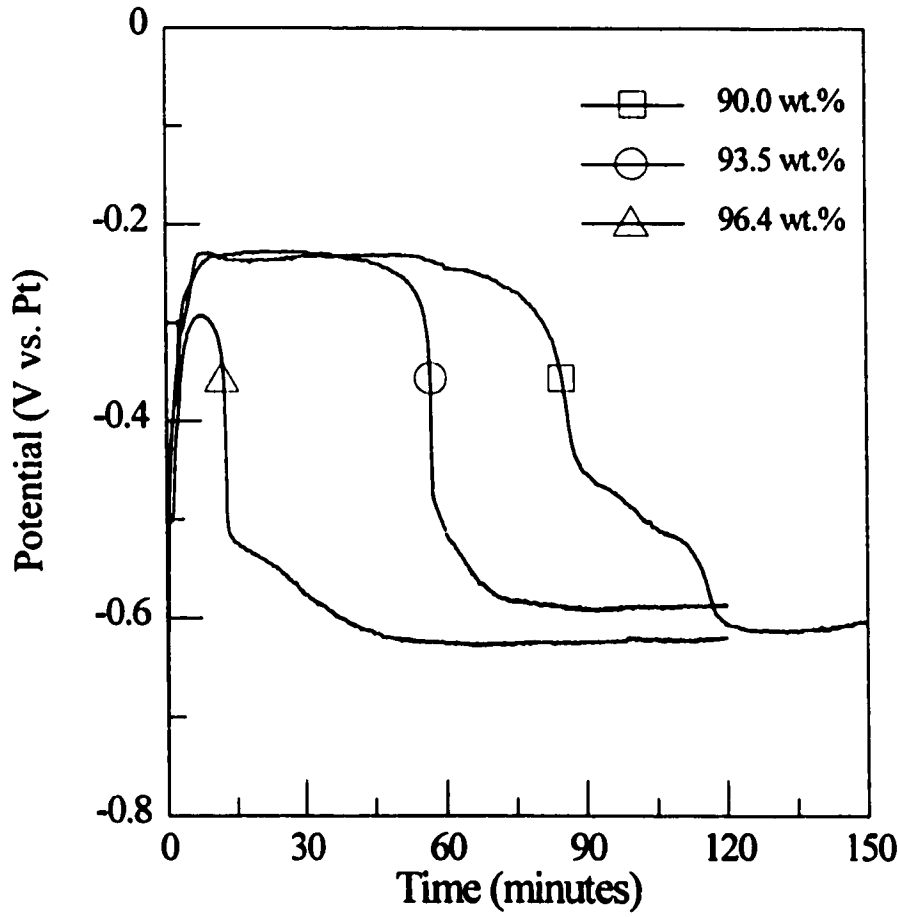


Figure 6.16. Influence of $[H_2SO_4]$ on the corrosion potential of a nickel RCE (1000 rpm) at 60oC as a function of time immediately after immersion.

transport controlled rate results in a reduced transition time. Increasing either the temperature or the electrode rotation rate increased the mass transport controlled dissolution rate resulting in a reduced potential transition time. Weight loss measurements conducted for each [$H_2SO_4$] studied, Table 6.5 showed that this is not the case for a change in [$H_2SO_4$]. The weight loss of nickel progressively decreased as [$H_2SO_4$] increased. The likely cause of the lower weight loss in the more concentrated solutions is the decreased solubility of $NiSO_4$[118,1119].

A possible explanation for the shortened transition time involves the quantity of NiS produced, more specifically, the maximum $\theta$ obtained, $\theta^m$, during the initial stage of corrosion. Considering the redox potential of $H_2SO_4$-$H_2O$ solutions increases as [$H_2SO_4$] increases[48,97], it is reasonable that the potential difference between the corrosion potential and the $H_2S$ potential decreases as the [$H_2SO_4$] increases. As a consequence of a smaller potential difference, a smaller quantity of NiS is required to produce a sufficient $\theta$ which polarizes the potential of nickel more positive than the $H_2S$ potential. A smaller quantity of NiS produced in the more concentrated solutions likely results in a lower $\theta^m$ which in turn requires less time for complete dissolution, despite the decrease in the overall dissolution rate.

### 6.4.4 Galvanic Passivation Mechanism

Measurements conducted on the S43000 RCE and the nickel RCE show that the

conditions required for galvanic passivation are satisfied in 90.0, 93.5 and 96.4 wt.% $H_2SO_4$ at 60°C. As galvanic passivation is possible, it is the likely cause of the of the active-passive corrosion of the S30403 RCE which occurred in each of the [$H_2SO_4$] studied. The model provides the following explanation of the effect of [$H_2SO_4$] on the active-passive corrosion of S30403.

Potential measurements of the S30403 RCE in 90.0, 93.5 and 96.4 wt.% $H_2SO_4$ discussed above show that an increase in [$H_2SO_4$] decreases the active and passive state period. The decrease in the active state period does not result from a decrease in the growth stage time constant. In fact, considering the decrease in the weight loss of the nickel RCE with an increase in [$H_2SO_4$], the growth stage time constant likely increases with increasing [$H_2SO_4$]. The decrease in period with an increase in [$H_2SO_4$] is likely a result of the less noble passivation potential of the Fe-17wt.%Cr base alloy. A less noble passivation potential reduces the critical $\theta$ required for galvanic passivation, $\theta^*$. It is reasonable that the lower $\theta^*$ required in the more concentrated solutions more than compensates the influence of a lower i and leads to the reduced active state period.

Similar to the active state period, the decrease in the passive state period with an increase in [$H_2SO_4$] does not result from a decrease in the dissolution stage time constant. The decrease period likely results from the lower $\theta^m$ believed to occur in the more concentrated solutions. A lower $\theta^m$ reduces the time required for $\theta$ to reach $\theta^*$. It is reasonable that the lower $\theta^m$ more than compensates the influence of a lower mass transport

controlled dissolution rate and leads to the reduced passive state period.

## 6.5 Summary

The objectives of the research presented and discussed in this chapter are to clarify the conditions in which passivity (chromium-rich oxide surface film) is stable and to clarify the role of alloyed nickel in promoting the spontaneous passivation and subsequent depassivation of S30403. The experimental approach adopted to meet these objectives involved modelling the active-passive corrosion of S30403 in concentrated $H_2SO_4$-$H_2O$ solutions with a NiS(Ni)-S43000 galvanic couple.

Experiments conducted to explore the galvanic interaction between NiS(Ni), NiS grown *in situ* on nickel, and S43000 demonstrate that anodic passivation of S43000 occurs during the couple. The NiS phase promotes the cathodic reduction of $H_2SO_4$ to $SO_2$ which provides the necessary driving force and current to stabilize the passive oxide film. In fact, the corrosion current density of NiS is so high that the galvanic potential is actually controlled essentially at the NiS corrosion potential. Galvanic passivation reduces the corrosion rate of the S43000 electrode by two orders of magnitude.

The galvanic interaction between the S43000 and NiS(Ni) electrodes satisfies the conditions required for anodic passivity of S43000 in those $H_2SO_4$-$H_2O$ solution conditions where the active-passive corrosion of S30403 occurs. Modelling the S30403 electrode using a NiS(Ni)-S43000 galvanic couple reproduces the major features of an active-passive cycle:

active to passive transition, passive state corrosion, passive to active transition and active state corrosion. Galvanic potential transients calculated from kinetic equations established to model the growth and subsequent dissolution of NiS reproduce the oscillatory potential transient observed for a S30403 electrode, including the characteristic stages that occur during a spike.

# CHAPTER 7

## 7. CONCLUSIONS AND FURTHER WORK

The objective of this study was originally identified in Chapter 1. For convenience the objectives are reproduced here. The objective is to develop a better understanding of the reactivity and/or passivity of stainless steel in concentrated $H_2SO_4$-$H_2O$ solutions by clarifying the following:

1. The state of stainless steel passivity.
2. The conditions under which passivity is stable.
3. The role played by the major alloying elements in establishing and maintaining the passive state.

To meet the objective, the study evaluated the corrosion and electrochemical behaviour of sample electrodes prepared from stainless steels S30403 and S43000 along with iron,

chromium and nickel in quiet and stirred 90-98 wt.% $H_2SO_4$ at 25-80°C. This chapter summarizes the major conclusions drawn from the study and identifies several areas related to the study which require further research.

## 7.1 Contributions to Knowledge

Consideration of the content of the previous chapters shows that the objective of the study has been achieved. Application of immersion and electrochemical techniques, including rotating electrodes, to study the reactivity of stainless steels S43000 and S30403 in hot concentrated $H_2SO_4$-$H_2O$ solutions proved to be powerful. Conclusions drawn from the study include the following:

1. A content of 17-18 wt.% chromium is sufficient to anodically passivate stainless steel in concentrated $H_2SO_4$-$H_2O$ solutions as the potential is made more noble. Passivity involves the formation of an oxide-type film which is not stable and requires anodic polarization.
2. Alloyed nickel plays an active role in improving the corrosion resistance of stainless steel. A content of 8 wt.% nickel is sufficient promote a periodic passivation of the base Fe-(17-18)wt.% Cr stainless steel under open-circuit conditions which reduces the corrosion rate by at least an order of magnitude.
3. A galvanic couple between NiS-Ni (NiS grown *in situ* on nickel) and

the Fe-17wt.%Cr stainless steel (S43000) provides the necessary driving force and current to anodically passivate the Fe-17wt.%Cr stainless steel in all solution conditions in which NiS forms. Galvanic passivation by NiS-Ni reduces the corrosion rate of the Fe-17wt.%Cr stainless steel by two orders of magnitude.

4. A theoretical model considering the periodic growth and subsequent dissolution of a solid NiS corrosion product and its corresponding galvanic interaction with the uncovered stainless steel alloy can predict the active-passive corrosion of Fe-Cr-Ni stainless steel in concentrated $H_2SO_4$-$H_2O$ solutions.

5. The potential-dependent reduction of undissociated $H_2SO_4$ molecules plays an essential role in the periodic spontaneous passivation process of Fe-Cr-Ni stainless steel. Anodic passivity proceeds with the participation of $H_2SO_4$ molecules as the source of oxygen and is stabilized through a sufficient driving force and current provided by a nickel-catalyzed reduction of $H_2SO_4$ molecules.

From a technical point of view, the periodic galvanic passivation model of the active-passive corrosion of Fe-Cr-Ni stainless steels provides a framework in which to:

1. Predict the influence of temperature, acid velocity and acid concentration on the corrosion resistance.

2. Improve the corrosion resistance through compositional changes which would result in either a decrease in the weight loss per spike or an extension in the passive state period or both.

## 7.2 Suggestions for Further Research

As a result of employing only stainless steels S43000 and S30403, this study essentially analyzed the effect of 8 wt.% nickel on the corrosion of Fe-(17-18)wt.% Cr stainless steel in 93.5 wt.% $H_2SO_4$. It is concluded that alloyed chromium and nickel play a significant role in the active state corrosion process and their corresponding solid corrosion products play a significant role in the passive state corrosion process. Therefore, the corrosion resistance should be sensitive to level of alloying of either chromium or nickel or both. Studying the active-passive corrosion as a function of the chromium content and the nickel content will be useful in achieving a better understanding of the synergy involved and identify an optimum composition for corrosion resistance.

Alloying elements known to have an influence on the corrosion resistance of stainless steel in concentrated $H_2SO_4$-$H_2O$ solutions include silicon, molybdenum and copper. The approach of studying the corrosion and electrochemical behaviour of the major alloying elements proved to be powerful to delineate the corresponding role of the elements in imparting corrosion resistance to the stainless steel alloy. Therefore, characterizing the electrochemical and corrosion behaviour of silicon, molybdenum and copper in concentrated

$H_2SO_4$-$H_2O$ solutions will be helpful in delineating the role of these alloying additions in providing corrosion resistance. For silicon, it may prove better to study the corrosion and electrochemical behaviour of Fe-Cr-Si alloys since silicon is believed to improve the corrosion resistance by stabilizing a silicon-enriched passive oxide film.

A key component in the periodic galvanic passivation model is the growth and dissolution process of the NiS deposit. The exact mechanism of the growth and dissolution process is not well understood. Therefore, studying the corrosion of a series of Fe-Ni binary alloys may be useful to better understand the NiS growth and dissolution processes. A series of Fe-Ni binary alloys provides a system in which to study the NiS growth and subsequent dissolution without the interference of a simultaneously growing passive oxide film. According to the conclusions drawn from this study, the Fe-Ni binary alloy system should possess corrosion potential oscillations resulting from a galvanic interaction with NiS.

Another key component in the mechanistic model is the role played by the NiS deposit. It is assumed that NiS undergoes an oxidative dissolution in concentrated $H_2SO_4$-$H_2O$ solutions and has an appreciable bulk electronic conductivity to support a galvanic interaction with Fe-Cr stainless steels. Neither the oxidative dissolution nor the electronic conductivity of the NiS deposit was characterized in this study. Therefore, characterizing the properties of the NiS deposit formed along with the properties of monolithic NiS will be helpful to better understand the beneficial role of NiS in improving the corrosion resistance of Fe-Cr-Ni stainless steels. Furthermore, the galvanic passivation ability of other metal

sulphides should be explored along with NiS. The galvanic passivation of stainless steel by coupling with metal sulphides is a possible technically significant means of corrosion protection for the concentrated sulphuric acid processing industry that should be explored in some detail.

This study only characterized the films formed on stainless steels S43000 and S30403 using *ex situ* techniques. The results may not be a true representative of surface films or deposits that form *in situ* due to possible surface chemistry alterations introduced during removal from the hydrophilic concentrated $H_2SO_4$-$H_2O$ solution and subsequent drying in an oxygen-containing atmosphere. Therefore, *in situ* analysis would be preferable when attempting to characterize the films or deposits that form. Assuming successful application of in situ techniques is possible, the analysis would be a powerful tool to probe the changes in the surface condition that are believed to occur with time during the active-passive corrosion. Possible *in situ* surface analytical techniques include ellipsometry and infra-red/Raman spectroscopy.

# 8. REFERENCES

[1]. G.M. Cameron, Chem. Eng. Prog., 78, 71 (1982).

[2]. D.R. McAlister, A.G. Corey, L.J. Ewing and S.A. Ziebold, Chem. Eng. Prog., 77, 34 (1986).

[3]. R.M. Kain and P.E. Morris, "Anodic Protection of Fe-Cr-Ni-Mo Alloys in Concentrated Sulfuric Acid", Paper No.149, CORROSION 76, NACE, Houston (1976).

[4]. Y.-S. Chang, "Active-Passive Corrosion Behaviour", PhD Thesis, University of Cambridge (1984).

[5]. R. Matsuhashi, H. Abo, S. Abe and H. Kihira, Corros. Eng., 36, 531 (1987).

[6]. F.W.S. Jones, US-Patent No. 4 543 244 (1985).

[7]. M. Davies, D.S. Hodgson, J. Rodda, "Applications of Saramet in $H_2SO_4$ Plants", in Proceedings SULPHUR 88, The British Sulphur Corporation Ltd., Vienna (1988).

[8]. M.B. Ives, J.R. Kish, J.R. Rodda, Mat. Sci. Forum, 185-188, 887 (1995).

[9]. C. Wagner and W. Traud, Z. Elektrochem., 44, 391 (1938).

[10]. M. Stern and A.L. Geary, J. Electrochem. Soc., 104, 56 (1957).

[11]. H.H. Uhlig, Corrosion and Corrosion Control, 2nd ed., John Wiley & Sons, Inc., New York, 1971.

[12]. N.D. Thomashov, Theory of Corrosion and Protection of Metals, The MacMillan Company, New York (1966).

[13]. H.H. Uhlig, "History of Passivity, Experiments and Theories" in Passvity of Metals, R.P. Frankenthal and J. Kruger (eds.), 1, The Electrochemical Society Inc., Princeton, New Jersey (1978).

[14]. J.O'M. Bockris and A.K.N. Reddy, Modern Electrochemistry, Vol. II, Plenum Press, New York (1970).

[15]. N. Sato, "The Passivity of Metals and Passivating Films", in Passivity of Metals, R. Frankenthal and J. Kruger (eds.), 29, The Electrochemical Society, Princeton, New Jersey (1978).

[16]. H.H. Uhlig and P.F. King, J. Electrochem. Soc., 106, 1 (1959).

[17]. B.N. Kabonov and D.I. Leikis, Z. Elektrochem., 62, 660 (1958).

[18]. Y.M. Kolotyrkin, Z. Elektrochem., 62, 664 (1958).

[19]. A. MacRae, Surf. Sci., 1, 319 (1964).

[20]. A. Pignocco and G. Pellister, J. Electrochem. Soc., 112, 1188 (1965).

[21]. U.R. Evans, Z. Elektrochem., 62, 619 (1958).

[22]. M. Flieschmann and H.R. Thirsk, J. Electrochem. Soc., 110, 688 (1963).

[23]. N. Sato and G. Okamoto, J. Electrochem. Soc., 110, 605 (1963).

[24]. J.O'M. Brockris, A.K.N. Reddy and B. Rao, J. Electrochem. Soc., 113, 1133 (1966).

[25]. D. Pavlov, Z. Elektrochem., 71, 398 (1967).

[26]. N. Sato, "Passivity of Iron, Nickel and Cobalt – General Theory of Passivity", in Passivity and Its Breakdown of Iron and Iron Base Alloys, R.W. Staehle and H. Okada (eds.), 1, NACE, Houston, Texas (1976).

[27]. F. Mansfeld, J. Electrochem. Soc., 120, 188 (1973).

[28]. K. Schwabe, S. Hermann and W. Oelssner, "Influence of Water on Anodic Dissolution and Passivation Metals", in Passivity of Metals, R. Frankenthal and J. Kruger (eds.), 413, The Electrochemical Society, Princeton, New Jersey (1978).

[29]. B. Elsener and H, Boehni, "The Role of Water in the Kinetics of Stainless Steel Dissolution and Passivation in Organic Media", in Passivity of Metals and Semiconductors, M. Froment (ed.), 555, Elsevier Science Publishing Co. Inc., New York (1983).

[30]. R.J. Gillespie and E.A. Robinson, "The Sulfuric Acid Solvent System", in Advances in Inorganic Chemistry and Radiochemisrty, Vol. I, 385, Acedemic Press, New York (1959).

[31]. R.J. Gillespie and E.A. Robinson, "Sulfuric Acid", in Non-Aqueous Solvent Systems, T.C. Waddington (ed.), 117, Acedemic Press, New York (1965).

[32]. R.J. Gillespie "Sulphuric Acid as a Solvent System" in Inorganic Sulphur Chemistry, G. Nickless (ed.), 563, Elsevier Publishing Company, New York (1968).

[33]. R. Pascard, C. R. Acad. Sci. Paris, 240, 2162 (1955).

[34]. P.W. Atkins, Physical Chemistry, W.H. Freeman and Co., New York (1986).

[35]. J. Timmermans, The Physico-Chemical Constants of Binary Systems in Concentrated Solutions, (1960).

[36]. J.E. Roughton, J. Appl. Chem., I. Suppl., 2, 141 (1951).

[37]. R.H. Rhodes and C.B. Barbour, Ind. Eng. Chem., 15, 850 (1923).

[38]. C.M. Gable, H.F. Betz and S.H. Maron, J. Amer. Chem. Soc., 72, 1445 (1950).

[39]. T.F. Young, L.F. Maranville and H.M. Smith in The Structure of Electrolyte Solutions, W.J. Hammer (ed.), John Wiley, New York (1959).

[40]. N.G. Zarakhani and M.I. Vinnik, Zh. Fiz. Kim., 36, 916 (1962).

[41]. M. Liler, Reaction Mechanisms In Sulphuric Acid, Acedemic Press Inc., New York (1971).

[42]. G. Charlot and B. Tremillon, Chemical Reactions in Solvents and Melts, Pergamon Press, New York (1969).

[43]. E. Högfeldt, Acta Cientif. Venezolana, 17, 13 (1966).

[44]. M. Pourbaix, Atlas of Electrochemical Equilibria in Aqueous Solutions, NACE, Houston (1974).

[45]. L.P. Hammet and A.J. Deyrup, J. Amer. Chem., Soc., 55, 1900 (1933).

[46]. L.P. Hammet and M.A. Paul, J. Amer. Chem. Soc., 56, 827 (1934).

[47]. T.E. Evans and A.C. Hart, Electrochem. Acta, 16, 1955 (1971).

[48]. N. Sridhar, "Mechanism of Corrosion in Concentrated Sulfuric Acid", in Proceedings SULPHUR 85, The British Sulphur Corporation Ltd., London (1985).

[49]. H. Hoffman, Z. Elektrochem., 27, 442 (1921).

[50]. F. Beck, Electochim. Acta, 17, 2317 (1972).

[51]. A.J. Arvía and J.S.W. Carrozza, Electrochim. Acta, 11, 1641 (1966).

[52]. H.A. Garrera, J.W.S. Carrozza and A.J. Arvía, Electrochim. Acta, 13, 771 (1968).

[53]. J.W.S. Carrozza, H.A. Garrera and A.J. Arvía, Electrochim. Acta, 14, 205 (1969).

[54]. A.J. Arvía, H.A. Garrera and J.W.S. Carrozza, Electrochim. Acta, 16, 79 (1971).

[55]. G.C. Kiefer and W.G. Renshaw, Corrosion, 6, 235 (1950).

[56]. E.H. Phelphs and D.C. Vreeland, Corrosion, 13, 619 (1957).

[57]. C. Edeleanu, Metallurgia, 50, 113 (1954).

[58]. F. D'Alba, S. Di Lorenzo and C. Lucarini, J. Electroanal. Chem., 271, 49 (1989).

[59]. A. Ishihara and S. Asakura, Corros. Eng., 42, 685 (1992).

[60]. M.R.F. Hurtado, P.T.A. Sumodjo and A.V. Benedetti, J. Electrochem. Soc., 140, 1567 (1993).

[61]. F. D'Albo, S. Di Lorenzo and C. Lucarini, Electrochim. Acta, 39, 443 (1994).

[62]. J. Wojtowicz, "Oscillatory Behaviour in Electrochemical Sysytems", in Modern Aspects of Electrochemistry, J.O. Bockris and B. Conway (eds.), 47, Plenum, New York (1972).

[63]. J.L. Hudson and R.M. Basset, Rev. Chem. Eng., 7, 111 (1991).

[64]. J.L. Hudson and T.T. Tsotsis, Chem. Eng. Sci., 49, 1493 (1994).

[65]. R. Matsuhashi, E. Sato, S. Abe and H. Abo, Corros. Eng., 39, 89 (1991).

[66]. H.S. Tong, "Corrosion and Electrochemical Behaviour of Iron-Chromium-Nickel Alloys in Concentrated Sulphuric Acid Solutions" in Electrochemical Corrosion Testing, ASTM STP 727, F. Mansfeld and U. Bertocci, (eds.), 96, ASTM (1981).

[67]. M. Renner, Werkst. Korros., 47, 246 (1996).

[68]. V.S. Kuzob, V.P. Krikun and V.S. Novitskii, Protection of Metals, 21, 425 (1986).

[69]. D. Kuron, F. Paulekat, H. Gräfen and E-M. Horn, Werkst. Korros., 36, 489 (1987).

[70]. M.H.W. Renner and P.A. Maughan "Influence of Molybdenum on the Corrosion Resistance of Iron- and Nickel- Based Alloys in Static Hot Concentrated Sulphuric Acid", Paper No. 160, CORROSION 91, NACE Houston (1991).

[71]. G. Okamoto, Corros. Sci., 13, 471 (1973).

[72]. A.E. Yaniv, J.B. Lumsden and R.W. Staehle, J. Electrochem. Soc., 124, 490 (1978).

[73]. H. Ogawa, H. Omata, I. Itoh, and H. Okada, Corrosion, 34, 52 (1978).

[74]. K. Asami, K. Hashimoto and S. Shimodaira, Corros. Sci., 18, 551 (1978).

[75]. A.R. Brooks, C.R. Clayton, K. Doss and Y.C. Lu, J. Electrochem., Soc., 133, 2459 (1986).

[76]. P. Marcus and I. Oleflord, Corros. Sci., 28, 589 (1988).

[77]. R. Kircheim, B. Heinze, H. Fischmeister, S. Hofmann, H. Knote and U. Stolz, Corros. Sci., 29, 899 (1989).

[78]. J.E. Castle and J.H. Qiu, Corros. Sci., 29, 591 (1989).

[79]. J. Banas, Electrochim. Acta, 32, 871 (1987).

[80]. J. Banas, B. Mazurkiewicz and B. Stypula, Electrochim. Acta, 37, 1069 (1992).

[81]. J. Banas, B. Stypula and B. Mazurkiewicz, ACH-Models in Chemistry, 132, 607 (1995).

[82]. J.C. Hines and R.C. Williamson, Corros. Sci., 4, 201 (1964).

[83]. J.C. Hines and R.C. Williamson, Corros. Sci., 4, 221 (1964).

[84]. G. Gilli and F. Zucchi, Corros. Sci., 8, 801 (1968).

[85]. B. Mazurkiewicz, Electrochim. Acta, 38, 495 (1993).

[86]. L.A. Poluboyarteseva, P.I. Zarubin and V.M. Vobakovskii, J. Appl. Chem. USSR, 36, 1210 (1963).

[87]. B.T. Ellison and W.R. Schmeal, J. Electrochem. Soc., 125, 524 (1978).

[88]. T.N. Andersen, N. Vanorden and W.J. Schlitt, Met. Trans. A., 11A, 1421 (1980).

[89]. S.W. Dean and G.D. Grab, Mater. Perform., 24 (6), 22 (1985).

[90]. S.L. Pohlman and T.N. Andersen, Mater. Perform, 26 (11), 41 (1987).

[91]. I. Epelboin and M. Keddam, C.R. Hebd. Séanc. Acad. Sci., Paris, 258, 137 (1964).

[92]. U. Ebersbach, K. Schwabe and K. Ritter, Electrochim. Acta, 12, 927 (1967).

[93]. G. Gilli, P. Borea, F. Zucchi and G. Trabanelli, Corros. Sci., 9, 673 (1969).

[94]. M. Turner, G.E. Thomson and P.A. Brook, Corros. Sci, 13, 985 (1973).

[95]. B. Mazurkiewicz, Werkst. Korros., 43, 565 (1992).

[96]. B. Stypula, Z. Naukowe AGH, 16, 119 (1990).

[97]. B. Stypula and J. Banas, Electrochim. Acta, 38, 2309 (1993).

[98]. B. Stypula and J. Stoch, Corros. Sci., 36, 2159 (1994).

[99]. B. Stypula, Mater. Sci. Forum, 185-188, 897 (1995).

[100]. K. Osozawa and H.J. Engell, Corros. Sci., 6, 389 (1966).

[101]. J.R. Rodda, unpublished data, McMaster University (1992).

[102]. ASTM G5-94 Standard Reference, "Test Method for Making Potentiostatic and Ptentiodynamic Anodic Polarization Measurements", in Annual Book of ASTM Standards 03.02, 63, ASTM, Philadelphia, PA.(1994).

[103]. J.A. von Fraunhofer and C. N. Banks, Potentiostat and Its Applications, Butterworth and Co. Ltd, New York (1972).

[104]. O.L. Riggs, Jr. and C.E. Locke, Anodic Protection Theory and Practice in the Prevention of Corrosion, Plenum Press, New York (1981).

[105]. E.P. Bertin, Introduction to X-Ray Spectrometric Analysis, Plenum Press, New York (1978).

[106]. E.P. Bertin, Principles and Practice of X-Ray Spectrometric Analysis, 2nd ed., Plenum Press, New York (1975).

[107]. D. Roy and J.D. Carette,, "Electron Spectroscopy for Chemical Analysis", p. 13 in Topics in Chemical Physics, Vol. 4, Springer Verlag (1972).

[108]. A. Christoff, Z. Phys. Chem., 55, 622 (1906).

[109]. A.E. Harvey Jr., J.A. Smart and E.S. Amis, Anal. Chem., 27, 1 (1955).

[110]. S.W. Dean Jr. and G.D. Grab, Mater. Peform., June, 21 (1985).

[111]. J. Chastain, Hanbook of X-ray Photoelectron Spectroscopy, Perkin-Elmer, Eden Prairie, (1992).

[112]. J.P. Hoare, The Electrochemistry of Oxygen, Interscience Publishers, John Wiley & Sons, New York (1968).

[113]. M.R. Tarasevich, A. Sadkowski and E. Yeager, "Oxygen Electrochemistry" in Comprehensive Treatise of Electrochemistry, Vol. 7, B.E. Conway (eds.), 301, Plenum Press, New York (19).

[114]. IUPAC Solubility Data Series, Vol. 18, O. Popovych (ed.), 79, Pergamon Press, Toronto (1981).

[115]. M.R.F. Hurtado, P.T.A. Sumodjo and A.V. Benedetti, J. Electrochem. Soc., 140, 1567 (1993).

[116]. M. Seo, R. Furuichi, G. Okamoto and N. Sato, Trans. Jpn. Inst. Met., 16, 519 (1975).

[117]. Y.-H Yau and M.A. Streicher, Corrosion, 47, 352 (1991).

[118]. J. Kendall and W. Davidson, J. Am. Chem. Soc., 43, 979 (1921).

[119]. W.D. Halsted and B.F. Lovey, J. Appl. Chem., Biotechnol., 27, 585 (1977).

[120]. F.D. Miles and T. Carson, J. Chem., 786 (1946).

[121]. W.T. Hall, Analytical Chemistry, Volume II, 9th Edition, p. 583, John Wiley & Sons, Inc., New York (1955).

[122]. E.G. Kremko, I.A. Kakovskii and L.D. Sheveleva, Protection of Metals, 20, 73 (1985).

[123]. A. Siedell, Solubilities of Inorganic and Metal Organic Compounds, 3rd Edition. Volume I, D. van Nostrand Company Inc., New York (1940).

[124]. CRC hanbook of Chemistry and Physics, 46th Ed., CRC Press, Cleveland (1965-66).

[125]. A. Senning, Sulfur in Organic and Inorganic Chemistry, M.. Dekker (1971).

[126]. K.J. Vetter, Electrochemical Kinetics, Academic Press, New York (1967).

[127]. V.G. Levich, Physicochemical Hydrodynamics, Prentice Hall, Inc., Englewood Cliffs, N.J. (1962).

[128]. M. Eisenberg, C.W. Tobias and C.R. Wilke, J. Electrochem. Soc., 101, 306 (1954).

[129]. T.P Hoar, "The Anodic Behaviour of Metals" in Modern Aspects of Electrochemistry No.2, J. O'M Bockris (ed.), 262, Academic Press Inc., New York (1959).

[130]. D.A. Vermilyea, "Anodic Films" in Advances in Electrochemistry & Electrochemical Engineering, Vol. 3, P. Delahay and C.W. Tobias (eds.), 211, Interscience Publishers, New York (1963).

[131]. G. Schmitt, Corrosion, 47, 285 (1991).

[132]. D.D. MacDonald, B. Roberts, and J.B. Hyne, Corros. Sci., 18, 411 (1978).

[133]. J.S. Smith and J.D.A. Miller, Brit. Corros. J., 10, 136 (1975).

[134]. T.W. Farrer and F. Wormwell, Chem. and Ind., 106, (1953).

[135]. D.F.A. Koch, "Electrochemistry of Sulfide Minerals" in Modern Aspects of Electrochemistry, No. 10, J.O'M. Bockris ed., 211, Plenum, New York (1984).

[136]. N.E. Wadsworth, "Heterogeneous Rate Processes in the Leaching of Base Metal Sulfides" in Hydrometallurgical Process Fundamentals, R.G. Bautista (ed.), 41, Plenum, New York (1984).

[137]. K. Osseo-Asare, Hydrometallurgy, 29, 61 (1992).

[138]. E. Peters, I.H. Warren, and H. Veltman, First Tutorial Symposium on Hydrometallurgy, The University of Denver (1972).

[139]. V.K. Berry, L.E. Murr and J.B. Hiskey, Hydrometallurgy, 3, 209 (1978).

[140]. J.L. Nickerson, Characterization of a Ni-Si Alloy via Electrochemical and Surface Analysis, M. Sci. Thesis, University of Notre Dame (1983).

[141]. F. Mansfeld, Corrosion, 27, 436 (1971).

[142]. T.P. Hoar, J. Inst. Met., 81, 668 (1952).

# APPENDIX A

## X-RAY FLUORESCENCE SPECTROSCOPY RESULTS

### Appendix A.1

**Insoluble Corrosion Product Formed During Corrosion of a UNS S30403 Electrode in 93.5 wt.% $H_2SO_4$ at 60°C**

### Appendix A.2

**Insoluble Corrosion Product Formed During Corrosion of a Nickel Electrode in 93.5 wt.% $H_2SO_4$ at 60°C**

# Appendix A.1

## Insoluble Corrosion Product Formed During Corrosion of a UNS S30403 Electrode in 93.5 wt.% $H_2SO_4$ at 60°C

McMaster University Department Of Geology
1280 Main Street West,
Hamilton, Ontario
L8S 4M1

Tel: (416) 525-9140 Fax: (416) 522-3141

JOB.609 14-Jul-95
Company name..... McMaster ScMo 100kV LiF220 Ge111 PE TlAP
**Tape & Holder re 251-0**

No Supporting Film is used
BackgroundModel used is Al
Given Effective Area is 452.16 mm2 ( 24.0 mm )
Assumed grain size = 0 Micrometer
Given rest is 0 %
Given Diluent/Sample is 0
The Viewed Mass (layer thickness) is to be calculated
A < sign means that the concentration is < 50 ppm

| Z | wt% | StdErr | Z | wt% | StdErr | Z | wt% | StdErr |
|---|---|---|---|---|---|---|---|---|
| 9 F | 0.19 | 0.1 | 32 Ge | | | 56 Ba | 23.0 | 0.3 |
| 11 Na | < | | 33 As | 0.74 | 0.2 | 57 La | < | |
| 12 Mg | < | | 34 Se | < | | 58 Ce | < | |
| 13 Al | < | | 35 Br | 0.12 | 0.04 | 59 Pr | | |
| 14 Si | 0.14 | 0.01 | 37 Rb | 0.0078 | 0.05 | 60 Nd | 0.053 | 0.03 |
| 15 P | 0.11 | 0.009 | 38 Sr | < | | 62 Sm | < | |
| 16 S | 2.2 | 0.07 | 39 Y | < | | 64 Gd | | |
| 17 Cl | 0.18 | 0.01 | 40 Zr | < | | 65 Tb | | |
| 19 K | 0.11 | 0.01 | 41 Nb | 0.36 | 0.06 | 72 Hf | | |
| 20 Ca | 0.92 | 0.04 | 42 Mo | 0.060 | 0.06 | 73 Ta | 2.3 | 0.07 |
| 22 Ti | < | | 45 Rh | 0.30 | 0.06 | 74 W | < | |
| 23 V | < | | 46 Pd | 0.22 | 0.07 | 77 Ir | | |
| 24 Cr | 0.039 | 0.006 | 47 Ag | 0.046 | 0.1 | 78 Pt | 0.030 | 0.1 |
| 25 Mn | < | | 48 Cd | 0.34 | 0.1 | 79 Au | < | |
| 26 Fe | 0.40 | 0.02 | 49 In | | | 80 Hg | < | |
| 27 Co | 0.46 | 0.03 | 50 Sn | 1.7 | 0.1 | 81 Tl | 0.19 | 0.09 |
| 28 Ni | 0.58 | 0.03 | 51 Sb | 2.5 | 0.2 | 82 Pb | < | |
| 29 Cu | 0.67 | 0.03 | 52 Te | 2.8 | 0.2 | 83 Bi | < | |
| 30 Zn | 56.2 | 0.2 | 53 I | < | | 90 Th | 0.55 | 0.1 |
| 31 Ga | | | 55 Cs | 2.3 | 0.4 | 92 U | 0.030 | 0.08 |

KnownConc 0 REST= 0 Dil/Smpl= 0

Mass/Area found : 3.90 mg /4.52 cm2 8.62 g/m2 with CountPrec= 0.5%

McMaster University Department Of Geology
1280 Main Street West,
Hamilton, Ontario
L8S 4M1

Tel: (416) 525-9140 Fax: (416) 522-3141

JOB.601 14-Jul-95
Company name..... McMaster ScMo 100kV LiF220 Ge111 PE TlAP
**Blank filter 251-1**

No Supporting Film is used
BackgroundModel used is Al
Given Effective Area is 452.16 mm2 ( 24.0 mm )
Assumed grain size = 0 Micrometer
Given rest is 0 %
Given Diluent/Sample is 0
The Viewed Mass (layer thickness) is to be calculated
A < sign means that the concentration is < 50 ppm

| Z | wt% | StdErr | Z | wt% | StdErr | Z | wt% | StdErr |
|---|---|---|---|---|---|---|---|---|
| 9 F | 0.13 | 0.3 | 32 Ge | | | 56 Ba | 2.8 | 0.08 |
| 11 Na | < | | 33 As | 0.083 | 0.03 | 57 La | < | |
| 12 Mg | < | | 34 Se | < | | 58 Ce | < | |
| 13 Al | 8.4 | 0.1 | 35 Br | 0.013 | 0.005 | 59 Pr | | |
| 14 Si | 29.3 | 0.2 | 37 Rb | 0.0087 | 0.005 | 60 Nd | < | |
| 15 P | < | | 38 Sr | 0.20 | 0.01 | 62 Sm | < | |
| 16 S | 0.23 | 0.02 | 39 Y | < | | 64 Gd | | |
| 17 Cl | < | | 40 Zr | < | | 65 Tb | | |
| 19 K | 0.12 | 0.009 | 41 Nb | 0.045 | 0.008 | 72 Hf | | |
| 20 Ca | 49.7 | 0.2 | 42 Mo | < | | 73 Ta | 0.20 | 0.01 |
| 22 Ti | 0.66 | 0.03 | 45 Rh | 0.044 | 0.007 | 74 W | < | |
| 23 V | < | | 46 Pd | 0.031 | 0.008 | 77 Ir | | |
| 24 Cr | 0.013 | 0.002 | 47 Ag | 0.0091 | 0.01 | 78 Pt | 0.0055 | 0.01 |
| 25 Mn | < | | 48 Cd | 0.044 | 0.01 | 79 Au | < | |
| 26 Fe | 0.37 | 0.02 | 49 In | | | 80 Hg | < | |
| 27 Co | 0.056 | 0.005 | 50 Sn | 0.20 | 0.02 | 81 Tl | 0.018 | 0.01 |
| 28 Ni | 0.073 | 0.006 | 51 Sb | 0.32 | 0.02 | 82 Pb | 0.027 | 0.01 |
| 29 Cu | 0.043 | 0.007 | 52 Te | 0.33 | 0.03 | 83 Bi | < | |
| 30 Zn | 6.1 | 0.1 | 53 I | < | | 90 Th | 0.086 | 0.01 |
| 31 Ga | | | 55 Cs | 0.32 | 0.1 | 92 U | 0.0056 | 0.010 |

KnownConc 0 REST= 0 Dil/Smpl= 0

Mass/Area found : 34.52 mg /4.52 cm2 76.3 g/m2 with CountPrec= 3.3%

McMaster University Department Of Geology
1280 Main Street West,
Hamilton, Ontario
L8S 4M1

Tel: (416) 525-9140 Fax: (416) 522-3141

JOB.602 14-Jul-95

Company name..... McMaster ScMo 100kV LiF220 GeIII PE TlAP

**Sample Filter 251-2**

No Supporting Film is used
BackgroundModel used is Al
Given Effective Area is 452.16 mm2 ( 24.0 mm )
Assumed grain size = 0 Micrometer
Given rest is 0 %
Given Diluent/Sample is 0
The Viewed Mass (layer thickness) is to be calculated
A < sign means that the concentration is < 50 ppm

| Z | wt% | StdErr | Z | wt% | StdErr | Z | wt% | StdErr |
|---|---|---|---|---|---|---|---|---|
| 9 F | 0.32 | 0.2 | 32 Ge | | | 56 Ba | 0.11 | 0.009 |
| 11 Na | < | | 33 As | 0.037 | 0.01 | 57 La | < | |
| 12 Mg | < | | 34 Se | < | | 58 Ce | < | |
| 13 Al | 3.1 | 0.08 | 35 Br | < | | 59 Pr | | |
| 14 Si | 20.0 | 0.2 | 37 Rb | < | | 60 Nd | < | |
| 15 P | 0.039 | 0.003 | 38 Sr | 0.062 | 0.005 | 62 Sm | < | |
| 16 S | 41.1 | 0.2 | 39 Y | < | | 64 Gd | | |
| 17 Cl | < | | 40 Zr | < | | 65 Tb | | |
| 19 K | 0.076 | 0.006 | 41 Nb | 0.012 | 0.002 | 72 Hf | | |
| 20 Ca | 29.8 | 0.2 | 42 Mo | 0.016 | 0.002 | 73 Ta | 0.14 | 0.01 |
| 22 Ti | 0.44 | 0.03 | 45 Rh | 0.0056 | 0.0010 | 74 W | < | |
| 23 V | < | | 46 Pd | 0.0085 | 0.0009 | 77 Ir | | |
| 24 Cr | 0.043 | 0.004 | 47 Ag | 0.027 | 0.002 | 78 Pt | < | |
| 25 Mn | < | | 48 Cd | 0.012 | 0.001 | 79 Au | < | |
| 26 Fe | 0.25 | 0.02 | 49 In | | | 80 Hg | < | |
| 27 Co | 0.039 | 0.003 | 50 Sn | 0.021 | 0.002 | 81 Tl | 0.0082 | 0.005 |
| 28 Ni | 0.054 | 0.005 | 51 Sb | 0.020 | 0.002 | 82 Pb | 0.0059 | 0.005 |
| 29 Cu | 0.034 | 0.005 | 52 Te | 0.022 | 0.002 | 83 Bi | < | |
| 30 Zn | 4.2 | 0.10 | 53 I | < | | 90 Th | 0.020 | 0.003 |
| 31 Ga | | | 55 Cs | 0.010 | 0.005 | 92 U | < | |

KnownConc 0 REST= 0 Dil/Smpl= 0

Mass/Area found to be 'infinite'

## Appendix A.2

## Insoluble Corrosion Product Formed During Corrosion of a Nickel Electrode in 93.5 wt.% $H_2SO_4$ at 60°C

McMaster University Department of Geology
1280 Main Street West,
Hamilton, Ontario
L8S 4M1

Tel: (416) 525-9140 Fax: (416) 522-3141

JOB.755 15-Dec-95
Company name..... McMaster Rh 100kV LiF220 Ge111 PE TlAP
**Filter Blank 272-1**

A Supporting Film is used
BackgroundModel used is Al
Given Effective Area is 452.16 mm2 ( 24.0 mm )
Assumed grain size = 0 Micrometer
Given rest is 0 %
Given Diluent/Sample is 0
Given Viewed Mass is 18000.00 mg / 4.522 cm2 = 3.981 g/cm2
A < sign means that the concentration is < 50 ppm

| Z | wt% | StdErr | Z | wt% | StdErr | Z | wt% | StdErr |
|---|---|---|---|---|---|---|---|---|
| 9 F | | | 32 Ge | | | 56 Ba | 0.88 | 0.04 |
| 11 Na | 0.62 | 0.03 | 33 As | 0.028 | 0.04 | 57 La | < | |
| 12 Mg | 0.61 | 0.03 | 34 Se | | | 58 Ce | < | |
| 13 Al | 11.2 | 0.2 | 35 Br | < | | 59 Pr | | |
| 14 Si | 47.5 | 0.2 | 37 Rb | < | | 60 Nd | 0.048 | 0.008 |
| 15 P | 0.69 | 0.03 | 38 Sr | 0.20 | 0.01 | 62 Sm | 0.026 | 0.010 |
| 16 S | 0.73 | 0.04 | 39 Y | < | | 64 Gd | | |
| 17 Cl | 0.029 | 0.003 | 40 Zr | < | | 65 Tb | | |
| 19 K | 0.021 | 0.01 | 41 Nb | < | | 72 Hf | | |
| 20 Ca | 35.2 | 0.2 | 42 Mo | < | | 73 Ta | 0.66 | 0.1 |
| 22 Ti | 0.64 | 0.03 | 45 Rh | < | | 74 W | 0.23 | 0.08 |
| 23 V | < | | 46 Pd | 0.067 | 0.01 | 77 Ir | < | |
| 24 Cr | 0.034 | 0.005 | 47 Ag | 0.021 | 0.01 | 78 Pt | 0.035 | 0.01 |
| 25 Mn | 0.017 | 0.005 | 48 Cd | 0.012 | 0.009 | 79 Au | 0.040 | 0.006 |
| 26 Fe | < | | 49 In | | | 80 Hg | < | |
| 27 Co | 0.095 | 0.008 | 50 Sn | < | | 81 Tl | < | |
| 28 Ni | 0.24 | 0.02 | 51 Sb | 0.012 | 0.02 | 82 Pb | < | |
| 29 Cu | < | | 52 Te | 0.014 | 0.02 | 83 Bi | 0.022 | 0.01 |
| 30 Zn | 0.062 | 0.02 | 53 I | < | | 90 Th | 0.0055 | 0.04 |
| 31 Ga | | | 55 Cs | < | | 92 U | < | |

KnownConc 0 REST= 0 Dil/Smpl= 0

The sum before normalisation to 100% was 45.7 %

McMaster University Department of Geology
1280 Main Street West,
Hamilton, Ontario
L8S 4M1

Tel: (416) 525-9140 Fax: (416) 522-3141

JOB.756 15-Dec-9E
Company name..... McMaster Rh 100kV LiF220 Ge111 PE TlAP
Ni 272-2

A Supporting Film is used
BackgroundModel used is Al
Given Effective Area is 452.16 mm2 ( 24.0 mm )
Assumed grain size = 0 Micrometer
Given rest is 0 %
Given Diluent/Sample is 0
Given Viewed Mass is 18000.00 mg / 4.522 cm2 = 3.981 g/cm2
A < sign means that the concentration is < 50 ppm

| Z | wt% | StdErr | Z | wt% | StdErr | Z | wt% | StdErr |
|---|---|---|---|---|---|---|---|---|
| 9 F | | | 32 Ge | | | 56 Ba | 0.10 | 0.008 |
| 11 Na | 0.11 | 0.009 | 33 As | 0.011 | 0.02 | 57 La | < | |
| 12 Mg | 0.16 | 0.01 | 34 Se | | | 58 Ce | < | |
| 13 Al | 2.2 | 0.07 | 35 Br | < | | 59 Pr | | |
| 14 Si | 8.8 | 0.1 | 37 Rb | < | | 60 Nd | 0.012 | 0.004 |
| 15 P | 0.23 | 0.02 | 38 Sr | 0.11 | 0.009 | 62 Sm | 0.0050 | 0.005 |
| 16 S | 74.2 | 0.2 | 39 Y | < | | 64 Gd | | |
| 17 Cl | 0.028 | 0.002 | 40 Zr | < | | 65 Tb | | |
| 19 K | < | | 41 Nb | < | | 72 Hf | | |
| 20 Ca | 12.9 | 0.2 | 42 Mo | < | | 73 Ta | 0.37 | 0.06 |
| 22 Ti | 0.18 | 0.01 | 45 Rh | < | | 74 W | 0.15 | 0.04 |
| 23 V | < | | 46 Pd | 0.042 | 0.005 | 77 Ir | < | |
| 24 Cr | 0.012 | 0.002 | 47 Ag | 0.010 | 0.007 | 78 Pt | 0.021 | 0.007 |
| 25 Mn | 0.0089 | 0.002 | 48 Cd | 0.0059 | 0.005 | 79 Au | 0.020 | 0.003 |
| 26 Fe | < | | 49 In | | | 80 Hg | < | |
| 27 Co | 0.048 | 0.004 | 50 Sn | < | | 81 Tl | < | |
| 28 Ni | 0.13 | 0.01 | 51 Sb | < | | 82 Pb | < | |
| 29 Cu | 0.017 | 0.03 | 52 Te | 0.010 | 0.01 | 83 Bi | 0.012 | 0.007 |
| 30 Zn | 0.033 | 0.01 | 53 I | < | | 90 Th | < | |
| 31 Ga | | | 55 Cs | < | | 92 U | < | |

KnownConc 0 REST= 0 Dil/Smpl= 0

The sum before normalisation to 100% was 80.8 %

McMaster University Department of Geology
1280 Main Street West,
Hamilton, Ontario
L8S 4M1

Tel: (416) 525-9140 Fax: (416) 522-3141

JOB.758 15-Dec-95

Company name..... McMaster Rh 100kV LiF220 Ge111 PE TlAP
Suspended 272-4

A Supporting Film is used
BackgroundModel used is Al
Given Effective Area is 452.16 mm2 ( 24.0 mm )
Assumed grain size = 0 Micrometer
Given rest is 0 %
Given Diluent/Sample is 0
Given Viewed Mass is 18000.00 mg / 4.522 cm2 = 3.981 g/cm2
A < sign means that the concentration is < 50 ppm

| Z | wt% | StdErr | Z | wt% | StdErr | Z | wt% | StdErr |
|---|---|---|---|---|---|---|---|---|
| 9 F | | | 32 Ge | | | 56 Ba | 0.052 | 0.007 |
| 11 Na | 0.020 | 0.006 | 33 As | 0.013 | 0.02 | 57 La | < | |
| 12 Mg | 0.081 | 0.007 | 34 Se | | | 58 Ce | < | |
| 13 Al | 1.2 | 0.05 | 35 Br | < | | 59 Pr | | |
| 14 Si | 4.8 | 0.1 | 37 Rb | < | | 60 Nd | 0.016 | 0.003 |
| 15 P | 0.19 | 0.01 | 38 Sr | 0.097 | 0.008 | 62 Sm | 0.0060 | 0.005 |
| 16 S | 84.3 | 0.2 | 39 Y | < | | 64 Gd | | |
| 17 Cl | 0.027 | 0.002 | 40 Zr | < | | 65 Tb | | |
| 19 K | < | | 41 Nb | < | | 72 Hf | | |
| 20 Ca | 8.2 | 0.1 | 42 Mo | < | | 73 Ta | 0.34 | 0.05 |
| 22 Ti | 0.12 | 0.009 | 45 Rh | < | | 74 W | 0.14 | 0.03 |
| 23 V | < | | 46 Pd | 0.037 | 0.005 | 77 Ir | < | |
| 24 Cr | 0.015 | 0.002 | 47 Ag | 0.0086 | 0.006 | 78 Pt | 0.021 | 0.006 |
| 25 Mn | 0.0096 | 0.002 | 48 Cd | 0.0053 | 0.004 | 79 Au | 0.019 | 0.003 |
| 26 Fe | < | | 49 In | | | 80 Hg | < | |
| 27 Co | 0.047 | 0.004 | 50 Sn | < | | 81 Tl | < | |
| 28 Ni | 0.17 | 0.01 | 51 Sb | < | | 82 Pb | < | |
| 29 Cu | 0.027 | 0.03 | 52 Te | 0.010 | 0.01 | 83 Bi | 0.011 | 0.007 |
| 30 Zn | 0.038 | 0.01 | 53 I | < | | 90 Th | < | |
| 31 Ga | | | 55 Cs | < | | 92 U | < | |

KnownConc 0 REST= 0 Dil/Smpl= 0

The sum before normalisation to 100% was 83.4 %